INTERNATIONAL ATOMIC ENERGY AGENCY
UNITED NATIONS EDUCATIONAL, SCIENTIFIC AND CULTURAL ORGANIZATION
INTERNATIONAL CENTRE FOR THEORETICAL PHYSICS
I.C.T.P., P.O. BOX 586, 34100 TRIESTE, ITALY, CABLE: CENTRATOM TRIESTE

SMR.764 - 3

RESEARCH WORKSHOP ON CONDENSED MATTER PHYSICS
13 JUNE - 19 AUGUST 1994

MINIWORKSHOP ON "NONLINEAR TIME SERIES ANALYSIS" 8 - 12 AUGUST 1994

"Experimental Applications of Controlling Chaos"

Rajarshi ROY
School of Physics
Georgia Institute of Technology
Atlanta, GA 30332
U.S.A.

OPTICS & PHOTONICS NEWS
MAY 1994

Controlling Chaotic Lasers

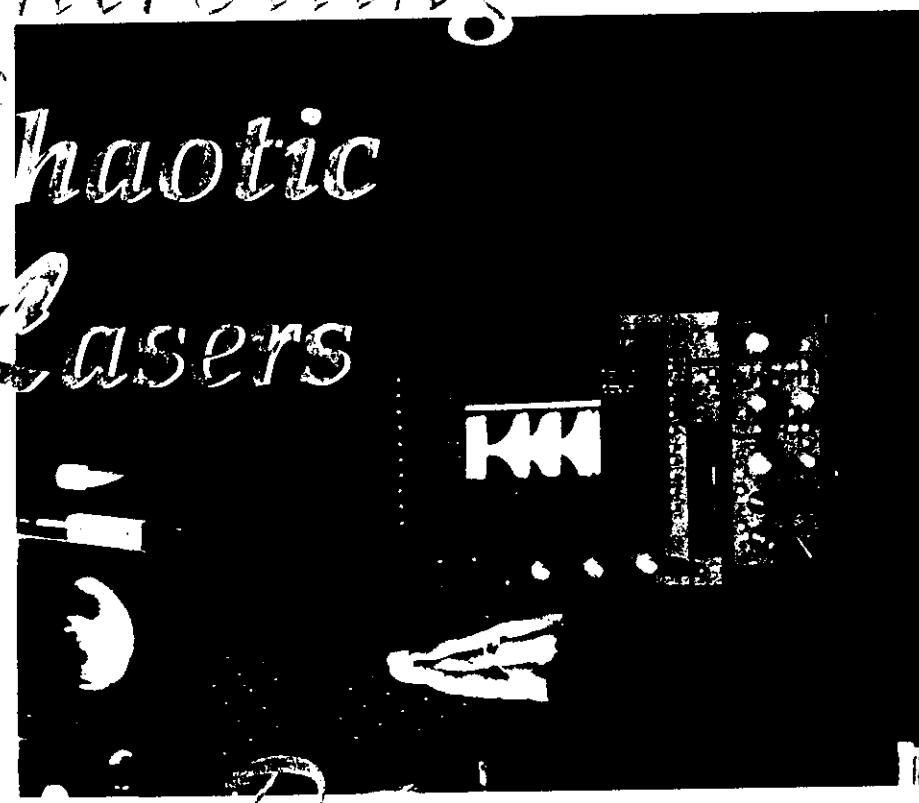

BY RAJARSHI ROY, ZELDA GILLS, AND K. SCOTT THORNBURG

Do lasers really exhibit chaos? Irregular intensity fluctuations were observed even in the earliest days of lasers. For example, the "spiking" fluctuations present in the output of a ruby laser were difficult to miss. All fluctuation phenomena observed were then commonly labeled "noise." Since that time, however, it has become evident that apparently random fluctuations can also occur in totally deterministic systems—those that are modeled by systems of equations containing no sources of noise. Such behavior is commonly called chaos.

The purpose of this article is to describe the advances made in the identification of chaotic behavior in lasers and to focus on the specific theme of controlling chaotic lasers. We will first briefly review the origins of the basic concepts of chaos and nonlinear dynamics in a general context and see how beautifully the history of chaotic lasers is intertwined with that of meteorology and fluid dynamics, the fields in which the crucial role of chaos was first recognized.

One of the most important realizations of the last 30 years has been that chaotic behavior is commonplace in physical, chemical, and biological systems. Most scientists and engineers have begun to recognize this inescapable fact. The advent of computers has been responsible for this awakening, not just in meteorology, but in every branch of science, from astronomy to zoology. A new branch of mathematics, dynamical systems theory, has developed rapidly and now forms the universal mathematical language for the description of chaotic systems in science and engineering. Nonlinear dynamics is the discipline that includes experimental and theoretical investigations of chaos and instabilities.

Chaos and the Weather

John Von Neumann, the father of modern computers, dreamed that one day we would be able to predict accurately, and perhaps even control, weather patterns around the globe.[1] In his book *Infinite in All Directions*, physicist Freeman Dyson discusses the views of Von Neumann, who had the "reputation of being the cleverest man in the world." Von Neumann hoped that computers would allow us to "divide the phenomena of meteorology cleanly into two categories, the stable and the unstable. The unstable phenomena are those that are upset by small disturbances, the stable phenomena are those that are resilient to small disturbances . . . . All processes that are stable we shall predict. All processes that are unstable we shall control."

Dyson remarks that few people took Von Neumann's dream seriously, including meteorologists. In fact, studies on the problem of convection of a fluid heated from below (a highly simplified model of the Earth's atmosphere) by Edward Lorenz, an MIT meteorologist, seemed to indicate that Von Neumann's dream could never be realized. Lorenz's numerical computations[2] revealed a totally new aspect of behavior in this dynamical system; large, irregular fluctuations appeared to originate from an innocuous looking set of three-coupled, nonlinear ordinary differential equations without any sources of noise or fluctuations included in them.

Even more surprising was the incredible sensitivity of a solution of these equations to a small difference in initial conditions. Lorenz found that very slightly different initial conditions resulted in an exponential divergence of solutions. Lorenz engraved this aspect of chaotic dynamics in our minds through the title of a talk he gave in 1972, "Predictability: Does the Flap of a Butterfly's Wings in Brazil set off a Tornado in Texas?"[3(a)] Indeed, Dyson comments that "a chaotic motion is generally neither predictable nor controllable. It is unpredictable because a small disturbance will produce exponentially growing perturbation of the motion. It is uncontrollable because small disturbances lead to other chaotic motions and not to any stable and predictable alternative. Von Neumann's mistake was to imagine that every unstable motion could be nudged into a stable motion by small pushes and pulls applied at the right places."

In the few years since Dyson wrote about the failure of Von Neumann's dream, there has, in fact, been significant progress toward its realization; reasonably accurate predictions can be made for chaotic motion over fairly long periods of time,[3] and the control of chaotic motion has been demonstrated for some "simple" chaotic systems, including lasers.

Chaotic Lasers

The connection between chaotic dynamics and laser instabilities was not made until Hermann Haken, in a short paper,[4] remarked on a beautiful similarity that he had discovered between the equations for a fluid studied by Lorenz a dozen years earlier, and the semi-classical equations that describe the operation of a single-mode laser. He found that the three equations of motion for the electric field of the laser, the polarization of the active medium, and the population inversion were identical in form to the Lorenz equations after appropriate transformations of the variables. These equations contained no noise sources, yet their similarity to the Lorenz equations implied that a laser should display irregular deterministic fluctuations in certain parameter regimes.

A search for laser chaos ensued, and several groups around the world searched for the right laser system to display Lorenz chaos.[5] This was not as simple as it may seem. A single-mode laser system had to be found where the decay rates of the polarization and population inversion of the active medium, as well as that of the electric field were of the same order of magnitude, for a valid comparison with the Haken-Lorenz equations. In most laser systems (He-Ne, CO_2, semiconductor, Nd:YAG, etc.), the polarization decay rate is much greater than the inversion and field decay rates, resulting in the effective reduction of the three variable system of equations to two dynamical variables. Chaos cannot occur in a two variable system of equations; a mathematical theorem tells us that we can only have stable or periodic dynamics in a two-dimensional system. We thus have to find a single-mode laser in which all three decay rates are comparable to see this type of chaotic behavior. Finally, a rather exotic laser system, the far-infrared ammonia laser, was settled upon, which had the right features to display Lorenz-like chaos.[6]

How can we tell if the observed intensity fluctuations in such a laser are really a signature of chaotic behavior? One of the most straightforward approaches to this question is to examine the system behavior while varying one of the parameters. If a sequence of behavior, or route to chaos, is found that has been identified from the study of deterministic model equations for the system, one may be reasonably sure that chaotic behavior has been observed. Extensive experiments and numerical modeling by several groups have now established that chaotic behavior is indeed displayed by the ammonia laser.

The reader may ask if laser chaos is restricted to exotic systems such as the ammonia laser. Many "garden variety" laser systems can exhibit chaotic behavior if they operate in multiple longitudinal or transverse modes; once again, these additional modes provide the three or more degrees of freedom necessary for the system to be chaotic. If the modes are nonlinearly coupled to each other, chaos can result. For example, nonlinear mode-coupling through four-wave-mixing in the active medium may generate chaotic intensity fluctuations of individual modes in a multimode dye laser.[10] External feedback often leads to chaos in semiconductor lasers,[11] a matter of great practical concern. During the 1980s, there were also several observations of chaotic behavior in single-mode lasers with modulated losses and pumps. Arecchi and colleagues demonstrated chaos in a loss modulated CO_2 laser,[12] while Winful and colleagues[13] showed that under certain conditions a semiconductor laser could be driven chaotic by periodic modulation of its injection current. The periodic modulation effectively provides the third degree of freedom necessary to observe chaos in these laser systems. One of the most interesting examples of laser chaos was discovered by Tom Baer (then at Spectra-Physics), who studied the generation of green light from a diode laser pumped Nd:YAG laser with an intracavity KTP crystal.[14]

The Green Problem

Baer found that though the Nd:YAG laser operated in a stable steady state without the intracavity crystal, large irregular intensity fluctuations were sometimes observed when the intracavity KTP crystal was used to generate green light from the system (Fig. 1). Baer noted that this behavior occurred when the laser operated in three or more longitudinal modes. He hypothesized that sum-frequency generation in the KTP crystal could provide mode-mode coupling that would destabilize the laser. This was not a desirable situation for proposed practical applications of the system, in optical disk readers, for example. The unstable behavior of this system soon came to be known as the "green problem."

The chaotic nature of the green laser was investigated in some detail and connected to the destabilization of relaxation oscillations.[15] Relaxation oscillations are always present in a laser; they are the result of power exchange between the atoms of the active medium and the electric field in the cavity and are normally very small in amplitude. It was found that the nonlinear coupling of the modes through sum-frequency generation resulted in the destabilization of relaxation oscillations in the green laser system. A reasonably accurate model was developed for the system, that could predict many aspects of system behavior, both chaotic and non-chaotic.

As may be expected, several methods were proposed and implemented to get rid of the fluctuations. These methods consisted of system modifications such as restricting the laser to operate in two orthogonally polarized modes by adding wave plates to the laser cavity[16,17] or proper orientation of the YAG and KTP crystals.[18] These are typical examples of what has been the traditional reaction of scientists and engineers when faced with irregular fluctuations in a laser system—redesign the system so that it is inherently stable or try to find a parameter regime of the system where chaos does not exist. A departure from this traditional mindset required a radically new perspective and approach toward grappling with chaotic systems.

Controlling Chaos

In the spring of 1990, Ott, Grebogi, and Yorke (OGY) of the University of Maryland introduced such a new perspective in a seminal paper[19] entitled "Controlling Chaos." "Control" refers to achieving periodic or stable output from a chaotic system without changing the parameters of the system, or the system itself, in a permanent way; only small time-dependent perturbations about the ambient parameter values are allowed. OGY observed that when irregular, chaotic behavior is observed, we often do not have available a detailed mathematical model for the dynamical system that will accurately describe its behavior over a wide range of operating parameters. If we want to develop techniques for control of such chaotic systems, two crucial questions arise.

- Can we develop a dynamical control strategy based primarily on experimental measurements made on the system, without trying to build a mathematical model that is globally accurate?
- Can we control the system without making large changes in parameters or variables?

OGY showed that both these goals can be achieved, at least for some chaotic systems. A chaotic system can be controlled with small, judiciously chosen changes to parame-

Figure 1

The laser system in which the "green problem" was observed by Tom Baer. Large, irregular amplitude fluctuations of the green light emitted by an Nd:YAG laser with an intracavity KTP crystal for frequency doubling. The fluctuations are not present without the intracavity KTP crystal.[14]

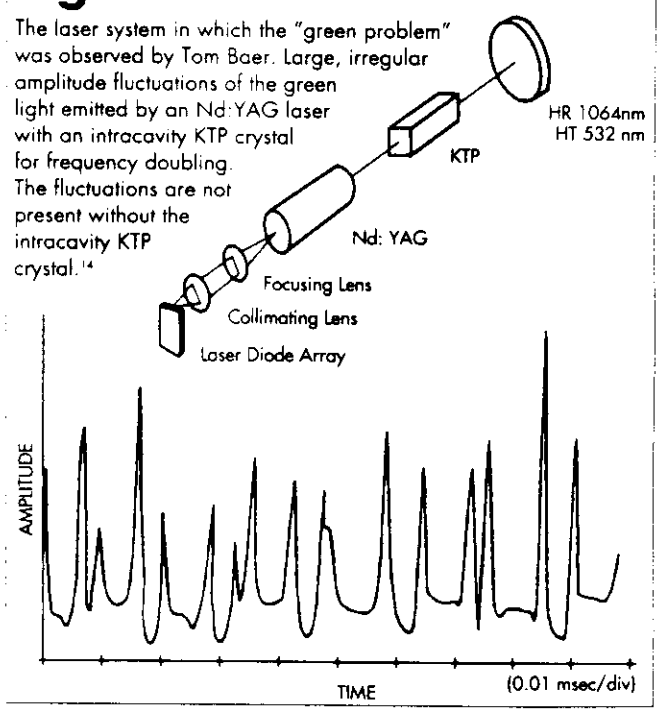

ters made on the basis of observations of a system variable, such as the fluctuating output intensity of a laser. It is the very sensitivity of a chaotic system to small perturbations that allows us to control it with such corrective changes.

The OGY algorithm for chaos control was based on the observation that a chaotic attractor—the geometrical object toward which a system's trajectory in phase space converges—typically has a large number of unstable periodic orbits embedded in it. The system visits the neighborhood of these unstable periodic orbits from time to time; what is needed for control is a technique to nudge the system back to a periodic orbit when the system shows its inherent tendency to depart from it. The basic elements of the OGY algorithm are simple. Even a nonlinear system can be described by a linear approximation, once it approaches close enough to a periodic state or fixed point (for example, an unstable steady state). By observing the dynamics of the system in the neighborhood of the fixed point or periodic state, the direction and amount of instability can be determined. We can then use that information to keep the system near the fixed point or periodic orbit.

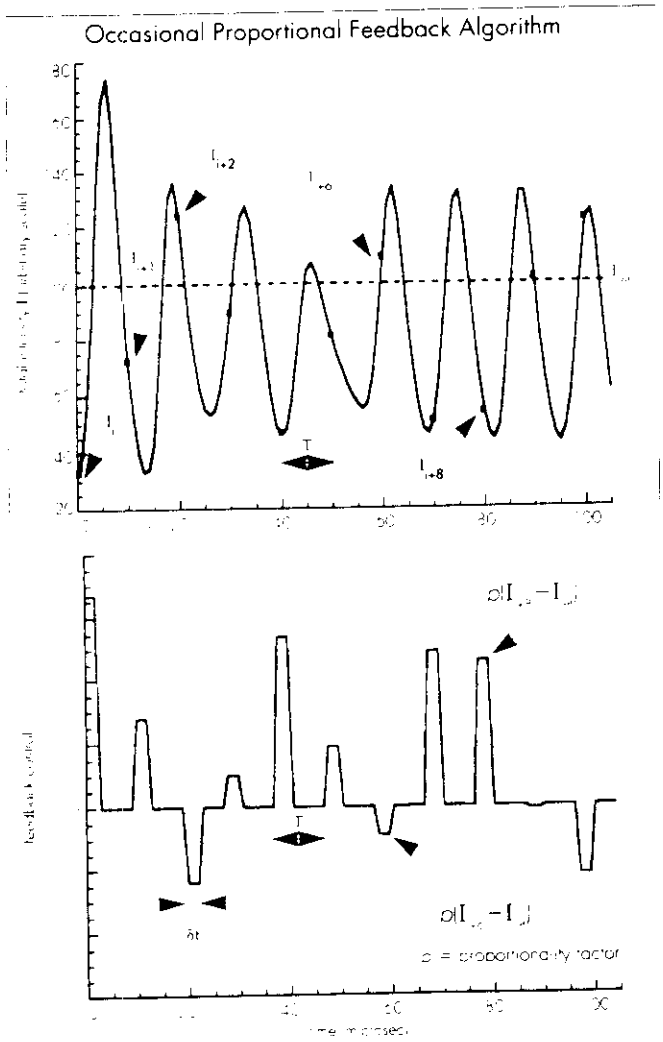

Figure 2

The occasional proportional feedback (OPF) algorithm used for control of the chaotic laser. The four parameters of the control circuit, T, dt, p and I_{ref} are shown.

To make this point clear, imagine trying to balance a ball at the center of a saddle. The saddle surface is unstable in the direction of convexity; the ball will fall off along the sides of the saddle. The amount of instability, or how fast the ball falls off, is determined by the curvature of the saddle. In the other direction, the saddle is stable; the ball returns toward the center if displaced along the ridge of the saddle. The OGY algorithm tells us essentially how to move a saddle under the ball so as to keep it balanced at the center. Once we know the curvature of the saddle in the unstable direction, we can balance the ball at the center by making observations of the position of the ball from time to time. If control is initiated when the ball is sufficiently close to the center, we can maintain control in a small neighborhood of the center with only small corrective motions.

The OGY algorithm was implemented in a beautiful experiment in late 1990. Ditto, Rauseo, and Spano showed how the OGY algorithm could be applied to stabilize the irregular motion of a mechanical system—a tinsel-like ribbon of magnetoelastic material that swayed chaotically in an applied alternating magnetic field.[20,21] The OGY method and related theoretical and experimental developments in physics, chemistry, and biology have recently been reviewed by Shinbrot *et al.*[22]

The dynamical control of chaotic systems offers several possibilites that are difficult to achieve with the traditional approach in which we adjust system parameters to be in a periodic or stable regime. First, it is possible to switch between two or more periodic waveforms rapidly with dynamical control. Second, it is possible to stabilize complex waveforms that may only occur over a very small parameter range for the system without control. Finally, with active feedback we can extend the range of system parameters over which a periodic orbit or steady state can be maintained.

Dynamical Control of a Chaotic Laser

It was clear to us at Georgia Tech, soon after publication of the OGY paper, that it would be of great interest to try and apply these new techniques to the chaotic green laser. There was the purely scientific motivation: Could we demonstrate control of a chaotic laser in an experiment and stabilize several different periodic waveforms for the same laser parameters? There was also the practical motivation: Could such control techniques be used to stabilize chaotic lasers without having to redesign the system?

It was at this point that one of us (Roy) happened to learn that Earle Hunt (Ohio University) had developed an analog circuit to stabilize periodic waveforms generated by a chaotic diode resonator circuit. Hunt used a variant of the OGY approach, which he called occasional proportional feedback (OPF).[23,24] The name arose from the fact that the

feedback consisted of a series of perturbations of limited duration dt ("kicks") delivered to the input drive signal at periodic intervals (T) in proportion to the difference of the chaotic output signal from a reference value. The OPF technique seemed perfectly suited for an attempt to stabilize periodic orbits of the green laser, since the circuit could be easily operated in the microsecond time scale required for the laser.

The laser intensity was detected with a fast photodiode and this signal provided the input for the control circuit. The output of the control circuit modified the injection current of the diode laser used to pump the Nd:YAG crystal. This seemed to be the most natural and convenient choice of control parameter. To adapt Hunt's circuit for control of the autonomously chaotic laser, we had to supply an external timing signal from a function generator. This determined the interval T between "kicks" applied to the pump laser injection current. Even though there was no external periodic modulation responsible for the chaotic dynamics, the relaxation oscillations of the laser intensity provided a natural time scale for perturbative corrections. The interval between kicks was thus adjusted to be roughly at the relaxation oscillation period (approximately 100 kHz), or a fractional multiple of it. The OPF algorithm is shown schematically in Figure 2. The four parameters of the control circuit are: The period T, duration of the kicks dt, reference level I_{ref}, which measures the deviation of the signal, and the proportionality factor p, which determines the amplitude of the kicks.

The results of application of OPF to the laser were quite remarkable.[25] We were able to demonstrate stabilization of a large variety of periodic waveforms with perturbations of a few percent applied to the pump laser injection current. A typical chaotic waveform, together with several periodic waveforms stabilized in this way, are shown in Figure 3. The control signal fluctuations are shown above the intensity waveforms. The particular waveforms stabilized can be selected by changes of control circuit parameters, mainly the time period T and the reference level I_{ref}.

For the control circuit to work successfully, the laser had to be operated so as to generate very little green light. The laser is "weakly" chaotic in this regime; the rate of separation of initially close trajectories in phase space is small, and only one direction of instability occurs. If a significant amount of green light was generated, and the laser was highly chaotic (particularly if the laser has more than one direction of instability in phase space), the circuit may be unable to stabilize the laser.

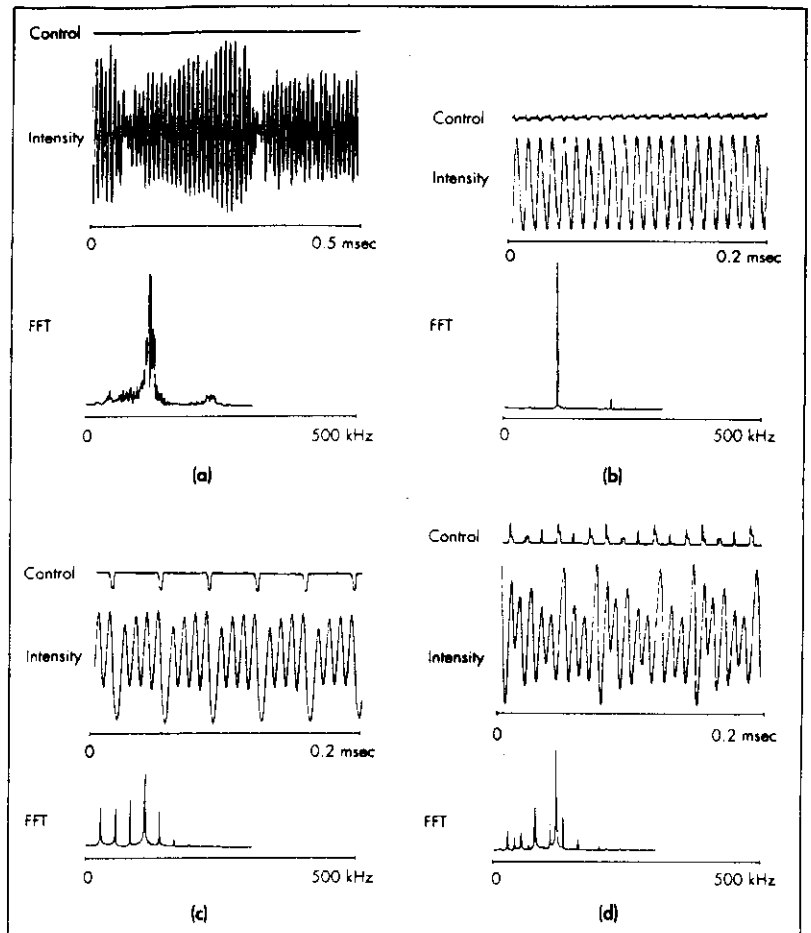

Figure 3

An example of stabilization of periodic orbits or waveforms of the chaotic laser. A typical chaotic time trace for the fundamental wavelength is shown in (a), in which the underlying relaxation oscillations are present. The control signals, waveforms and their fast Fourier transforms are shown in (b), (c), and (d) for three periodic orbits that have been stabilized. The relative fluctuations of the control signal about the ambient value are of the order of a few percent.[25]

Stabilization of the Steady State

Of course, these experiments beg the question: If the laser is in a chaotic state, can we apply small corrective perturbations to obtain a stable output? This is, of course, interesting from an engineering standpoint and for practical application. Much to our own surprise, we found that we could indeed achieve a stable output by adjusting the reference level to the mean of the chaotic fluctuations and matching the period T to the relaxation oscillation period. The control voltage fluctuations became extremely small once the steady state was controlled. Figure 4 shows the transient behavior of the laser intensity fluctuations as they are reduced to small fluctuations about the steady state as well as the control signal fluctuations during the stabilization process.

If the control parameters are fixed and the pump power of the laser is increased or decreased after the steady state is stabilized, the control signal fluctuations increase rapidly, and control is lost as the laser goes into periodic or chaotic oscillations. Clearly, one needs to change the control circuit parameters as the laser pump power is changed. A procedure called "tracking" accomplishes this change of control parameters in a systematic fashion. We applied such a tracking procedure to our laser; the control circuit parameters are varied to minimize the control signal fluctuations at each value of the pump power, which is increased in small increments. Our experiment illustrated the general algorithms

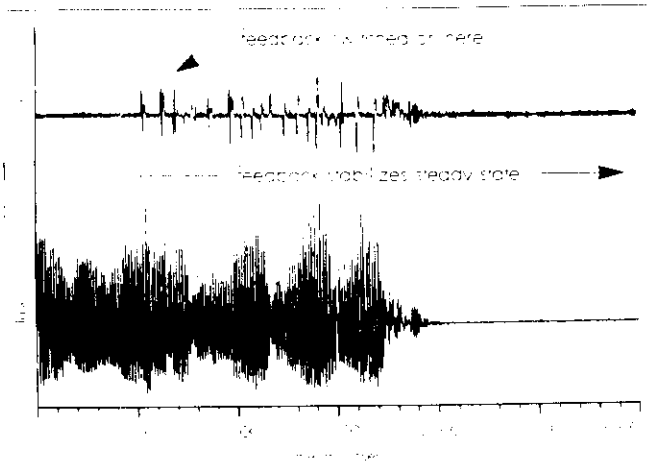

Figure 4

Stabilization of the steady state. The transients toward the steady state are shown when the control signal is applied to a chaotic laser. The chaos here is due to reflective feedback, not the intracavity crystal.

for tracking periodic orbits developed recently by Ira Schwartz and his colleagues at the Naval Research Laboratory.[26,27] By combining stabilization and tracking, we maintained a stable steady state (Fig. 5) as the laser pump power was increased from threshold (21 mW) to more than three times above threshold (about 80 mW).[28] Without the control circuit, the laser intensity went into periodic oscillations at a pump power of about 25 mW, and then into chaotic fluctuations, as indicated in the figure by open circles and crosses.

Current Research and Future Directions

Experiments on the control of chaotic lasers have been performed in several laboratories around the world. In a series of elegant experiments, Pierre Glorieux and his co-workers in Lille, France, have demonstrated both stabilization of periodic orbits and of the unstable steady state in an Nd:fiber laser.[29-31] Stabilization of the steady state was achieved by continuous derivative feedback in their experiments. They also demonstrated the tracking of unstable periodic orbits as system parameters were varied. Another experiment in Lille showed that the unstable branch of a bistable optical system could be stabilized by these feedback techniques.[32] The experiments of Brun and colleagues in Zurich on an NMR laser succeeded in systematically stabilizing several periodic orbits by an extension of the OGY technique.[33] Apart from these experiments, several groups have investigated the application of such control techniques to models of semiconductor laser diodes destabilized by optical feedback from an external reflector.[33,34]

The implementation of the control algorithm has been done electronically so far either by digital techniques or by analog hardware. An alternative approach, particularly if speed is crucial, may be the development of all-optical processing and feedback. To our knowledge, no experiments have demonstrated dynamical control and stabilization of chaos through purely optical techniques. Could neural networks (optically implemented, for speed) be used to predict future behavior of the chaotic system and help determine optimal corrections?[35]

In the OGY technique, the system must come sufficiently close to an unstable periodic orbit to stabilize it successfully with small perturbations. What if we don't want to wait for long periods of time, as is typically the case for complex waveforms? The Maryland group has developed a technique called "targeting," in which a chaotic system moves from its current state to a desired state in as short a time as possible through small perturbations. This is still a very active area of theoretical research, and the technique has yet to be implemented on an optical system or device. The targeting algorithm has been demonstrated experimentally on the magnetoelastic ribbon system by Shinbrot *et al.* with impressive results.[36]

The robustness of control techniques to external noise and drift of parameters is a crucial technical issue that will have to be investigated in detail for the practical implementa-

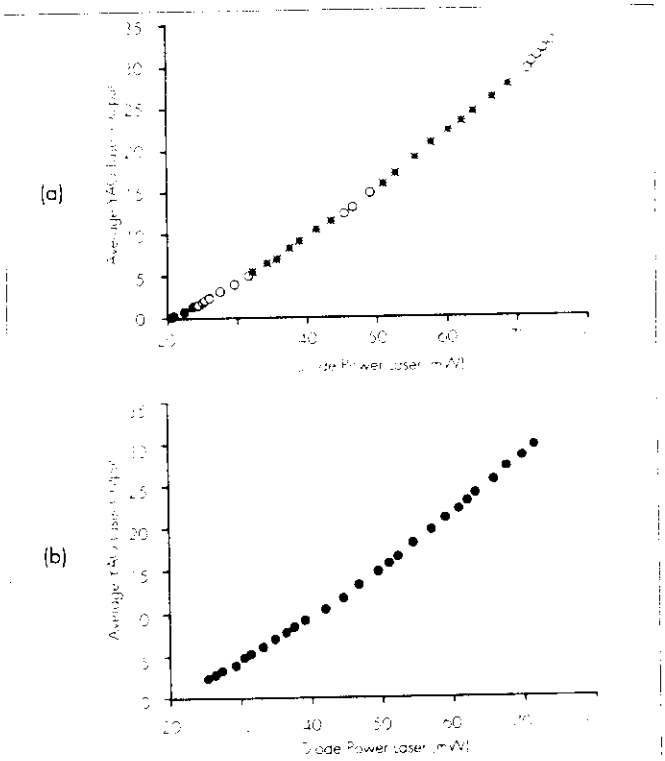

Figure 5

Stabilization of the steady state; control combined with a tracking algorithm allowed us to extend the stability regime of the laser. In (a) the solid circles represent stable output, the open circles periodic oscillations, and the crosses chaotic fluctuations; no control or tracking is done. In (b), stable output is obtained over the entire pump power range with control and tracking. The y-axis shows the Nd:YAG 1.06 μ output on a relative scale.[28]

tion of these techniques. On the more fundamental side, a difficult issue that is sure to emerge in the near future is the influence of intrinsic (quantum) noise on nonlinear dynamics and the resulting limitations on control of chaotic systems.

Finally, an important area of research in the future will be the control of chaotic systems with higher dimensional chaotic attractors (for example, those with more than one direction of instability in phase space) and sytems that possess both spatial and temporal degrees of freedom.[37,38] Laser arrays may be the test-bed for application for techniques that are being developed to control spatio-temporal chaos. Here the emphasis may be on the dynamical control of spatial profiles, including the periodic (or aperiodic) scanning of beams in space.

ACKNOWLEDGMENTS

It is a pleasure to acknowledge collaborations and discussions over the past five years with Tom Baer, Chris Bracikowski, Pere Colet, Ron Fox, Evans Harrell, Robert Hilborn, Earle Hunt, Christina Iwata, Glen James, Greg Kintz, Tom Maier, Tom Murphy, Ira Schwartz, Ioana Triadaf, and Kurt Wiesenfeld. We apologize to the authors of papers we have not referenced, either inadvertently, or due to lack of space.

REFERENCES

1. (a) J. Gleick, *Chaos, Making a New Science*, Viking, New York, N.Y. 1987. (b) F.C. Moon, *Chaotic and Fractal Dynamics*, J. Wiley, New York, N.Y. 1992. (c) R. C. Hilborn, *Chaos and Nonlinear Dynamics: An Introduction for Scientists and Engineers*, Oxford University Press, New York, N.Y. 1994. (d) E.N. Lorenz, *The Essence of Chaos*, University of Washington Press, Seattle, Wash. (1993).
2. J. Von Neumann, *Can We Survive Technology*, Fortune (1955), reprinted in *John Von Neumann, Collected Works, Vol. VI*, edited by A.H. Taub, The Macmillan Co., New York, N.Y., 1963.
3. F. J. Dyson, *Infinite in All Directions*, Harper and Row, New York, N.Y., 1988, p. 182.
4. E.N. Lorenz, "Deterministic nonperiodic flow," J. Atmos. Sci. **20**, 130-141 (1963).
5. N. Gershenfeld and A. S. Weigend, *The Future of Time Series*, in *Time Series Prediction: Forecasting the Future and Understanding the Past*, A.S. Weigend and N. Gershenfeld, editors, Addison-Wesley, Reading, Mass. (1993).
6. H. Haken, "Analogy between higher instabilities in fluids and lasers," Phys. Lett. **53A**, 77-78 (1975).
7. (a) L.M. Narducci and N.B. Abraham, *Laser Physics and Laser Instabilities* World Scientific, Singapore, 1988. (b) P.W. Milonni, M-L. Shih and J.R. Ackerhalt, *Chaos in Laser Matter Interactions*, World Scientific, Singapore, 1987. (c) C.O. Weiss and R. Vilaseca, *Dynamics of Lasers*, VCH Publishers, New York, N.Y. 1991.
8. U. Hubner *et al.*, "Dimensions and entropies of chaotic intensity pulsations in a single-mode far-infrared NH_3 laser," Phys. Rev. **A40**, 6354-6365 (1989).
9. R.G. Harrison and W. Lu, "Origin of periodic, chaotic, and bistable emission from Raman lasers," Phys. Rev. Lett. **63**, 1372-1375 (1989).
10. I. McMackin *et al.*, "Instabilities and chaos in a multimode, standing-wave, CW dye laser," Phys. Rev. **A38**, 320-332 (1988).
11. J. Sacher *et al.*, "Intermittency in the coherence collapse of a semiconductor laser with external feedback," Phys. Rev. Lett. **63**, 2224-2227 (1989).
12. F.T. Arecchi *et al.*, "Experimental evidence of subharmonic bifurcations, multistability, and turbulence in a Q-switched gas laser," Phys. Rev. Lett. **49**, 1217-1219 (1982)
13. H.G. Winful *et al.*, "Frequency locking, quasiperiodicity, and chaos in modulated self-pulsing semiconductor lasers," Appl. Phys. Lett. **48**, 616-618 (1986).
14. T. Baer, "Large amplitude fluctuations due to longitudinal mode coupling in diode-pumped intracavity-doubled Nd:YAG lasers," J. Opt. Soc. Am. **B3**, 1175-1180 (1986).
15. C. Bracikowski and R. Roy, "Chaos in a multimode solid-state laser system," Chaos **1**, 49-64 (1991).
16. M. Oka and S. Kubota, "Stable intracavity doubling of orthogonal linearly polarized modes in diode-pumped Nd:YAG lasers," Opt. Lett. **13**, 805-807 (1988).
17. D. Anthon *et al.*, "Intracavity doubling of CW diode-pumped Nd:YAG lasers with KTP," IEEE J. Quant. Elect. **28**, 1148-1157 (1992).
18. G.E. James *et al.*, "Elimination of chaos in an intracavity-doubled Nd:YAG laser," Opt. Lett. **15**, 1141-1143 (1990).
19. E. Ott *et al.*, "Controlling chaos," Phys. Rev. Lett. **64**, 1196-1199 (1990).
20. W. L. Ditto *et al.*, "Experimental control of chaos," Phys. Rev. Lett. **65**, 3211-3214 (1990).
21. W.L. Ditto and L. M. Pecora, "*Mastering Chaos*," Scientific American **269**, 78 (1993)
22. T. Shinbrot *et al.*, "Using small perturbations to control chaos," Nature **363**, 411-417 (1993).
23. E.R. Hunt, "Stabilizing high-period orbits in a chaotic system: The diode resonator," Phys. Rev. Lett. **67**, 1953-1955 (1991).
24. E. R. Hunt and G. Johnson, "Keeping chaos at bay," IEEE Spectrum **30**, 32-36 (1993).
25. R. Roy *et al.*, "Dynamical control of a chaotic laser: Experimental stabilization of a globally coupled system," Phys. Rev. Lett. **68**, 1259-1262 (1992).
26. I.B. Schwartz and I. Triandaf, "Tracking unstable orbits in experiments," Phys. Rev. **A46**, 7439-7444 (1992).
27. T. Carroll *et al.*, "Tracking unstable orbits in an experiment," Phys. Rev. **A46**, 6189-6192 (1992).
28. Z. Gills *et al.*, "Tracking unstable steady states: Expending the stability regime of a multimode laser system," Phys. Rev. Lett. **69**, 3169-3172 (1992).
29. S. Bielawski *et al.*, "Stabilization and characterization of unstable steady states in a laser," Phys. Rev. **A47**, 3276-3279 (1993).
30. S. Bielawski *et al.*, "Experimental characterization of unstable periodic orbits by controlling chaos," Phys. Rev. **A47**, R2492-2495 (1993).
31. B. Macke *et al.*, "Stabilization of unstable stationary states in optical bistability," Phys. Rev. **A47**, R1609-1611 (1993).
32. C. Reyl *et al.*, "Control of NMR-laser chaos in high-dimensional embedding space," Phys. Rev. **E47**, 267-272 (1993).
33. A. Gavrielides *et al.*, *Chaos in Optics*, SPIE Proc. Vol. 2039, ed. R. Roy (1993), p. 239.
34. G.R. Gray *et al.*, *Chaos in Optics*, SPIE Proc. Vol. 2039, ed. R. Roy (1993), p. 45.
35. S.D. Pethel *et al.*, *Chaos in Optics*, SPIE Proc. Vol. 2039, ed. R. Roy (1993)p. 129.
36. T. Shinbrot *et al.*, "Using the sensitive dependence of chaos (the 'butterfly effect') to direct trajectories in an experimental chaotic system," Phys. Rev. Lett. **68**, 2863-2866 (1992).
37. D. Auerbach *et al.*, "Controlling chaos in a high dimensional system," Phys. Rev. Lett. **69**, 3479-3482 (1992).
38. Hu Gang and Qu Zhilin, "Controlling spatiotemporal chaos in coupled map lattice systems," Phys. Rev. Lett. **72**, 68-71 (1994).

RAJARSHI ROY, ZELDA GILLS, *and* **K. SCOTT THORNBURG** *are with the Georgia Institute of Technology School of Physics, Atlanta, Ga.*

Chaos in a multimode solid-state laser system

C. Bracikowski and Rajarshi Roy
Georgia Institute of Technology, School of Physics, Atlanta, Georgia 30332

(Received 3 April 1991; accepted for publication 14 May 1991)

When a nonlinear crystal is placed within a multimode solid-state laser cavity, deterministic fluctuations are induced in the output intensity. In this paper, the results of our studies of the intensity noise in a diode pumped, intracavity frequency doubled Nd:YAG (neodymium doped yttrium aluminum garnet) laser will be presented. First, a novel technique to eliminate these fluctuations is described. Second, the observation of antiphase states in the laser output is discussed. These states are characterized by a cyclic periodic pulsing of the individual longitudinal mode intensities. Finally, the statistical properties of chaotic intensity fluctuations are characterized. It is be demonstrated that it is possible to accurately model the laser dynamics by a system of globally coupled, nonlinear oscillators.

I. INTRODUCTION

In this paper we will study the periodic and chaotic fluctuations present in the output intensity of a multimode solid-state laser system. Many optical systems exhibit chaotic dynamics.[1-3] Our studies have been performed on an Nd:YAG laser which normally lases at the fundamental wavelength of 1064 nm in the infrared. When a nonlinear optical crystal such as KTP (potassium titanyl phosphate) is inserted into the cavity, some of the infrared fundamental is converted into green light ($\sim$532 nm) by the processes of second harmonic and sum frequency generation. Sum frequency generation provides a nonlinear loss mechanism that globally couples the longitudinal modes, i.e., each lasing mode is coupled to all other lasing modes. This nonlinear mode coupling produces deterministic intensity fluctuations in the laser output. The laser output is stable without the intracavity doubling crystal; with the crystal inserted into the laser cavity the output intensity can show periodic and chaotic fluctuations.

An early prediction of instability in a laser system with nonlinearly coupled modes was made by Arecchi and Ricca.[4] Chaotic intensity fluctuations in this laser system were observed and analyzed by Baer,[5] who developed a deterministic rate equation model to explain the fluctuations. A detailed linear stability analysis of Baer's rate equations was performed by Wu and Mandel.[6,7] A significant step was taken by Oka and Kubota[8] who recognized that the polarizations of the cavity modes play a critical role in the laser dynamics. Their analysis, however, was limited to the case of only two orthogonally polarized cavity modes. We have generalized previous models to include multiple longitudinal modes. We have shown that these modes can lase in only two orthogonal polarizations. Our analysis includes the possible birefringence of the YAG crystal that was neglected in previous analyses.

In Sec. II we present the generalized laser model. We briefly outline the derivation of the model and discuss the physical origin and magnitudes of the various parameters. Section III contains the results of a linear stability analysis of the laser rate equations. This analysis predicts that the laser can be stabilized by proper rotational orientation of the YAG and KTP crystals. Experimental results that verify this prediction are shown. Numerical integration of the laser equations predicts the existence of antiphase states in the laser output. These states are characterized by a cyclic periodic pulsing of the individual longitudinal mode intensities. This theoretical prediction as well as the experimental observation of antiphase states in the laser intensity are discussed in Sec. IV. The rich variety of complex nonlinear dynamical behavior of this laser is explored in Sec. V. We use fast Fourier transforms (FFT), time delay plots, phase plots, probability distributions, correlation functions, and a calculation of the Liapunov exponent to provide a detailed picture of the dynamics. In particular, the probability distributions associated with the total intensity and its two orthogonally polarized components in the chaotic state are measured and compared with the results of the numerical model. Section VI presents our conclusions and a discussion of the interesting new questions that are raised by this work.

II. LASER SYSTEM AND MODEL

Figure 1 is a schematic of the intracavity doubled Nd:YAG laser we have studied. The laser cavity contained a nonlinear KTP (potassium titanyl phosphate) crystal which served as the frequency doubling element.[9,10] The intensity at the fundamental wavelength is highest within the laser cavity. Since the intensity of green light produced by the KTP crystal is proportional to the square of the intensity at the fundamental wavelength, the KTP crystal is placed inside the laser cavity. The Nd:YAG crystal was pumped by a commercial ten element phased array laser diode[11,12] with a maximum output power of 200 mW. The highly divergent and elliptical pump beam is first collimated and then circularized before being focussed into the cylindrical YAG rod by a 5 cm focal length lens. The flat front face of the Nd:YAG crystal acted as the cavity high reflector, and was highly reflecting at both the fundamental ($\sim$1064 nm, infrared) and doubled ($\sim$532 nm, green) wavelengths and highly transmitting at the pump wavelength ($\sim$810 nm). The laser output coupler had a 3.75 cm radius of curvature and was highly transmitting at the

 1054-1500/91/010049-16$01.00

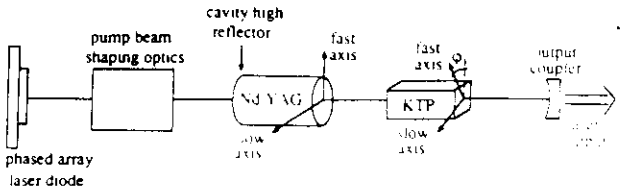

FIG. 1. Schematic of the diode pumped Nd:YAG (neodymium doped yttrium aluminum garnet) laser with an intracavity KTP (potassium titanyl phosphate) crystal showing the angle φ between the YAG and KTP fast axes. The KTP crystal produces green light at half the wavelength of the fundamental emission (1.064 μm) from the laser.

doubled frequency and highly reflecting ($>99.9\%$) at the fundamental, such that only the fundamental circulated in the laser cavity; the doubled frequency is simply transmitted by the output coupler. The KTP crystal was antireflection coated at both the fundamental and doubled wavelengths. The Nd:YAG and KTP crystals were both 5 mm long and the entire laser cavity was about 3.5 cm long. The threshold pump power for this laser was ~ 10 mW.

The analysis and results that follow are for a laser cavity with a birefringent YAG rod and a birefringent KTP crystal (Fig. 1). A birefringent material contains two orthogonal directions along which the material has a different index of refraction such that light polarized along one axis travels faster than light polarized along the orthogonal axis. Because of this property, one of the axes is usually called the "fast" axis and the other is called the "slow" axis. Undoped YAG (yttrium aluminum garnet) is normally isotropic and homogeneous and exhibits no birefringence. However, when the YAG crystal is doped with the neodymium ion Nd^{3+} (typically 1% of the Y^{3+} ions are replaced with Nd^{3+}), which serves as the active ion to produce the infrared laser light, the crystal growth process itself, and the fact that the neodymium ion is slightly larger than the yttrium ion that it replaces can cause some residual stress induced birefringence in the Nd:YAG rod.[13] Birefringence may also be produced thermally in the Nd:YAG rod due to inefficient conversion of pump beam energy to laser light.

We have measured the residual birefringence in our unpumped YAG rod to be $|n_f - n_s| \sim 3\times 10^{-7}$, where n_s and n_f are the indices of refraction along the slow and fast axes, respectively. If the YAG rod is mechanically stressed, by a mounting screw for example, its birefringence can increase by orders of magnitude. The KTP crystal is naturally birefringent with $|n_f - n_s| \sim 0.08$. A phase difference will build up between the two orthogonally polarized components as they propagate through the birefringent crystals. The amount of phase difference that is accumulated will depend on the difference between the two indices of refraction along the two orthogonal directions, the wavelength of light used, and the length of the birefringent crystal itself. The relative phase delays ξ and δ due to the birefringence of the YAG and KTP crystals, respectively, are calculated from $2\pi L|n_f - n_s|/\lambda$, where L is the crystal length and λ is the YAG fundamental wavelength. Even though the birefringence of the YAG crystal is much smaller than that of the KTP, it is sufficient to induce a significant phase delay. As shown in Fig. 1, φ is the angle between the fast axes of the YAG rod and the KTP crystal.

As first pointed out by Oka and Kubota,[8] a complete analysis of this laser system must include the polarizations of the cavity modes. These polarizations are given by the eigenvectors of the round trip Jones matrix M for this laser cavity. This matrix describes how a given polarization of light is affected after one round trip in the laser cavity which contains birefringent elements. The round trip matrix M is the product of the individual Jones matrices that describe how each element in the cavity affects the polarization of light.[14] M is unitary since all the matrices that describe the individual cavity elements are unitary. The eigenvalues of M thus have unit magnitude and its eigenvectors are real and orthogonal. These two orthogonal eigenvectors are the only two polarization states that are unchanged after one round trip in the cavity. The laser output is polarized in either one or both of these orthogonal polarization directions. Our experimental observations confirm that the laser modes are linearly polarized along two orthogonal directions. The analysis described above does not allow us to predict the number of modes that will lase in the two polarization directions. We have observed different numbers of linearly polarized modes ranging from one to ten. Note that the gain of the laser medium and the nonlinearity of the KTP crystal have not been incorporated into the geometrical analysis; the final lasing mode configuration is crucially dependent on these considerations.

Green light is produced in the KTP crystal by second harmonic generation from a single cavity mode and by sum frequency generation between pairs of modes. In second harmonic generation two photons from the same cavity mode of fundamental frequency ω combine to create one photon of green at frequency 2ω. In sum frequency generation one photon from a cavity mode at frequency ω_1 and one photon from a different mode at frequency ω_2 combine to create one photon of green at frequency $(\omega_1 + \omega_2)$. The amount of green light produced by sum frequency generation depends on whether the contributing fundamental modes are polarized parallel or orthogonal to each other. These two processes for the generation of green light must be included into the laser rate equations as loss terms for the fundamental intensity.

Each cavity mode can exist in one of the two orthogonal eigenpolarization directions, which we label as x and y. Let m and n be the number of modes polarized in the x and y directions, respectively, where $N = m + n$ is the total number of lasing modes. The rate equations for the fundamental intensities I_k and gains G_k are[15-17]

$$\tau_c \frac{dI_k}{dt} = \left(G_k - \alpha_k - g\epsilon I_k - 2\epsilon \sum_{j\neq k} \mu_j I_j \right) I_k,$$

$$\tau_f \frac{dG_k}{dt} = \gamma - \left(1 + I_k + \beta \sum_{j\neq k} I_j \right) G_k, \tag{1}$$

where τ_c (0.2 ns) and τ_f (240 μs) are the cavity round trip time and fluorescence lifetime of the Nd^{3+} ion, respectively; I_k and G_k are, respectively, the intensity and gain

associated with the kth longitudinal mode; α_k is the cavity loss parameter for the kth mode, γ is the small signal gain which is related to the pump rate, β is the cross-saturation parameter, and g is a geometrical factor whose value depends on the angle φ between the YAG and KTP fast axes, as well as on the phase delays ξ and δ due to their birefringence. For modes having the same polarization as the kth mode $\mu_j = g$, while $\mu_j = (1 - g)$ for modes having the orthogonal polarization. This difference is due to the different amounts of sum frequency generated green light produced by pairs of parallel polarized modes or by pairs of orthogonally polarized modes. Here, ϵ is a nonlinear coefficient whose value depends on the crystal properties of the KTP and describes the conversion efficiency of the fundamental intensity into doubled intensity. In these rate equations we have made the simplifying approximation that the gain γ and cross-saturation parameter β are the same for all modes. The individual mode losses are assumed to differ only slightly, with $\alpha_k \sim 0.01$. The parameter values given above represent typical experimental operating conditions.

The cross-saturation parameter β is a measure of the competition among the various longitudinal modes for a given population inversion. It reflects the amount of spatial overlap of two standing wave cavity modes inside the gain medium and the extent of homogeneous broadening of the laser transition.[18,19] The greater the spatial overlap of the longitudinal modes in the gain medium, the greater the value of β ($0 < \beta < 2$). Since the gain medium is located at one of the cavity mirrors, the amount of spatial overlap among the various lasing modes is great. This occurs because all the mode fields must go to zero at the mirror in order to satisfy the cavity boundary conditions. If the gain medium was located farther away from the mirror, in the middle of the cavity for example, the amount of spatial overlap of the modes and the mode competition would both be reduced.[19] In general, the cross-saturation parameter β will be different for each pair of cavity modes. However, for simplicity, we assume the same value of β for all mode pairs.

The parameter g is a geometrical factor whose value depends on the angle φ between the YAG and KTP fast axes, as well as the phase delays ξ and δ due to their birefringence. Its value varies between 0 and 1. For the laser in Fig. 1, g can be calculated from[15,17]

$$g = 4u_1^2 u_2^2/(u_1^2 + u_2^2)^2 = 4v_1^2 v_2^2/(v_1^2 + v_2^2)^2, \tag{2a}$$

$$\mathbf{u} = \begin{bmatrix} u_1 \\ u_2 \end{bmatrix} = \begin{bmatrix} 2\,\mathrm{Im}(a) - 2\sqrt{1 - [\mathrm{Re}(a)]^2} \\ 2y \end{bmatrix}, \quad y \neq 0, \tag{2b}$$

$$\mathbf{v} = \begin{bmatrix} v_1 \\ v_2 \end{bmatrix} = \begin{bmatrix} 2\,\mathrm{Im}(a) + 2\sqrt{1 - [\mathrm{Re}(a)]^2} \\ 2y \end{bmatrix}, \quad y \neq 0, \tag{2c}$$

$$a = e^{i\xi}(\cos^2\varphi e^{i\delta} + \sin^2\varphi e^{-i\delta}), \tag{2d}$$

$$y = \sin 2\varphi \sin\delta, \tag{2e}$$

where $\mathbf{u}$ and $\mathbf{v}$ are the orthogonal eigenvectors of the unitary matrix M. Also, $g = 0$ if $y = 0$.

Cross saturation of the active medium [represented by the $\beta I_j G_k$ terms in Eq. (1)] and sum frequency generation in the nonlinear crystal [represented by the $2\epsilon\mu_j I_j I_k$ terms in Eq. (1)] introduce comparable amounts of global coupling among the laser modes. This means that each mode intensity I_j is coupled to every other cavity mode intensity I_k, $k \neq j$. We have thus modeled the laser as a set of globally coupled nonlinear oscillators that represent the cavity modes.

The model presented here describes deterministic low-frequency fluctuations in the mode intensities, but does not include longitudinal mode beating phenomena. The lowest intermode beat frequency for our laser is about 4 GHz; the phenomena observed and discussed in this paper lie in the submegaHertz range. Low-frequency (~ 100 kHz) oscillations due to differences in intermode beat frequencies that arise from unequal phase shifts of the modes are not accounted for in the model presented here. Such phenomena can be included appropriately in a model that uses field equations rather than the intensity equations employed here. A motivation in using the model of Eqs. (1) is to determine to what extent the intensity rate equations are able to predict phenomena observed in this laser system.

A characteristic frequency for exchange of energy between the light and the active medium is specified by the relaxation oscillations which may be observed in the laser output with or without the doubling crystal. These oscillations occur when the laser is perturbed away from stable steady state due to noise, and may be observed directly in the photocurrent with an rf spectrum analyzer. The magnitude of the oscillations is less than a fraction of a percent of the average steady-state intensity. Detailed calculations of the relaxation oscillation frequency for our laser system[17] show that the doubling crystal has a very small effect (less than a percent) on the relaxation oscillation frequency for typical parameter values. We have observed relaxation oscillation frequencies in the range of 20–150 kHz for pumping up to five times above threshold. The frequency increases as the square root of the pump power, which is well known. In the rest of the paper we will describe large periodic and chaotic intensity fluctuations that occur with similar characteristic frequencies.

III. STABILITY ANALYSIS

A linear stability analysis of the rate equations (1) was carried out to find the conditions on the parameter g for which the laser output is predicted to be stable.[15,17] Recall [from Eqs. (2)] that g depends on the parameters ξ, δ, and φ. To simplify the analysis, all modes were assumed to have the same loss, cross saturation, and small signal gain parameters. Numerical integration of the rate equations (1) shows that the results of this stability analysis are qualitatively unchanged even if the mode parameters are unequal. For the three specific cases of $(m,n) = (N,0),(1,1),(N/2,N/2)$ the output will be stable if[15,17]

$$g < \frac{\tau_c}{\tau_f}\frac{[1 + (N-1)\beta]}{\epsilon}\left(\frac{1+p}{p}\right), \quad m = N, n = 0, \tag{3a}$$

$$g > \frac{2}{3} - \frac{1}{3}\frac{\tau_c}{\tau_f}\frac{(1+\beta)}{\epsilon}\left(\frac{1+p}{p}\right), \quad n=m=1, \tag{3b}$$

$$\begin{cases} g > \left(\dfrac{N}{2N-1}\right) - \dfrac{1}{(2N-1)}\dfrac{\tau_c}{\tau_f}\dfrac{[1+(N-1)\beta]}{\epsilon}\left(\dfrac{1+p}{p}\right) \\ g < \dfrac{\tau_c}{\tau_f}\dfrac{[1+(N-1)\beta]}{\epsilon}\left(\dfrac{1+p}{p}\right) \end{cases},$$

$$n=m=\frac{N}{2}; \quad N=2,4,6,\ldots, \tag{3c}$$

where $p=(\gamma-\alpha)/\alpha$. The general case of m modes in one polarization direction and n modes in the orthogonal polarization, i.e., $m \neq n$; $m,n>0$, must be examined numerically.

The importance of these theoretical predictions is that we have discovered a technique for stabilizing the laser through proper choice of the parameter g, exploiting the birefringence of the YAG crystal. For each of the mode configurations, stability is predicted for a range of values of the parameter g. Since g is a function of the relative orientation angle φ between the YAG and KTP fast axes, these stability conditions predict that the laser output should be stable for a range of orientation angles φ between the YAG and KTP crystals. That is, the fluctuations in the output intensity can be eliminated merely by proper rotational orientation of these two birefringent crystals. We should note here that in all previous studies, the YAG crystal was assumed to be isotropic, and the importance of its rotational orientation with respect to the KTP crystal was not recognized.

Figure 2 shows the experimental verification of this prediction. In this experiment, the orientation of the YAG crystal was unchanged, only the KTP crystal was rotated and the output intensity was detected by a photodiode and observed on a digital oscilloscope. A filter was positioned in front of the photodiode to transmit only the green intensity. The KTP crystal was rotated until the output intensity became stable. This particular orientation angle was labeled 0°. The KTP was then rotated beyond this point and the laser intensity was observed to remain stable for 80° of rotation between the YAG and KTP fast axes. Figure 2(a) shows one sample stable intensity time trace at an orientation angle of 70°. As the KTP crystal was rotated past 80° the laser output showed simple periodic oscillations [Fig. 2(b)], becoming more complex (but still periodic) [Fig. 2(c) and (d)], and eventually becoming chaotic [Fig. 2(e)]. As the KTP crystal was rotated even further, the laser output returned to a simple periodic behavior [Fig. 2(f)], finally becoming stable again, and the whole sequence then repeated itself. This technique is currently being used by a commercial manufacturer of mode locked, intracavity doubled Nd:YAG lasers to eliminate the output intensity fluctuations.[20]

Figure 3 shows the dependence of the parameter g on the angle φ between the YAG and KTP fast axes and on the KTP birefringence δ for a given amount of YAG birefringence $\xi = 0.1\pi$ with three modes all polarized in one direction, i.e., $m = N = 3$, $n = 0$. The shaded region in the

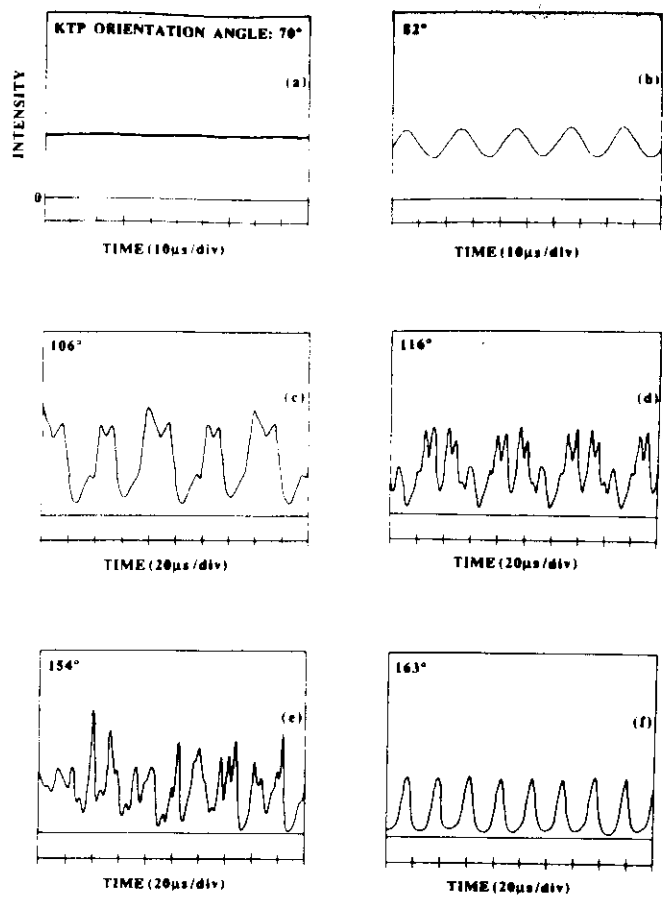

FIG. 2. Representative experimental time traces of the doubled output intensity for various KTP–YAG orientation angles. Stable operation was observed from 0° to 80°, where 0° was defined to be the relative orientation angle corresponding to the onset of stable laser output.

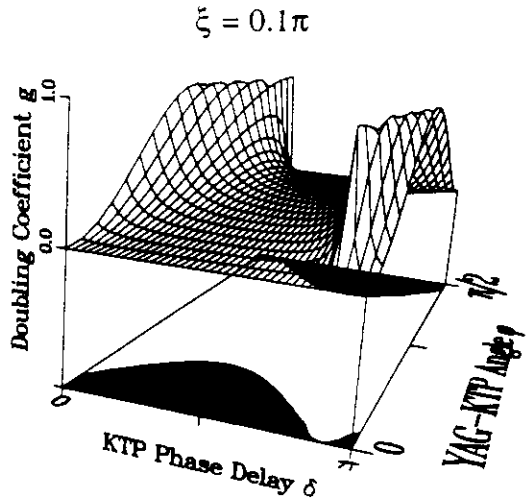

FIG. 3. Dependence of the parameter g on the angle φ between the YAG and KTP fast axes and the KTP phase delay δ for the case of three similarly polarized modes, i.e., $m = 3$, $n = 0$, for a given value of YAG birefringence $\xi = 0.1\pi$. The shaded region in the δ-φ plane corresponds to values of g where the stability constraint [inequality (3a)] holds, i.e., $g < 0.04$, for the parameter values given in the text.

$\delta - \varphi$ plane indicates the region in parameter space where the stability condition (3a) holds, i.e., $g < 0.04$. This condition is obtained for the following operating parameter: $\tau_c/\tau_f = 8.0 \times 10^{-7}$, $\beta = 0.6$, $\alpha = 0.01$, $\gamma = 0.08$, $p = (\gamma - \alpha)/\alpha = 7.0$, and $\epsilon = 5.0 \times 10^{-5}$.

We repeated this experiment rotating only the YAG crystal while keeping the KTP crystal orientation unchanged, which also eliminated the fluctuations. As discussed above, the value of g also depends on the phase delays ξ and δ due to the birefringence in the YAG and KTP crystals, respectively. We varied the temperature of the KTP crystal, which changed its length, which in turn changed its phase delay. This procedure also enabled us to obtain stable, periodic, and chaotic fluctuations in the output intensity. Control of fluctuations by temperature control alone is less effective than rotational orientation, since the length change that can be achieved by this method is limited.

IV. ANTIPHASE STATES

The numerical model (1) also predicts that the laser output can exhibit a curious periodic fluctuation called the "antiphase" state. Antiphase states have been theoretically predicted to exist for Josephson junction arrays,[21,22] but have never been experimentally observed. To explain what antiphase states actually are, let us consider N parallel polarized modes in the laser. In an antiphase state each mode intensity has the same periodic waveform as all the other modes, however, this common waveform is shifted in time by T/N from one mode to another, where T is the period of this common waveform (Fig. 4). That is

$$f_k(t) = f_0(t + Tk/N) \quad k = 1,...,N, \tag{4}$$

where f_k is the waveform of the kth mode and f_0 is a waveform of period T. For the specific example of $N = 3$ as depicted in Fig. 4, there are $(N-1)! = 2$ unique antiphase states as shown.

Now consider the more complicated situation of m modes in one polarization direction and n modes in the orthogonal polarization such that the total number of lasing modes is $N = m + n$. In this case there are $m!n!$ unique antiphase states. The distinct $m!n!$ antiphase states for the specific case of $n = 2$ and $m = 3$ are also shown in Fig. 4. Notice that for $(N,0)$ there are $(N-1)!$ unique antiphase states, and for (m,n) there are $m!n!$ unique antiphase states.

Equations (1) define a flow in a $2N$-dimensional phase space. Integration of these equations results in a trajectory

$$\mathbf{X}(t) = \{I_1(t), G_1(t), I_2(t), G_2(t), ..., I_N(t), G_N(t)\}.$$

The equations have an important symmetry, namely, invariance under interchange $(I_k, G_k) \leftrightarrow (I_j, G_j)$ of any two modes having the same polarization. It follows that, if $\mathbf{X}(t)$ is a solution, then so are all of the $m!n!$ trajectories that come from permutation of the indices within a given polarization group. Of course, these need not all define distinct trajectories in phase space. For example, if one has identical (I_k, G_k) for all modes of a given polarization, then

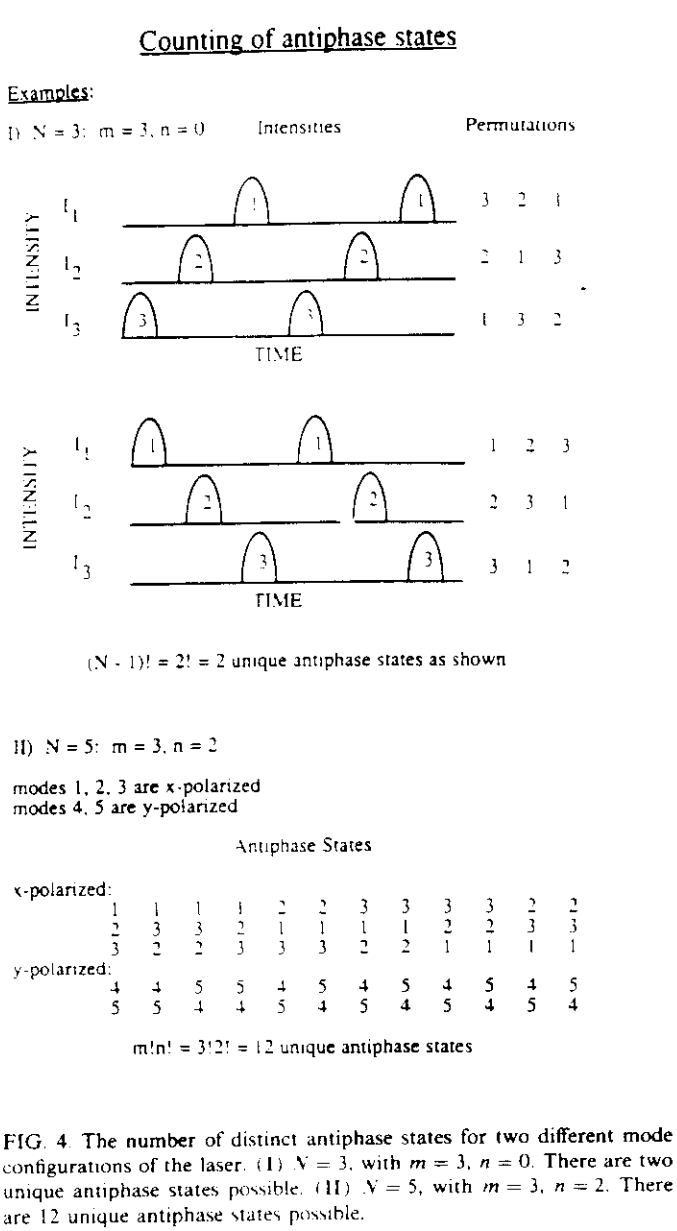

FIG. 4. The number of distinct antiphase states for two different mode configurations of the laser. (I) $N = 3$, with $m = 3$, $n = 0$. There are two unique antiphase states possible. (II) $N = 5$, with $m = 3$, $n = 2$. There are 12 unique antiphase states possible.

any exchange of indices labeling these modes gives the exact same orbit: This solution retains a high symmetry. At the other extreme, if one has a solution with no residual symmetry [so that $(I_k, G_k) \neq (I_j, G_j)$ for all $j \neq k$], there are $m!n!$ distinct solutions coexisting in the phase space. This illustrates a general rule: the lower the symmetry of a given solution, the greater its multiplicity. These considerations hold for all phase space orbits of the system, although in what follows we focus on periodic, attracting orbits.

Note that this analysis does not say whether or not any symmetry-broken states exist; rather, it says that such solutions must come in groups of a certain size. As a practical matter, the existence of solutions must be deduced either by integration of the differential equations, or by direct observation of the physical system.

Each antiphase state is a stable periodic solution to Eqs. (1), such that each antiphase state is an attractor in the phase space of all intensities and gains. Each stable solution will coexist with all the other stable solutions, and any nearby trajectory in the phase space will eventually

settle down onto one of these attractors.

As discussed above, the number of unique antiphase states grows "explosively," i.e., factorially, with the number of modes. This means that the stable attractors crowd ever more tightly in phase space with an increasing number of modes. If the number of modes is large enough, the attractors may become so tightly packed in phase space that even a small amount of noise can cause the system to hop from one stable solution to another. Such sensitive dependence on system noise has been demonstrated numerically for Josephson junction arrays.[22,23]

In all of the theoretical and experimental results given here, the number of cavity modes is fairly small. We can vary the total number of modes in the laser cavity N from 1 to ~ 10, with a number of accompanying polarization combinations, by varying the pump power above threshold and by varying the orientation angle φ between the YAG and KTP crystals. In contrast, some Josephson junction arrays contain thousands of junctions making attractor crowding more severe than in the laser.

Since each cavity mode is a different wavelength, the antiphase state represents a synchronized periodic switching among the various lasing wavelengths. If the dynamics of the laser could be appropriately controlled to switch at will among the various distinct antiphase states, this laser could be a convenient and versatile source of wavelength and time multiplexed signals. If all of the mode parameters are identical, then the particular antiphase state the system selects is determined purely by the initial conditions and there is nothing one could do short of "restarting" the system to make it change from one antiphase state to another. If the attractors are sufficiently crowded in the phase space or if the noise strength is sufficiently large, then the system will hop randomly among these attractors. If the mode parameters were significantly different such that the symmetry of the system was broken, i.e., the exchange of indices completely changed the system, then this difference in parameters could be exploited to force the system into a selected antiphase state.

We have actually observed antiphase states for a small number of lasing modes. In the experiment, the laser cavity was adjusted to support two modes in the x-polarization direction ($m = 2$) and one mode in the y-polarization direction ($n = 1$). The longitudinal mode structure was monitored during the experiment with a confocal Fabry–Perot interferometer. The numerical prediction for the intensity output from the laser is shown in Fig. 5. In Fig. 5(a) it can be seen that each mode intensity has the same periodic waveform as the other two modes. This common waveform is shifted in time from one mode to the next. Figure 5(b) shows the total intensity in the x- and y-polarized directions. The total intensity in the x-polarized direction is the sum of the intensities of the two x-polarized modes, and the total y-polarized intensity is just the intensity of the one y-polarized mode. Figure 5(b) provides a direct comparison to the experimental data in Fig. 6. Figure 6 shows the experimental laser intensity time traces for the intensity in the x-polarized ($m = 2$) and the y-polarized ($n = 1$) directions, respectively, as well as the total

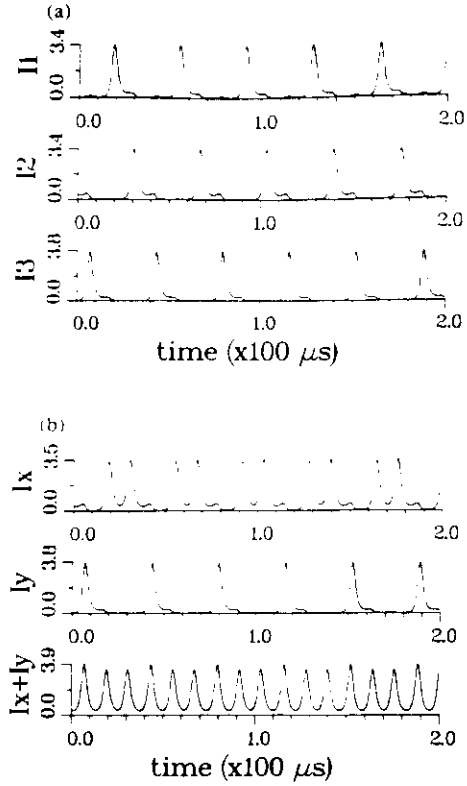

FIG. 5. Results of numerical integration of Eqs. (1) for $(m,n) = (2,1)$. (a) The individual antiphase mode intensities. (b) The x- and y-polarized intensities and the total intensity. This plot can be directly compared with the experimental observation in Fig. 6.

intensity. The similarity between the theoretical and experimental results is clear.

The cavity mode frequency spacing in this laser was so small (~ 4 GHz) that the individual lasing modes could not be separated by a prism or grating. The modes could be separated only by their polarization. To facilitate comparison between experiment and theory, the laser was oper-

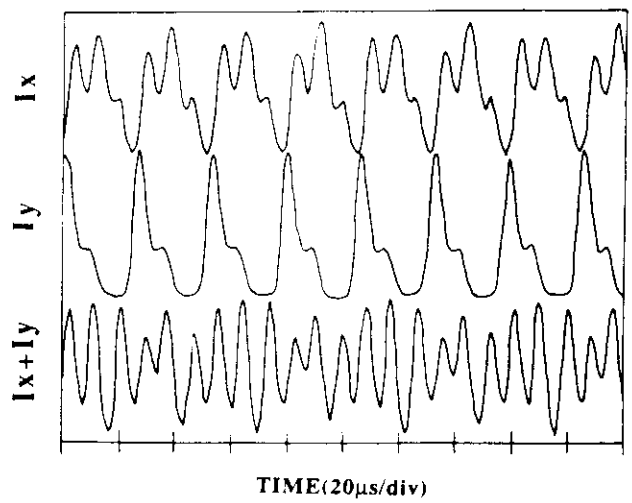

FIG. 6. Experimental observation of an antiphase state. Time traces of the x- and y-polarized intensities and the total intensity are shown. The measurements were not made simultaneously.

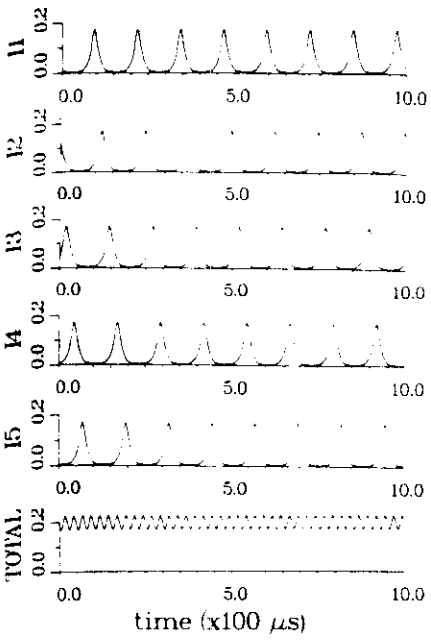

FIG. 7. Theoretical prediction of a higher-order antiphase state. Results of the numerical integration of Eqs. (1) for $(m,n) = (5,0)$ show the existence of an antiphase state.

ated with only three modes. Figure 7 shows a higher-order antiphase state in the laser output for $N = 5$, obtained from numerical integration of Eqs. (1) where in this case all five modes are polarized in the same direction. It would be very interesting to develop experimental techniques for the direct observation of higher-order antiphase states.

V. CHARACTERIZATION OF COMPLEX PERIODIC AND CHAOTIC INTENSITY FLUCTUATIONS

When the laser is operated in a parameter range where complex periodic and chaotic intensity fluctuations are observed, we may use a variety of techniques to characterize the statistical nature of these fluctuations. In order to perform quantitative studies, the laser intensity time trace was detected with a photodiode (1 ns rise time) and displayed on a (400 MHz) digital oscilloscope. The oscilloscope itself possesses the capability for extensive data analysis. The digitized intensity data could also be transferred to an IBM PC for further analysis. In the rest of this paper we will describe the behavior of the complex periodic and chaotic fluctuations in some detail.

Fast Fourier transforms (FFT) of the intensity time traces provide a direct means for analysis of the frequency components of the intensity fluctuations. The time traces and corresponding power spectra of periodic and chaotic intensity fluctuations are shown in Fig. 8. Figure 8(a)–(d) shows a variety of complex periodic waveforms, whose FFTs contain many discrete frequency components. Figure 8(d) shows a rather interesting case. The time trace appears to be somewhat periodic, and the FFT does contain some distinct low-frequency components with a broadband part at higher frequencies. The time traces in Fig. 8(e) and (f) have broadband power spectra with only a few remaining discrete frequencies, which is characteristic of chaos.

Two-dimensional time delay plots, produced by displaying the digitized intensity data at time t against the intensity at time $t + \Delta t$, are often used to illustrate the periodic or chaotic behavior of a nonlinear dynamical system. If carried to higher dimensions, i.e., $I(t)$ vs $I(t + \Delta t)$ vs $I(t + 2\Delta t)$..., time delay plots using only time series measurements of the total intensity can be used to reconstruct the original phase space attractor. This is a general result and is applicable to any dynamical system in which the time series of only one system variable is available.[24,25] Takens has shown that in order to capture the topological features of the original attractor in an N-dimensional phase space from a time series of only one dynamical system variable, the pseudophase space or embedding space must have at least $2N + 1$ dimensions.[26] Originally, time derivatives, i.e., $I(t)$ vs $dI(t)/dt$ vs $d^2I(t)/dt^2$..., were used instead of time delays to reconstruct the system attractor. However, time delay coordinates work just as well and are simpler to obtain experimentally.[27]

Figures 9–11 show time traces, time delay plots, and phase plots [$dI(t)/dt$ vs $I(t)$] for periodic and chaotic intensity output from the laser. The time delay and phase plots in both periodic cases (Figs. 9 and 10) show a ringed structure that vanishes when the laser output is chaotic (Fig. 11). The Δt used in the figures was arbitrarily chosen. Figures 12 and 13 show time delay plots for periodic laser output with two different values of Δt. In all cases shown, the two-dimensional time delay curve crosses itself. This means that the system dimensionality must be greater than two since the uniqueness theorem stipulates that valid solutions may not cross themselves in phase space.

The most convincing support for the claim that the seemingly random intensity output from the laser is actually chaotic comes from a calculation of the Liapunov exponents. Chaos is characterized by exponential divergence of initially close trajectories in phase space, indicating that one or more of the Liapunov exponents are positive. The rate of this exponential divergence of trajectories in time ($e^{\lambda t}$) is given, for low-dimensional systems, by the largest Liapunov exponent λ. A positive value of λ indicates the exponential separation of initially close trajectories in phase space. This implies the familiar statement that chaos is characterized by sensitive dependence on initial conditions, since time series originating from these nearby initial conditions will diverge exponentially. The rate of the exponential divergence of chaotic trajectories, or the rate of convergence for stable trajectories, is given by the magnitude of the Liapunov exponent. To determine whether or not a given system is chaotic, it is important to calculate the largest Liapunov exponent and determine if it is positive.

The method used here to calculate the largest Liapunov exponent in the integration of the numerical model requires rate equations for the time evolution of small deviations from a given trajectory in each dynamical variable (the I_j and the G_j). These rate equations are obtained from a linear stability analysis of Eqs. (1). The Liapunov expo-

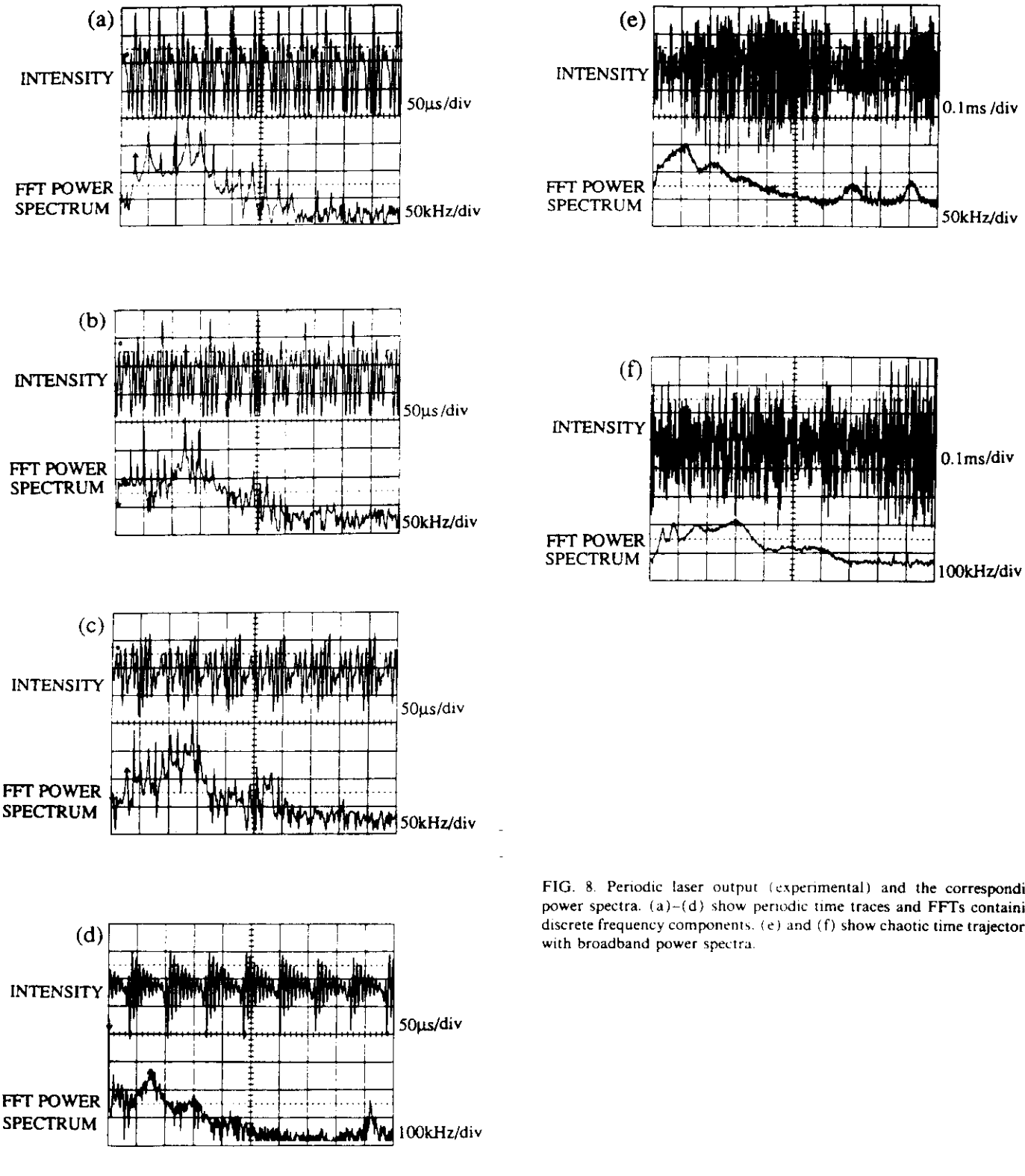

FIG. 8. Periodic laser output (experimental) and the corresponding power spectra. (a)–(d) show periodic time traces and FFTs containing discrete frequency components. (e) and (f) show chaotic time trajectories with broadband power spectra.

nent at time t is a function of the length of the vector of deviations at time t as well as the original length of this vector. The technique calculates the largest Liapunov exponent for the dynamics. If the system is in a periodic or stable state the calculated value of the Liapunov exponent is $\lambda = 0$. If the system is in a chaotic state, then $\lambda > 0$, as found in the sample calculation discussed below. We assume here that the dynamics of the phase space trajectories is dominated by the largest Liapunov exponent.

The outline of this calculation of the Liapunov exponent is as follows: Let

$$\mathbf{x}(t) = \{I_1(t), G_1(t), I_2(t), G_2(t), \ldots, I_N(t), G_N(t)\}$$

be the vector of dynamical system variables at time t, let

$$\Delta\mathbf{x}(t) = \{\Delta I_1(t), \Delta G_1(t), \ldots, \Delta I_N(t), \Delta G_N(t)\}$$

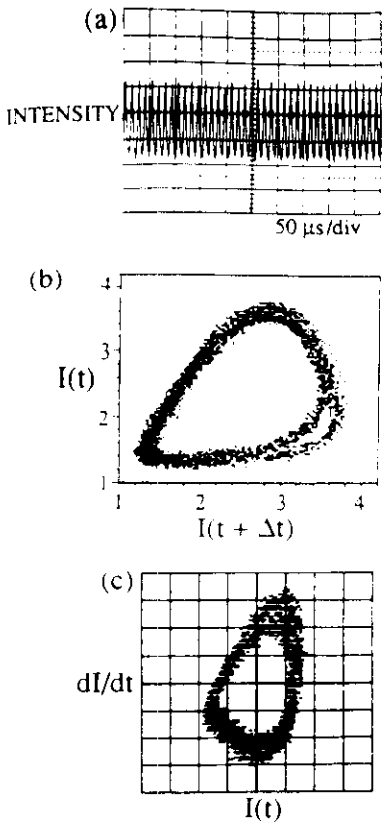

FIG. 9. (a) Periodic laser output (experimental). (b) Time delay plot $I(t)$ vs $I(t+\Delta t)$ for the data in (a) with $\Delta t = 2$ μsec. (c) Phase plot $dI(t)/dt$ vs $I(t)$ for the data in (a). The plots are in scaled units.

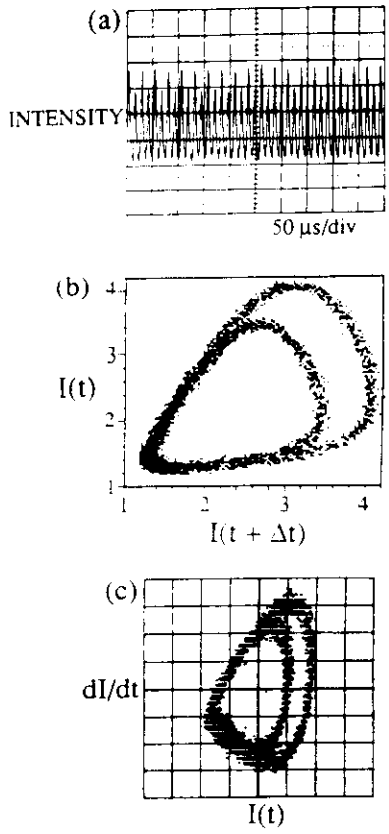

FIG. 10. (a) Period doubled laser output (experimental). (b) Time delay plot $I(t)$ vs $I(t-\Delta t)$ for the data in (a) with $\Delta t = 2$ μs. (c) Phase plot $dI(t)/dt$ vs $I(t)$ for the data in (a). The plots are in scaled units.

be the vector of small deviations from $\mathbf{x}$ at time t and let $d(t)$ be the length of the deviation vector $\Delta\mathbf{x}(t)$ at time t given by $d(t) = \|\Delta\mathbf{x}(t)\|$. Then the long time or asymptotic value of the largest Liapunov exponent λ is given by[28–30]

$$\lambda = \lim_{\substack{t\to\infty \\ d(0)\to 0}} \frac{1}{t} \ln\left(\frac{d(t)}{d(0)}\right). \tag{5}$$

When doing this calculation on a computer, the initial length of the deviation vector $d(0)$ is chosen to be unity for convenience. Since the length of the deviation vector $d(t)$ grows exponentially with time, the deviation vector must be renormalized periodically to prevent overflow problems in the calculation. The Liapunov exponent is then found by the average of these periodically calculated values.

The Liapunov exponent for one particular random time series produced from integration of the numerical model (1) is $\lambda \sim 1.6\times 10^4\ \mathrm{s}^{-1}$. This value for the largest Liapunov exponent is the steady state or asymptotic value. Figure 14(a) shows the time dependence of the estimate of the Liapunov exponent. The positive Liapunov exponent indicates the time series is in fact chaotic, and its magnitude indicates that the separation time (the inverse of the Liapunov exponent) is about 60 μs. In Fig. 14(b) we plot the magnitude of the separation of two total intensity time traces whose initial values differ by 10^{-10} as a function of time. The rate of exponential growth of the separation was found to be $\sim 2\times 10^4\ \mathrm{s}^{-1}$, which compares reasonably well to the Liapunov exponent given above. The time scale specified by these measures is also in reasonable agreement with the time for sequential energy sharing between modes, as seen in Figs. 5–7.

The positive Liapunov exponent calculated from the numerical model provides convincing evidence that this laser system can operate in a truly chaotic state. However, the Liapunov exponent gives us no information about the magnitude of the fluctuations in the laser output. Probability distributions can be used to obtain a measure of the magnitude of the fluctuations in a chaotic system.[31]

When a driven, dissipative, globally coupled oscillator system is in a chaotic state, a complex energy sharing process may occur among the oscillators.[32,33] Probability distributions can be used to characterize the fluctuations of the total energy of the system as well as the energy of an individual oscillator. Kaneko has recently used probability distributions to study N globally coupled logistic maps as a mean-field-type extension of coupled map lattices.[34,35] He has shown the interesting result that mean field fluctuations for these logistic maps are approximately Gaussian distributed despite the fact that they are coupled. That is, an approximately Gaussian distribution for the mean field was obtained in the limit of large $N(N\sim 20\,000)$, even though the maps are globally coupled. Kaneko also showed that for large N the two-point mutual information is extremely small but remains finite and is responsible for

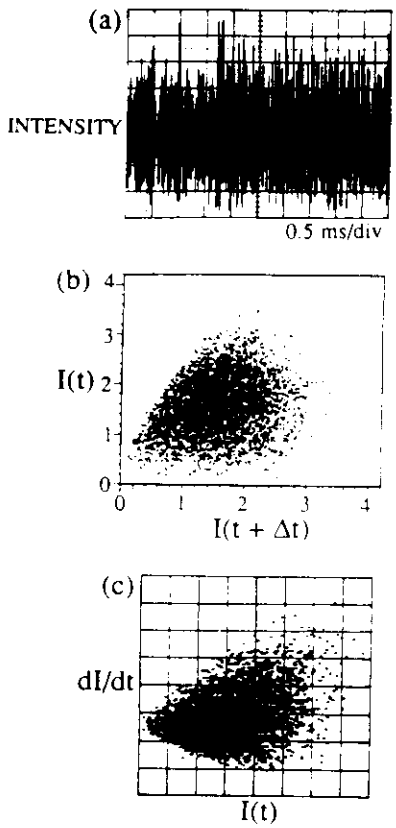

FIG. 11. (a) Chaotic laser output (experimental). (b) Time delay plot $I(t)$ vs $I(t+\Delta t)$ for the data in (a) with $\Delta t = 2\mu s$. (c) Phase plot $dI(t)/dt$ vs $I(t)$ for the data in (a). The plots are in scaled units.

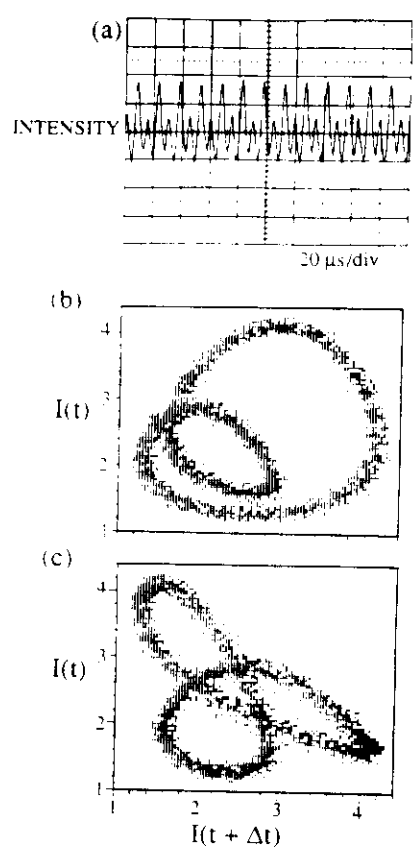

FIG. 12. (a) Periodic laser output (experimental). (b) Time delay plot $I(t)$ vs $I(t+\Delta t)$ for the data in (a) with $\Delta t = 2\ \mu s$. (c) Time delay plot $I(t)$ vs $I(t+\Delta t)$ for the data in (a) with $\Delta t = 10\ \mu s$. The plots are in scaled units.

the breakdown of the law of large numbers. This implies that any two individual maps are not statistically independent in their fluctuations.

Here, we use probability distributions to analyze the energy sharing among the globally coupled axial modes of a chaotic Nd:YAG laser system. However, unlike the mean field approximation, global coupling by sum frequency generation is a natural description for a multimode laser, and not a computationally expedient approximation. A characterization of the energy sharing is provided by the probability distributions of the total and x- and y-polarized mode intensities as well as by an examination of their time evolution. Integration of the numerical model (1) describing the laser dynamics yields predictions for the probability distributions and time traces that are remarkably similar to the experimental results. We find that even though the probability distribution of an individual mode intensity is highly non-Gaussian, the distribution of the total intensity is approximately Gaussian. This result is reminiscent of Kaneko's study of globally coupled maps. It is, however, observed for the case of a few ($N \sim 5$) globally coupled laser modes which are strongly statistically dependent, as will be shown.

The laser was aligned to produce either a periodic or chaotic intensity time trace. The second harmonic was filtered from the laser output, and only the fundamental intensity was incident upon a photodiode. The axial mode structure was monitored during the experiment with a confocal Fabry–Perot interferometer. The photodiode signal was observed and stored on a digital oscilloscope interfaced to an IBM PC. The digitized signal was transferred to the IBM PC and the total intensity probability distribution was calculated. Repeating this procedure allowed us to obtain a probability distribution accumulated from many time traces. A polarizing beamsplitter cube was then inserted in front of the photodiode, allowing us to obtain time traces and probability distributions of the x- and y-polarized intensities simultaneously.

Figure 15(b) shows a probability distribution obtained from the simple periodic experimental laser data in Fig. 15(a). The probability distribution is obtained by normalizing a histogram of the digitized laser intensity values. The distribution in Fig. 15(b) for the simple periodic time trace in Fig. 15(a) contains two peaks. Each of these two peaks corresponds to one of the two turning points in the periodic time trace. The laser intensity stays in the vicinity of a turning point for a relatively long period of time, which creates a peak in the probability distribution at the intensity value of that turning point. Figures 16 and 17 show the probability distributions for other more complex examples of periodic laser output. Notice that as the periodic time trace becomes more complicated, the corresponding probability distributions contain more peaks be-

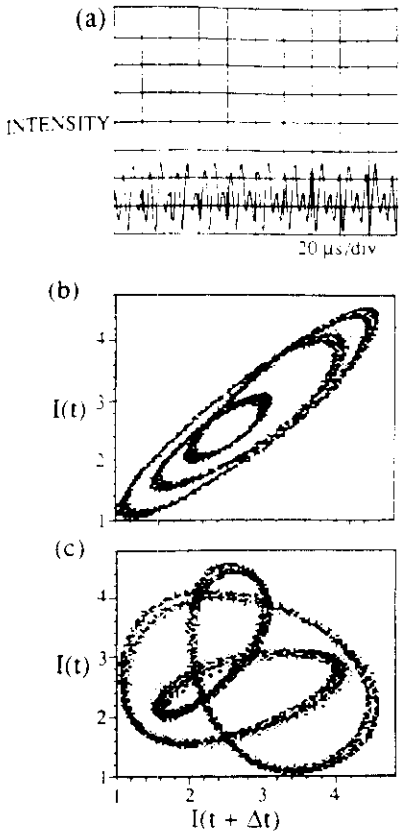

FIG. 13. (a) Periodic laser output (experimental). (b) Time delay plot $I(t)$ vs $I(t+\Delta t)$ for the data in (a) with $\Delta t = 0.5$ μs. (c) Time delay plot $I(t)$ vs $I(t+\Delta t)$ for the data in (a) with $\Delta t = 5$ μs. The plots are in scaled units.

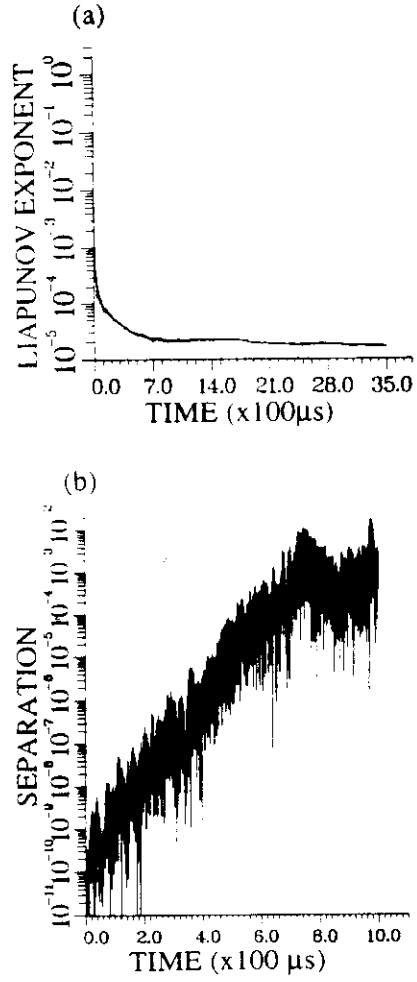

FIG. 14. (a) Largest Liapunov exponent for a chaotic time series of the total intensity produced from a numerical integration of Eqs. (1) with $(m,n) = (1,4)$. The asymptotic value of the Liapunov exponent is $\lambda \sim 1.6 \times 10^4\ s^{-1}$. The initial value was chosen to be unity. (b) Magnitude of the separation of two initially close chaotic intensity time series. The slope of the plot ($\sim 2 \times 10^4\ s^{-1}$) gives a measure of the exponential divergence of these intensities.

cause the trajectory contains more turning points.

Figures 18 and 19 show a comparison between experimental data and numerical results from the integration of Eqs. (1) for the case of one x-polarized mode ($m = 1$) and four y-polarized modes ($n = 4$). Figure 18(a)–(c) shows the time traces for the one x-polarized mode intensity, the intensity in the y-polarized direction (the sum of the four y-polarized mode intensities), and the total intensity, respectively, obtained from the experiment. Figure 18(d)–(f) contains the time traces obtained from the numerical model for the following parameter values: $\tau_c = 0.2$ ns, $\tau_f = 240$ μs, $\gamma = 0.05$, $\beta = 0.7$, $g = 0.1$, and $\epsilon = 5 \times 10^{-6}$. The individual mode losses are assumed to differ only slightly, with $\alpha_k \sim 0.01$.

The probability distributions shown in Fig. 19(a)–(c) (experimental data) were accumulated from 15 time traces of length 1 ms each, with 4000 digitized data values per trace. The numerical probability distributions in Fig. 19(d)–(f) were accumulated from three time traces of length 1.5 ms each. The length of the time traces was chosen to be long relative to the divergence time of 60 μs calculated from the Liapunov exponent given above, in order to obtain a comprehensive sampling of the laser dynamics.

In both the cases of the time traces and the probability distributions, the corresponding experimental and theoretical plots look very similar. Also, in both theory and experiment the total intensity has a probability distribution that is approximately Gaussian. The comparison to a Gaussian is facilitated by plotting a Gaussian curve calculated from the mean and variance of the total intensity fluctuations. This nearly Gaussian probability distribution for the total intensity is significant for three reasons. First, the intensity fluctuation distributions for the x- and y-polarized directions are very non-Gaussian. Second, the individual modes are strongly coupled through sum frequency generation. Third, only a small number of modes ($N = m + n = 5$) are involved. In contrast, Kaneko required several thousand globally coupled logistic maps to achieve an approximately Gaussian probability distribution. It is also significant to notice that in our experiments and in the case of Kaneko's study of globally coupled logistic maps, probability distributions that are only approximately Gaussian are obtained for some system parameters.[35] The central limit theorem does not usually apply to

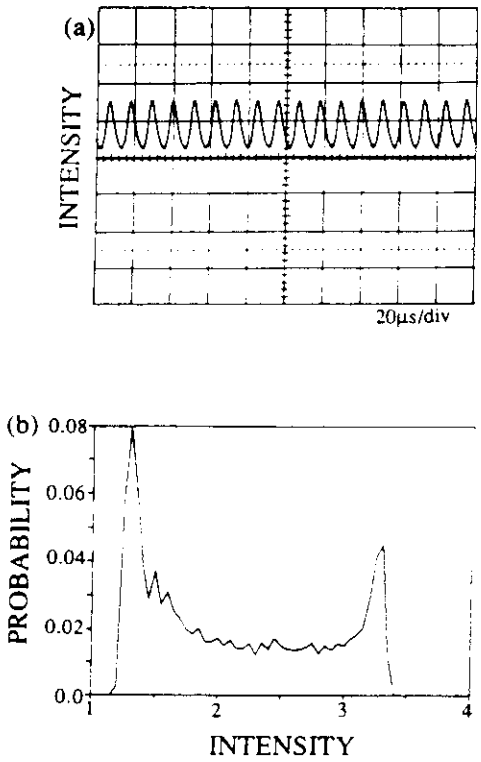

FIG. 15. Simple periodic laser intensity output (experimental) and its corresponding probability distribution. Each of the two peaks in the probability distribution corresponds to one of the two turning points in the time series. The intensity is given in scaled units.

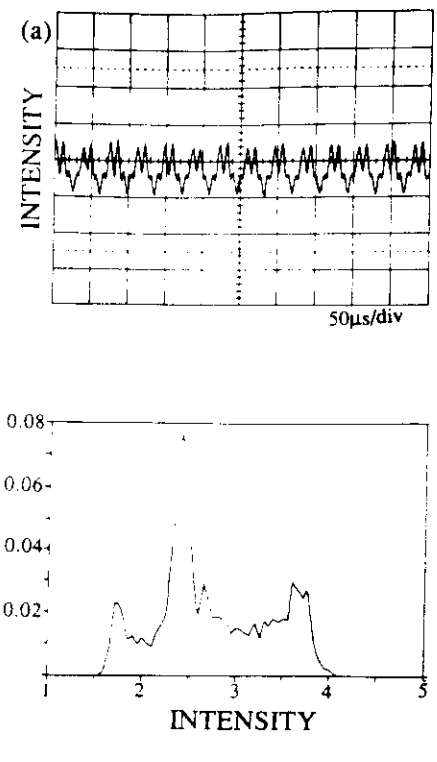

FIG. 16. Periodic laser intensity output (experimental) for a more complex waveform than in Fig. 15(a) and its corresponding probability distribution. Each of the peaks in the probability distribution corresponds to one of the turning points in the time series. The intensity is given in scaled units.

strongly dependent random variables.[36] The central limit theorem states that the sum of N random, independent variables is Gaussian distributed in the limit of large N. The laser modes, however, are coupled through sum frequency generation and few in number and their sum, the total intensity, is only approximately Gaussian distributed. This implies that the central limit theorem may not be responsible for the observed distribution of the total intensity fluctuations. However, the approximately Gaussian nature of chaotic probability distributions could be a general property of many chaotic systems, and not necessarily only a feature of the particular system discussed here.

The probability distributions associated with the x- and y-polarized intensities are very asymmetric and non-Gaussian. The x- and y-polarized intensities are anticorrelated as shown in Fig. 20. That is, only one polarization direction is "on" at any given time, and the two polarized intensities switch on and off in an approximately periodic anticorrelated fashion. The time between successive on or off states for one given polarization fluctuates with time. The polarized intensities calculated from the numerical model also show this nearly periodic energy sharing. A similar energy sharing between orthogonal linear polarized intensities, as well as between right- and left-handed circularly polarized light, has been observed in the dynamics of some gas lasers.[37]

In order to quantify the statistical dependence or independence of the intensity fluctuations, we will calculate the autocorrelation function of the total intensity and the cross-correlation function between the x- and y-polarized intensities. The cross-correlation function $C(\Delta n)$ between two data sets $f(n)$ and $g(n)$ relative to their respective means $\langle f\rangle$ and $\langle g\rangle$ is given by

$$\begin{aligned} C(\Delta n) &= \left(\frac{1}{(N-\Delta n)} \sum_{n=1}^{N-\Delta n} [f(n)-\langle f\rangle][g(n+\Delta n) \right. \\ &\quad \left. -\langle g\rangle]\right)(\langle f\rangle\langle g\rangle)^{-1}, \\ &= \left(\left(\frac{1}{N-\Delta n}\right) \sum_{n=1}^{N-\Delta n} f(n)g(n+\Delta n)\right) \\ &\quad \times(\langle f\rangle\langle g\rangle)^{-1}-1, \end{aligned} \tag{6}$$

where N is the number of data values in each set. The cross-correlation function is formed by displacing the data set $g(n)$ by Δn relative to the data set $f(n)$. Notice that the result of the cross-correlation calculation would be different if $f(n)$ were displaced relative to $g(n)$. The autocorrelation function $A(\Delta n)$ of the data set $f(n)$ is defined as the limiting case of the cross-correlation $C(\Delta n)$ with $g(n)=f(n)$. That is,

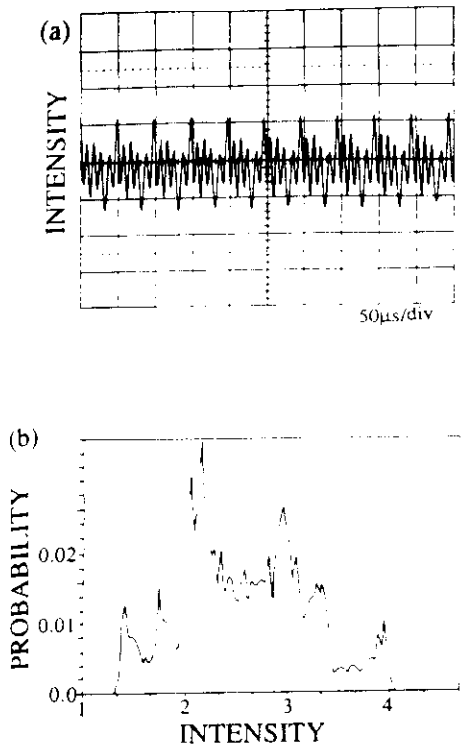

FIG. 17. Periodic laser intensity output (experimental) for a more complex waveform than in Fig. 15(a) and Fig. 16(a) and its corresponding probability distribution. Each of the peaks in the probability distribution corresponds to one of the turning points in the time series. The intensity is given in scaled units.

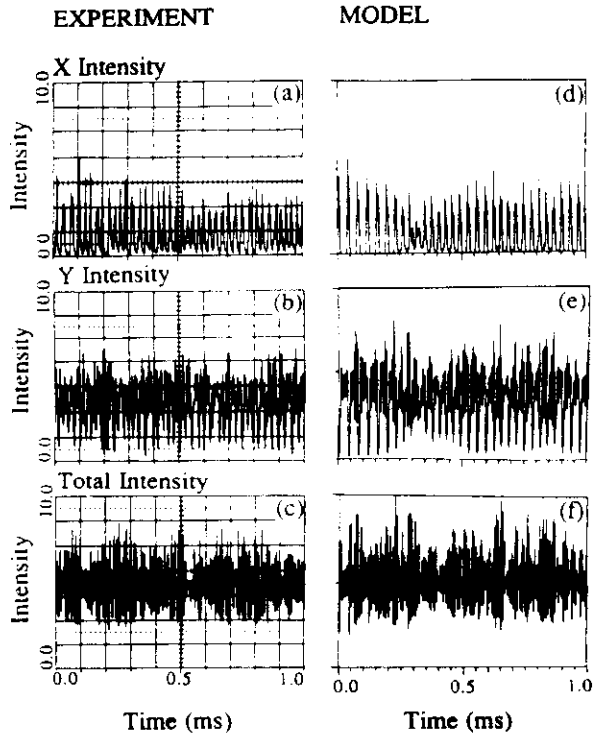

FIG. 18. (a)–(c) Experimental time traces for the x-polarized, y-polarized, and total intensities. (d)–(f) Corresponding time traces from the numerical integration of Eqs. (1). The experimental and numerical results are both for the case $(m,n) = (1,4)$.

$$A(\Delta n) = \left(\frac{1}{(N - \Delta n)} \sum_{n=1}^{N-\Delta n} f(n) f(n + \Delta n) \right) \times (\langle f \rangle^2)^{-1} - 1, \tag{7}$$

where $A(\Delta n = 0) = \sigma^2 / \langle f \rangle^2$, where $\sigma^2 = \langle f^2 \rangle - \langle f \rangle^2$ is the variance of $f(n)$.

Figure 21(a) and (b) shows the autocorrelation for a chaotic time series obtained from the numerical model for the case of one x-polarized modes ($m = 1$) and four y-polarized modes ($n = 4$). Figure 21(c) shows the cross-correlation between the one x-polarized intensity and the y-polarized intensity (the sum of the four y-polarized mode intensities). The correlation functions of the numerical data look very similar to typical experimental results for chaotic intensity fluctuations shown in Fig. 22(a)–(c), again for the case of $(m,n) = (1,4)$. The autocorrelation functions in Figs. 21(a) and 22(a) die out on a time scale of tens of microseconds, which is similar to the separation time given by the inverse of the Liapunov exponent. Notice that the cross-correlation function between the x- and y-polarized intensities is initially negative. This is because the x- and y-polarized intensities are anticorrelated as was shown in Fig. 20. The autocorrelation functions show oscillations at about five times the frequency of the slow oscillations present in the cross-correlation functions. The cross-correlation function shows an energy exchange between the single x-polarized mode intensity and the y-polarized intensity, which contains four modes. The autocorrelation function is computed for the total intensity, and reveals the time scale for exchange of energy among the five modes, which occurs in an approximately antiphase fashion, even though the total intensity is chaotic.

The time scale for the fast oscillations in the autocorrelation function is about ten microseconds, which compares closely with the time period for relaxation oscillations. The laser operated without the intracavity doubling crystal shows very small amplitude, damped relaxation oscillations generated by noise perturbations. The cross coupling of the modes introduced by sum frequency generation may lead deterministically to large amplitude intensity fluctuations that originate in the relaxation oscillations.

The reader may have noticed that the experimentally measured probability distributions in Fig. 19(a)–(c) shows many sharp peaks. This is most noticeable in the probability distribution for the intensity in the x-polarized direction. One may conjecture that these sharp features would disappear if the histograms were accumulated from many more time traces. This conjecture is disproved by the following experimental observations. Figure 23(a)–(d) shows probability distributions for the total intensity fluctuations accumulated from 1, 10, 50, and 100 time traces, respectively. The sharp peaks occur at the same intensities in all these distributions. This structure is reminiscent of the peaks observed in the probability distributions for periodic time traces which were related to the turning points for the intensity. That is, even though the time trace looks chaotic, certain well-defined maxima and minima in the

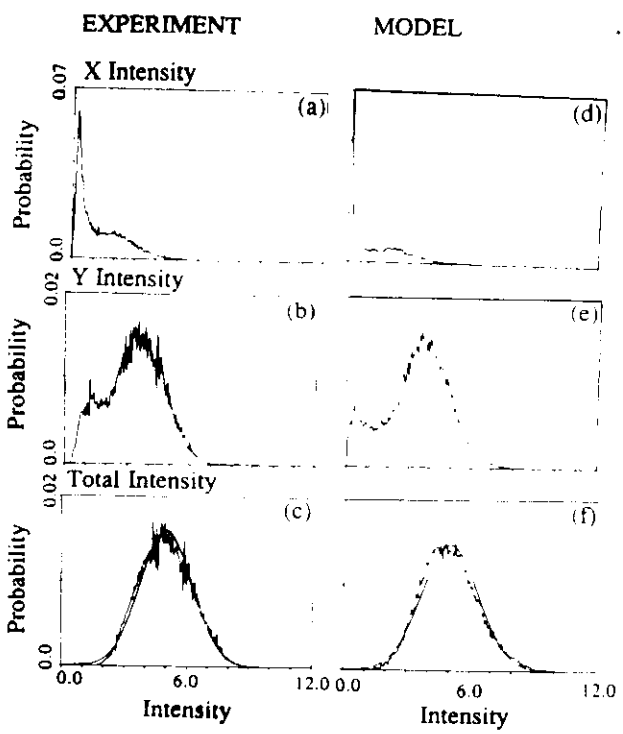

FIG. 19. (a)–(c) Experimental probability distributions for the x-polarized, y-polarized, and total intensities. (d)–(f) Corresponding probability distributions from the numerical integration of Eqs. (1). The experimental and numerical results are for the case $(m,n) = (1,4)$. The experimental time traces (and probability distributions) were not measured simultaneously.

total intensity time trace occur frequently, leading to the observed residual peaklike structures in the probability distributions.

The fine structure in the probability distributions obtained from integration of the numerical model in Fig. 19(d)–(f) is much less obvious than in the experimental measurements in Fig. 19(a)–(c). The difference could be that the numerical errors in the computation represent a noise source that is larger in magnitude than the spontaneous emission noise that is always present in the laser.

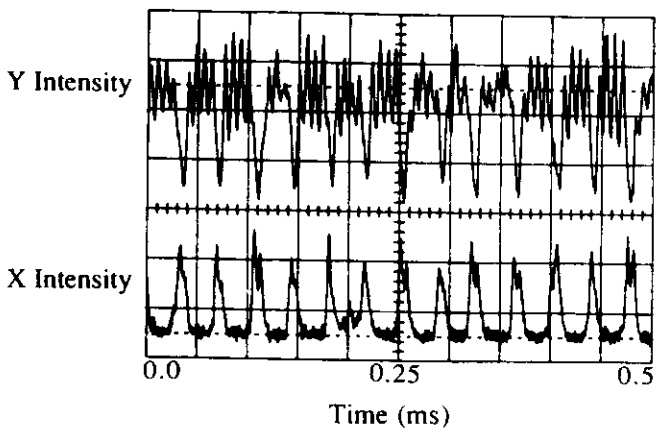

FIG. 20. Experimental time traces from simultaneously measured x-polarized and y-polarized intensities. Notice the anticorrelation between the orthogonally polarized intensities.

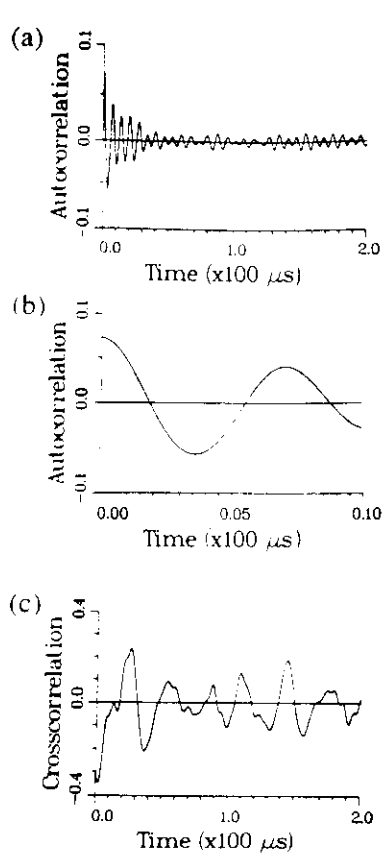

FIG. 21. (a) Autocorrelation function for a chaotic time series of the total intensity produced from a numerical integration of Eqs. (1). (b) Autocorrelation function of the same data as in (a) on a shorter time scale. (c) Cross-correlation function of the x-polarized intensity and the y-polarized intensity. The cross-correlation function is negative for $\Delta t = 0$ indicating that the x-polarized intensity and the y-polarized intensity are anticorrelated.

The fact that this structure is observed in the experimental results at all implies that the strength of the spontaneous emission noise in the laser is actually extremely small (the noise magnitude may also be independently estimated). This provides justification for our neglecting spontaneous emission in the laser model given by the rate equations (1), even though spontaneous emission is always present in the actual laser system.

VI. CONCLUSIONS

The laser system studied here is extremely convenient for detailed invetigations of complex periodic and chaotic phenomena. Its nonlinear dynamical behavior can be controlled by variation of a single system parameter (the relative orientation of the YAG and KTP crystals). It is possible to eliminate the chaotic fluctuations in this laser, obtain complex periodic waveforms, such as antiphase states, and to study the statistics of chaotic fluctuations. Our statistical studies raise many questions about the distribution of fluctuations in a system of globally coupled nonlinear oscillators. Why are the distributions approximately Gaussian in shape and what is responsible for the fine structure and significant deviations that are observed?

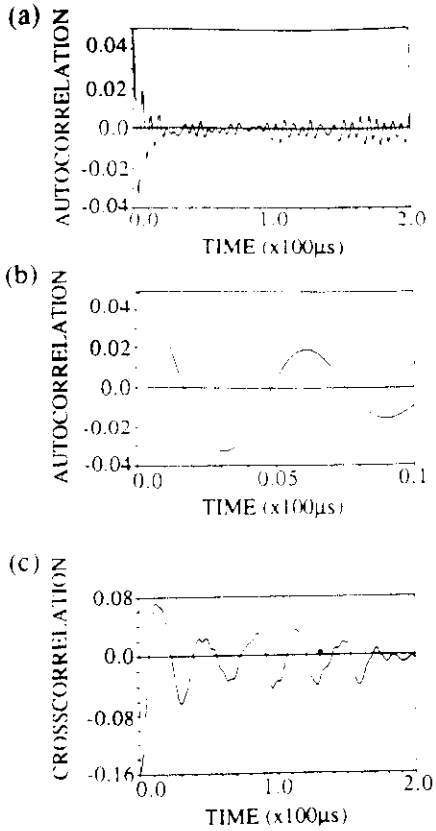

FIG. 22. Experimentally measured correlation functions for typical chaotic time traces of the laser. (a) Autocorrelation function for a chaotic total output intensity. (b) Autocorrelation function of the same data as in (a) on a shorter time scale. (c) Cross-correlation function of the x-polarized intensity and the y-polarized intensity. The cross-correlation function is negative for $\Delta t = 0$ indicating that the x-polarized intensity and the y-polarized intensity are anticorrelated. Notice the striking similarity to the numerical results in Fig. 21.

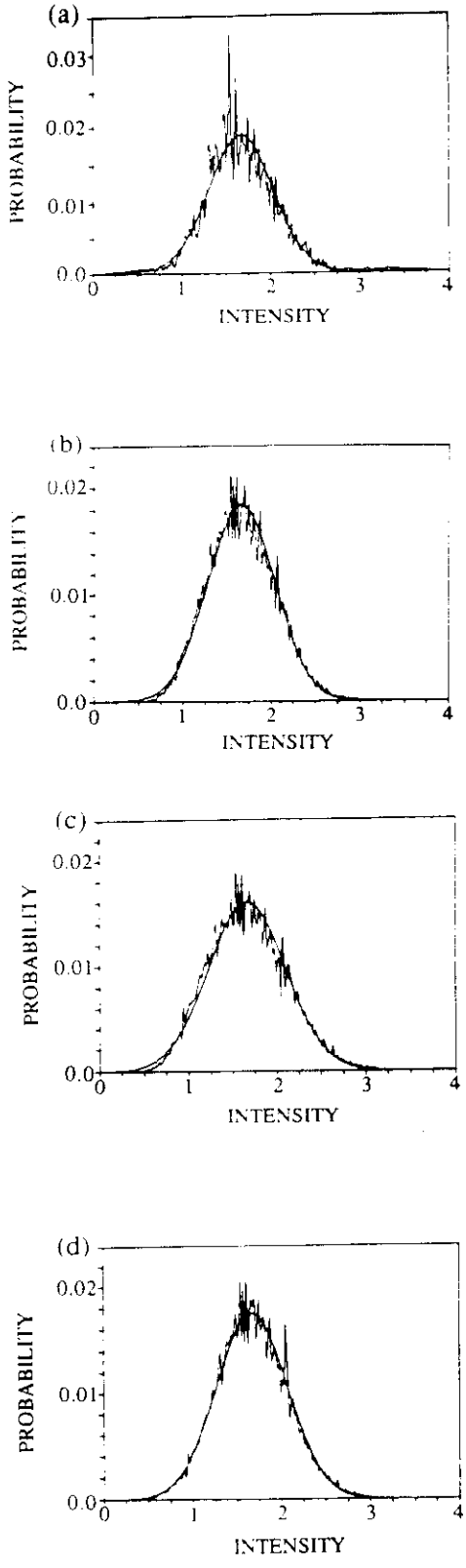

FIG. 23. Experimental probability distributions for the total output intensity accumulated from 1, 10, 50, and 100 time traces of length 1 ms each. (a) Probability distribution of 1 time trace. (b) Probability distribution accumulated from ten time traces. (c) Probability distribution accumulated from 50 time traces. (d) Probability distribution accumulated from 100 time traces. Notice that the fine structure in the probability distributions persists even when 100 time traces were accumulated. Also notice that the fine structure peaks occur at the same intensities in all four probability distributions. The intensity axes in the plots (a)–(d) are identically scaled.

What is the role of the central limit theorem in determining the nature of fluctuations in chaotic coupled systems?

Much theoretical and experimental work remains to be done to explore the answers to these questions, and the laser system is an excellent one for such investigations.

ACKNOWLEDGMENTS

We acknowledge support from NSF Grant ECS 8722216 and a research fellowship from Eastman Kodak Company. We thank Ron Fox, Joe Ford, Evans Harrell, Glenn James, and Kurt Wiesenfeld for many illuminating discussions and collaborations. In addition, we thank Tom Baer and Greg Kintz of Spectra Physics for the donation of laser components, and for sharing their expertise and insights on this laser system with us. Finally, we are grateful to Neal Abraham and Tito Arecchi for constructive criticism and many helpful remarks on the manuscript.

[1]N. B. Abraham, P. Mandel, and L. M. Narducci, "Dynamical Instabilities and Pulsations in Lasers," *Progress in Optics XXV*, edited by E. Wolf (North-Holland, Amsterdam, 1988), pp. 1–190, J. Chrostowski and N. B. Abraham, *Optical Chaos*, edited by SPIE Proceedings **667** (1986).
[2]D. K. Bandy, A. N. Oraevsky, and J. R. Tredicce, Eds., J. Opt. Soc. Am. B **5**, (1988), special issue on Nonlinear Dynamics of Lasers.
[3]R. G. Harrison and D J. Biswas, Nature **321**, 394 (1986).
[4]F. T. Arecchi and A. M. Ricca, in *Coherence and Quantum Optics IV*, edited by L. Mandel and E. Wolf (Plenum, New York, 1978), p. 975.
[5]T. Baer, J. Opt. Soc. Am. B **3**, 1175 (1986).
[6]P. Mandel and X.-G. Wu, J. Opt. Soc. Am. B **3**, 940 (1986).
[7]X.-G. Wu and P. Mandel, J. Opt. Soc. Am. B **4**, 1870 (1987).
[8]M. Oka and S. Kubota, Opt. Lett. **13**, 805 (1988).
[9]R. F. Belt, G. Gashurov, and Y. S. Liu, Laser Focus/Electro Optics **10**, 110 (October 1985).
[10]J. D. Bierlein and H. Vanherzeele, J. Opt. Soc. Am. B **6**, 622 (1989).
[11]W. Streifer, R. D. Burnham, T. L. Paoli, and D. R. Scifres, Laser Focus **20**, 100 (June 1984).
[12]W. Streifer, D. R. Scifres, G. L. Harnagel, D. F. Welch, J. Berger, and M. Sakamoto, IEEE J. Quantum Electron. **24**, 883 (1988).
[13]W. Koechner, *Solid State Laser Engineering* (Springer-Verlag, Berlin, 1988), p. 48.
[14]E. Hecht and A. Zajac, *Optics* (Addison-Wesley, Reading, MA, 1979), p. 268.
[15]G. E. James, E. M. Harrell II, C. Bracikowski, K. Wiesenfeld, and R. Roy, Opt. Lett. **15**, 1141 (1990).
[16]K. Wiesenfeld, C. Bracikowski, G. E. James, and R. Roy, Phys. Rev. Lett. **65**, 1749 (1990).
[17]G. E. James, Ph.D. dissertation, Georgia Institute of Technology, 1990 (unpublished).
[18]M. Sargent, M. O. Scully, and W. E. Lamb, Jr., *Laser Physics* (Addison-Wesley, Reading, MA 1974), pp. 120, 158.
[19]A. Siegman, *Lasers* (University Science Books, Mill Valley, CA, 1986), pp. 466, 992.
[20]L. Marshall, private communication. These results were presented in paper WA1, "High-power pulsed and cw diode-pumped mode-locked Nd:YAG lasers," Topical Meeting on Advanced Solid State Lasers, Hilton Head, 18–20 March, 1991.
[21]P. Hadley and M. Beasley, Appl. Phys. Lett. **50**, 621 (1987).
[22]K. Wiesenfeld and P. Hadley, Phys. Rev. Lett. **62**, 1335 (1989).
[23]K. Y. Tsang and K. Wiesenfeld, Appl. Phys. Lett. **56**, 495 (1990).
[24]H. L. Swinney, in *Order in Chaos*, edited by D. Campbell and H. Rose (North-Holland, Amsterdam, 1983), p. 3.
[25]D. Ruelle, *Chaotic Evolution and Strange Attractors* (Cambridge U. P., Cambridge, 1989), p. 28.
[26]F. Takens, "Detecting Strange Attractors in Turbulence," in *Lecture Notes in Mathematics*, Vol. 898, edited by D. A. Rand and L. S. Young (Springer-Verlag, Berlin, 1981), p. 366.
[27]N. H. Packard, J. P. Crutchfield, J. D. Farmer, and R. S. Shaw, Phys. Rev. Lett. **45**, 712 (1980).
[28]A. J. Lichtenberg and M. A. Lieberman, *Regular and Stochastic Motion* (Springer-Verlag, Berlin, 1983), p. 264.
[29]G. Benettin, L. Galgani, and J. M. Strelcyn, Phys. Rev. A **14**, 2338 (1976).
[30]R. F. Fox, Phys. Rev. A **41**, 2969 (1990).
[31]F. Moon, *Chaotic Vibrations: An Introduction for Applied Scientists and Engineers* (Wiley, New York, 1987), p. 151.
[32]E. Fermi, J. Pasta, and S. Ulam, Los Alamos Scientific Laboratory Rep. LA-1940 (1955).
[33]J. Ford and J. Waters, J. Math Phys. **4**, 1293 (1963).
[34]K. Kaneko, Phys. Rev. Lett. **65**, 1391 (1990).
[35]K. Kaneko, Phys. Rev. Lett. **66**, 243 (1991), errata for Ref. 34.
[36]J. V. Uspensky, *Introduction to Mathematical Probability* (McGraw-Hill, New York, 1965), Chap XIV.
[37]G. P. Puccioni, G. L. Lippi, N. B. Abraham, and F. T. Arecchi, Opt. Commun. **72**, 361 (1989).

Dynamical Control of a Chaotic Laser: Experimental Stabilization of a Globally Coupled System

Rajarshi Roy, T. W. Murphy, Jr., T. D. Maier, and Z. Gills
School of Physics, Georgia Institute of Technology, Atlanta, Georgia 30332

E. R. Hunt
Department of Physics and Astronomy, Ohio University, Athens, Ohio 45701-2979
(Received 25 November 1991)

A multimode, autonomously chaotic solid-state laser system has been controlled by the technique of occasional proportional feedback, related to the control scheme of Ott, Grebogi, and Yorke. We show that complex periodic wave forms can be stabilized in the laser output intensity. A detailed model of the system is not necessary. Our results indicate that this control technique may be widely applicable to autonomous, higher-dimensional chaotic systems, including globally coupled arrays of nonlinear oscillators.

PACS numbers: 05.45.+b, 42.50.−p

The possibility of obtaining complex periodic wave forms from a chaotic system has inspired much recent theoretical and experimental work [1–7]. The basic concept involved is that a chaotic attractor has a large number of unstable periodic orbits embedded in it. It should therefore serve as a rich source of complex periodic wave forms, if an appropriate dynamical control technique can be implemented to stabilize the system. The control algorithm proposed by Ott, Grebogi, and Yorke [1] (OGY) was a breakthrough in this direction and has been applied experimentally to a periodically driven magnetoelastic ribbon [2]. In the OGY scheme, an unstable periodic orbit is stabilized through the application of small, carefully computed perturbations to a system parameter; the perturbations are proportional to the deviation of the system from the unstable fixed point. Other systems studied experimentally with the aim of establishing control over chaos have been a thermal convection loop [3], a yttrium iron garnet (YIG) oscillator [4], and most recently, a diode resonator [5]. Control of the periodically driven diode resonator was achieved by the technique of occasional proportional feedback (OPF) and many higher-order periodic orbits were successfully generated. While Ref. [6] is concerned with the control of chaos through sinusoidal modulations of a control parameter, Ref. [7] clearly shows the relation of the OPF technique to the OGY algorithm.

In this Letter, we describe the application of the OPF technique to an autonomously chaotic multimode laser, a higher-dimensional system for which the chaotic attractor is not characterizable by a two-dimensional map. Further, the application of the control signal is performed on relatively fast time scales of the order of a few microseconds. This limits the application of schemes involving digital computations. In these circumstances, the OPF scheme provides an attractive means to attempt control of an autonomously chaotic laser. Though the OPF scheme does not require any detailed model of laser operation, a knowledge of the characteristic time scale of energy exchange between the active medium and the light in the laser cavity was important for its implementation in this system.

The multimode laser with an intracavity crystal [8] is an example of a system of globally coupled nonlinear oscillators; each longitudinal mode is a relaxation oscillator coupled to all the others [9–12]. Such globally coupled arrays have been found to be of relevance and interest in the study of Josephson-junction networks [13], models of chemical turbulence [14], and heartbeat rhythms [15]. The technique described here could possibly be applied to a wide range of physical, chemical, and biological systems, including arrays and networks of coupled nonlinear elements.

The laser used in our experiments is a diode-laser-pumped solid-state Nd-doped yttrium aluminum garnet (Nd:YAlG) system that contains a KTP (potassium titanyl phosphate) doubling crystal within a cavity of length ~3.5 cm. We have previously studied this system extensively and the equations that describe the laser operation in several longitudinal modes are well known [9–12]. In the experiments reported here, it was not necessary for us to utilize a detailed model of the system. The laser was pumped at 60 mW, about 3 times above threshold (~20 mW), and the chaotic operation was observed for a given rotational orientation between the YAlG and KTP crystals [9]. At this level of excitation, the laser operates in anywhere from five to ten longitudinal modes, depending on the rotational orientation of the crystals and the length of the laser cavity.

In a periodically driven system it is convenient to sample a system variable at the driving frequency or its submultiples. In the autonomously chaotic laser, there is no modulation applied, and hence one looks for a natural periodicity characteristic of the system. Such a periodicity is present in the form of relaxation oscillations in the laser with intracavity nonlinear crystal [11,12], representative of the fundamental periodicity in the exchange of energy between active atoms and light in the laser cavity. The frequency of the relaxation oscillations ν_r increases as the square root of the excitation level above threshold, and depends also on other parameters characterizing the laser, such as the cavity loss, fluorescence decay time of the active atoms, and the nonlinearity coefficient of the KTP crystal [12]. ν_r is in the range 20–150 kHz, for lev-

els of excitation of the laser up to 5 times above threshold. The source of chaotic behavior in this laser is the coupling of the longitudinal modes through the nonlinear process of sum-frequency generation. This process destabilizes the relaxation oscillations which are normally heavily damped in the system without the intracavity crystal. Autocorrelation functions of the total intensity reveal clear oscillations at the relaxation-oscillation frequency even when the laser is chaotic [11]. Alternatively, one may discern a peak at the relaxation-oscillation frequency in the fast Fourier transform (FFT) of the total intensity fluctuations.

The basic technique for achieving dynamical control is as follows. A system variable (the total laser output intensity) is sampled within a window of selected offset and width. The sampling frequency is related to the relaxation-oscillation frequency of the system. A signal proportional to the deviation of the sampled intensity from the center of the window is generated and applied to perturb a system parameter from its ambient value. This control signal repeatedly attempts to bring the system closer to a periodic unstable orbit that is embedded in the chaotic attractor, resulting in a realization of the periodic orbit with accuracy limited by the frequency and extent of feedback as well as by the positive Lyapunov exponent characterizing the orbit.

A block diagram of the laser system and controller is shown in Fig. 1. The fundamental 1.06-μm radiation is monitored by a photodiode, the output from which serves as the input to the control circuit. A stable oscillator is used to generate the synchronizing frequency with which the output from the chaotic laser is sampled. A variable offset is added to the laser signal to bring it within a window of adjustable width. The window comparator is activated when the wave form makes a transit through the window. When the synchronizing input is coincident with this event, the sample and hold acquires the wave-form voltage. The sampled signal is output through the gate only for time periods short compared to the period of the synchronizing oscillator. A typical time period for application of the correction signal is less than 10 μsec. An inverting amplifier with variable offset and gain delivers the control signal to the diode-laser driver.

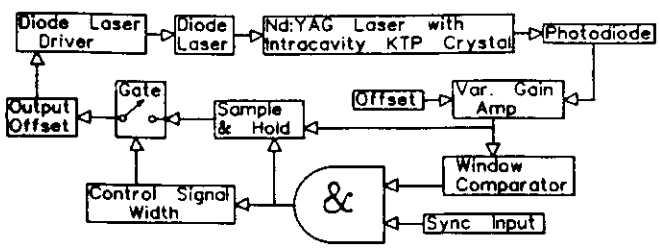

FIG. 1. Schematic of the laser system and occasional proportional feedback controller. The perturbation of the diode-laser drive current is proportional to the deviation of a sampled wave form value from the window center. The synchronizing oscillator frequency, wave-form offset, and control-signal width are varied to optimize stability of the periodic wave form.

The rotational orientation of the YAlG and KTP crystals was adjusted such that the laser was clearly chaotic in operation, but only a small amount (less than a few μW, typically) of green light was generated in the doubling crystal. This indicates that the effect of the nonlinearity is small, and that the laser is in a "weakly" chaotic regime. With the laser in chaotic operation, control is attempted by adjustment of the synchronizing frequency. The synchronizing oscillator frequency is varied near the relaxation-oscillation frequency observed for the laser, and the wave-form offset and window width are adjusted to initiate control. Further adjustments of the control signal width and gain, as well as the wave-form offset and window width, are necessary to optimize the stability of the wave forms obtained. The most effective adjustments were found to be the synchronizing frequency, the wave-form offset, and the control-signal width.

It is very easy to make these adjustments and to obtain many higher-order periodic wave forms of the laser intensity, a few of which are illustrated in Fig. 2. The wave form of the chaotic laser without any control signal is shown first. The FFT of this wave form shows a broad relaxation-oscillation peak centered at about 118 kHz. The time scale shown is 0–500 μsec. Period-1, -4, and -9 wave forms are also shown together with the control signals; a rich variety of wave forms can be obtained in practice and maintained in stable operation for many minutes. The time scale for these figures is 0–200 μsec. The sharp spikes on the control signal that are visible particularly in Fig. 2(d) are an artifact of the sample and hold circuit. The FFTs for the intensity fluctuations are shown below the intensity time traces. The range of frequencies shown is 0–500 kHz in all the figures. For the low-period orbits, control can be established with small perturbations applied near the relaxation-oscillation frequency or its submultiples [Figs. 2(b) and 2(c)]. In this manner we have observed orbits up to period 8. In Fig. 2, it is seen that the wave forms generated align themselves with the correction signal such that the wave form peaks are sampled. There is a range of frequencies of the synchronizing signal over which this alignment is noticeable, and robust, successful control is maintained. For the period-1 orbit, control was retained over a 110–165 kHz synchronizing frequency range. For higher-period orbits such as the period-9 orbit shown in Fig. 2(d), we often found that the synchronization frequency had to be adjusted to a simple rational fraction of the relaxation frequency. The nature of the control signal grows progressively more complex as higher-order periodic orbits are captured [Fig. 2(d)]. We note that in the example wave forms shown here, the control signal consists of only positive-going or negative-going corrections. However, many cases have been observed for complex wave forms in which the corrections are both positive and negative relative to the ambient bias. The perturbations applied to

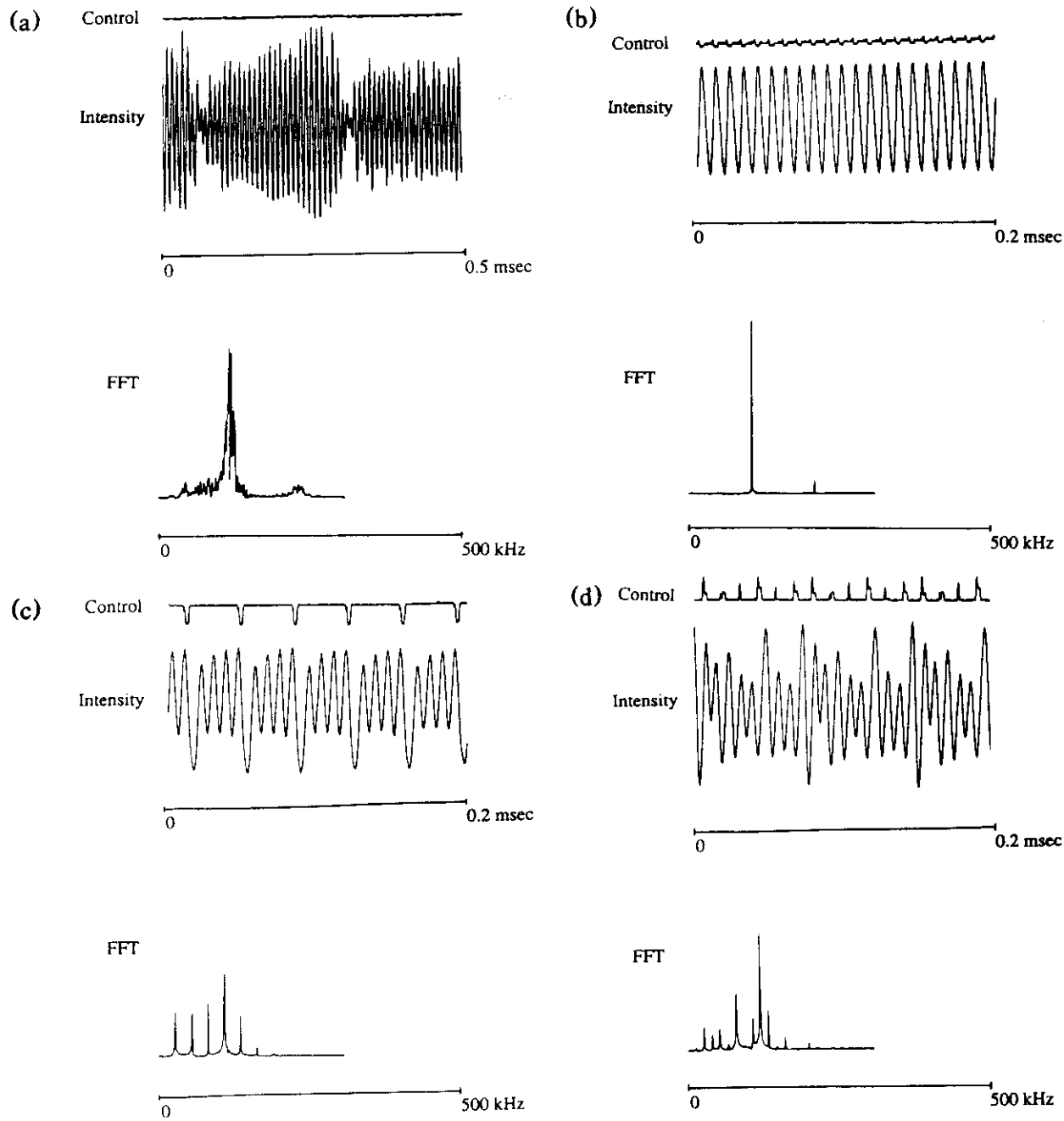

FIG. 2. Time traces of the laser intensity and the corresponding FFTs. The control signal is shown at the top, and then the intensity time trace and FFT. (a) The chaotic intensity fluctuations of the laser output without any applied control signal. The FFT below the wave form shows the broad relaxation-oscillation peak. (b) A period-1 orbit obtained by adjusting the synchronizing oscillator frequency to approximately the relaxation-oscillation frequency. (c) A period-4 orbit obtained by adjusting the synchronizing oscillator frequency to approximately $\frac{1}{4}$ of the relaxation-oscillation frequency. (d) A period-9 orbit obtained with the synchronizing oscillator frequency at $\frac{4}{9}$ of the dominant frequency shown in the FFT. The complex nature of the control signal is clearly visible. The spikes seen in the control signal are an artifact of the sample and hold circuit.

the drive current of the diode laser are only a few percent of the ambient-bias current for the low-order periodic orbits. Even for the higher-order orbits, the maximum perturbations observed were less than 10%. At these levels of control-signal magnitude, however, the original attractor may be modified to some extent by the feedback.

We have found experimentally that wave forms very similar to those obtained from the laser with dynamical control can be produced without control if operating parameters (the relative orientation of the crystals and the pump excitation) are changed. However, these uncontrolled wave forms are typically very unstable and cannot be maintained except

25

for very short periods of time. With control, they can be maintained for many minutes. We have also picked out segments of unstable periodic orbits from chaotic intensity time traces that are similar to the low-order periodic orbits that we have generated with dynamical control under the same operating conditions. Experimental results demonstrating this correspondence and a comparison of wave forms generated numerically from a detailed model of the laser [11,12] will be published separately.

We have also examined the effect of a simple periodic modulation of the pump. Though the laser is stabilized on low-order orbits by the modulation, the modulation amplitude necessary is often much larger than 10% for such stabilization. Further, the wave forms are stable for only short periods of time, and environmental changes such as air currents and temperature drifts tended to have a highly destabilizing influence on the system. In contrast, with OPF stabilization, the laser stays locked in a given orbit for much longer lengths (many minutes) of time.

In conclusion, we have demonstrated dynamical control of an autonomously chaotic, higher-dimensional optical system for the first time on microsecond time scales. The multimode laser system studied by us is an example of a globally coupled system of nonlinear oscillators. The proportional control signal applied to the pump excitation results in an ordered, periodic state of the originally chaotic ensemble of oscillators. The results reported here indicate that the technique of occasional proportional feedback should be widely applicable to a variety of physical, chemical, and biological systems, including arrays and networks of coupled elements.

We acknowledge support from NSF Grant No. ECS 8722216, a Goldwater fellowship (T.W.M.), and an AT&T graduate fellowship (Z.G.). We also thank Neal Abraham, Chris Bracikowski, Kenju Otsuka, and Kurt Wiesenfeld for helpful discussions. In particular, we thank Chris Bracikowski for design and construction of the laser system and for many previous collaborations over the past years.

[1] E. Ott, C. Grebogi, and J. A. Yorke, Phys. Rev. Lett. **64**, 1196 (1990).
[2] W. L. Ditto, S. N. Rauseo, and M. L. Spano, Phys. Rev. Lett. **65**, 3211 (1990).
[3] J. Singer, Y-Z. Wang, and H. H. Bau, Phys. Rev. Lett. **66**, 1123 (1991).
[4] A. Azevedo and S. M. Rezende, Phys. Rev. Lett. **66**, 1342 (1991).
[5] E. R. Hunt, Phys. Rev. Lett. **67**, 1953 (1991).
[6] Y. Braiman and I. Goldhirst, Phys. Rev. Lett. **66**, 2545 (1991).
[7] B. Peng, V. Petrov, and K. Showalter, J. Phys. Chem. **95**, 4957 (1991).
[8] T. Baer, J. Opt. Soc. Am. B **3**, 1175 (1986).
[9] G. E. James, E. H. Harrell, II, C. Bracikowski, K. Wiesenfeld, and Rajarshi Roy, Opt. Lett. **15**, 1141 (1990).
[10] K. Wiesenfeld, C. Bracikowski, G. E. James, and Rajarshi Roy, Phys. Rev. Lett. **65**, 1749 (1990).
[11] C. Bracikowski and Rajarshi Roy, Chaos **1**, 49 (1991).
[12] Rajarshi Roy, C. Bracikowski, and G. E. James, in Proceedings of the International Quantum Optics Conference, edited by R. Inguva and G. S. Agarwal (Plenum, New York, to be published).
[13] K. Wiesenfeld and P. Hadley, Phys. Rev. Lett. **62**, 1335 (1989).
[14] Y. Kuramoto, *Chemical Oscillations, Waves and Turbulence* (Springer-Verlag, New York, 1984).
[15] A. T. Winfree, *The Geometry of Biological Time* (Springer-Verlag, New York, 1980).

Tracking Unstable Steady States: Extending the Stability Regime of a Multimode Laser System

Zelda Gills, Christina Iwata, and Rajarshi Roy
School of Physics, Georgia Institute of Technology, Atlanta, Georgia 30332

Ira B. Schwartz and Ioana Triandaf
U.S. Naval Research Laboratory, Special Project for Nonlinear Science, Plasma Physics Division, Code 4700.3, Washington D.C. 20375-5000
(Received 23 July 1992)

It is shown that the unstable steady state of a multimode laser system may be stabilized by the occasional proportional feedback technique for dynamical control of chaotic systems. The range of pump excitations over which stabilization can be maintained is extended by more than an order of magnitude through application of a procedure for tracking the unstable steady state as the pump excitation is slowly varied.

PACS numbers: 05.45.+b, 42.50.−p

It was recently demonstrated in several experiments that dynamical control of chaos can be achieved in mechanical, fluid, electronic, and laser systems [1–4]. In these experiments, two related techniques were employed to establish control: the Ott-Grebogi-Yorke (OGY) algorithm [5] and the occasional proportional feedback (OPF) method [3,4,6], both of which consist of applying small, appropriately estimated perturbations to a system parameter. These perturbations stabilize the system on a chosen periodic orbit, or unstable steady state. A crucial question immediately arises: Can we maintain control of a particular orbit or unstable steady state over a wide range of parameter values for the system, including both chaotic and nonchaotic regions?

We study here the particular case of stabilization of an unstable steady state. In the case of the chaotic multimode laser system, it is of great relevance for practical applications that a stabilized steady state be maintained. It is found that when the laser is stabilized by a dynamical control technique, it remains stable only for a very limited range of pump powers, if the parameters of the control circuit are kept fixed. However, it is next demonstrated that through the application of a recently developed procedure for tracking the unstable steady state (through judicious changes in a control parameter), the stabilized steady state can be maintained over a greatly extended range of pump excitations. The tracking procedure was developed [7] particularly for experimental systems where a detailed theoretical model may not be available. For the laser system studied in these experiments, a reasonably accurate model is available [8], but we do not make use of the model for either the control or the tracking procedure. Furthermore, the laser system employed is a higher-dimensional one for which no simple return map is available [4,8], in contrast to the experiments of Refs. [1,3]. Our experiments are thus a striking demonstration that the procedures developed in Ref. [7] may be applied successfully to complex systems with no low-dimensional characterization of the chaotic attractor.

To obtain insight into the tracking technique, let us assume that the chaotic system under study may be controlled through application of a technique that consists of making small perturbations of a system parameter in response to the system output, as measured through detection of a system variable, or suitable combination of variables. Two techniques that have been developed for such control are the OGY method [1,5] and OPF method [3,4,6]. In the OGY algorithm, three basic elements are needed to implement control: a time series, a control point ξ_F about which control is achieved, and an accessible system parameter p. We suppose that there exists an unstable periodic orbit $\xi(p)$ which varies as a function of parameter p. For some initial parameter value p for which the orbit is chaotic, we assume we have determined the eigenvalues and eigenvectors of the orbit, and that the orbit is controlled. The OPF method is essentially a limiting case of the OGY algorithm when the contracting direction is infinite in strength, i.e., the stable eigenvalue λ_s is zero. We review the OGY method here since it is more general and is based on a first-principles attractor reconstruction technique.

To track the orbit, a small change is made in p. Since the orbit location is a function of p, a small error is made if the control point is not changed. To see this, we examine the OGY control algorithm. At a fixed value of p, we choose a small correction $\delta p = C(\xi_n - \xi_F)\mathbf{f}_u$, so that the next iterate falls on the local stable manifold. Here, ξ_F is the predicted fixed point, ξ_n is the current iterate of the map, $\mathbf{f}_u$ is the contravariant eigenvector along the unstable direction, and C is a constant $C = \lambda_u/(\lambda_u - 1)\mathbf{g}\cdot\mathbf{f}_u$, where $\mathbf{g} = \partial\xi_F(p)/\partial p$ and λ_u is the unstable eigenvalue. To implement the tracking procedure, we determine the error $\mathbf{e}$ between the predicted fixed point ξ_F and the true fixed point, by examining the mean of the control fluctuations $\langle\delta p\rangle$ about p. If the predicted value of the fixed point is equal to the exact value, it can be shown [7] that the mean of the fluctuations will be close to zero (to within the noise of the experiments). The mean of the fluctuations is given approximately by $\langle\delta p\rangle \approx C\mathbf{e}\cdot\mathbf{f}_u$. Therefore, the error is minimized by varying the estimate

of the fixed point at the new parameter value to that which minimizes $|\langle \delta p \rangle|$. This minimization is a correction to the prediction of the fixed point and locates a new point on the branch of orbits, which is now used for further prediction. The connection between the OGY and OPF methods has been addressed by Schwartz, Triandaf, and Roy [9], and it may be shown that the considerations discussed for tracking an orbit are easily extended to the OPF control technique as well.

We have applied the OPF control technique for dynamical stabilization of the unstable steady state of a chaotic multimode Nd:YAG (neodymium doped yttrium aluminum garnet) laser with a nonlinear intracavity KTP (potassium titanyl phosphate) crystal [4,8]. The diode laser pumped solid state laser system displays periodic and chaotic fluctuations of the output intensity for certain operating parameter regimes. To apply the OPF method, an analog electronic feedback system was developed, described in Ref. [4]. The laser output intensity is detected by a photodiode, the signal $V(t)$ from which [corresponding to the intensity $I(t)$] is amplified with a variable gain (proportionality factor "A") and offset with respect to a reference voltage V_{ref} (corresponding to the reference intensity I_{ref}). The signal is sampled periodically with the period determined by an external synchronizing pulse generator. The sampled signal is input to the laser diode driver as a small perturbation on the dc bias level, for a time short compared to the sampling period. A series of minute kicks of fluctuating magnitude and sign are thus applied to the diode drive current. The control parameters are (i) the reference level with respect to which the output intensity is measured, (ii) the proportionality factor A that multiplies $V(t) - V_{\text{ref}}$, (iii) the period T at which the output is sampled, and (iv) the gating period δt over which the correction $A[V(t) - V_{\text{ref}}]$ is applied to the ambient value of the diode drive current. For stabilization of the unstable steady state, I_{ref} is our guess for the average steady-state intensity. If this guess is incorrect, the control signal fluctuations acquire a net dc component. Thus we can zero this dc component by adjustment of I_{ref}, and minimize the control fluctuations by adjustment of the other control parameters.

In Fig. 1, the average value of the Nd:YAG laser output (relative units) is shown as a function of the dc bias applied to the diode laser driver. No control signal is applied. The symbols denote a complicated sequence of stable steady-state, periodic, and chaotic behavior. Note that stable steady-state output is obtained only for a very small range of pump powers, for the given set of laser operating parameters.

Figure 2(a) shows an example of unstable chaotic fluctuations of the output intensity, with no control signal applied. Application of dynamical control results in the stabilization of the steady state, Fig. 2(b). The control signal fluctuations are so small as to be virtually indistinguishable from noise in the digital oscilloscope trace and are significantly less than 1% of the ambient dc bias. The stabilized steady-state intensity has the same average value as that of the chaotic output. The fluctuations of the laser intensity are a few percent of the steady-state dc

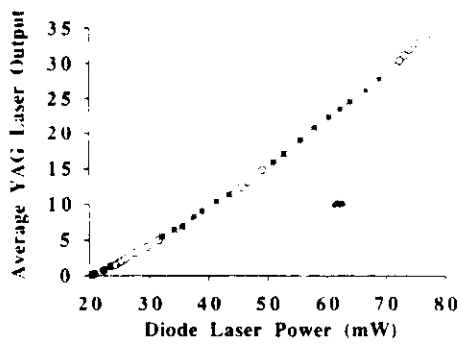

FIG. 1. The average laser output (relative units) at 1.06 μm, without application of the control signal. The symbols designate steady-state (●), periodic (○), and chaotic (*) behavior of the laser. Stable operation is obtained only very near threshold; for higher pump powers, a complex sequence of periodic and chaotic behavior is found.

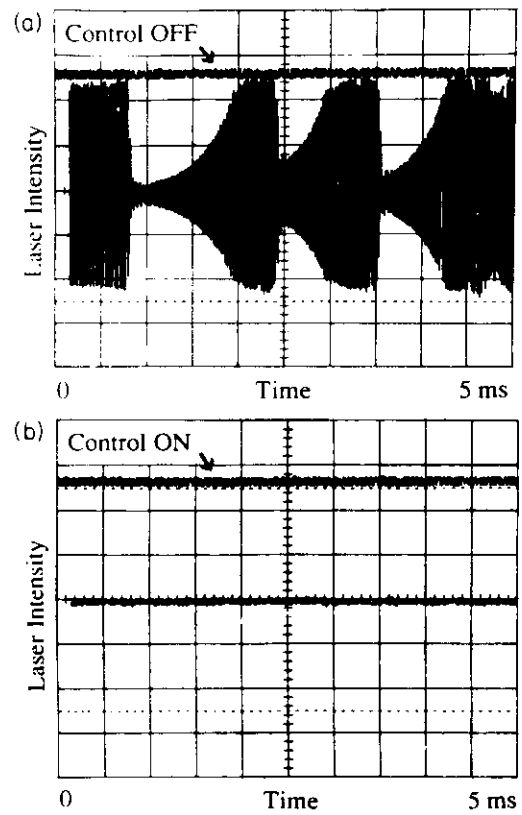

FIG. 2. (a) Digital oscilloscope trace showing the chaotic fluctuations of the laser output intensity vs time. The pump power is about 53 mW, and no control signal is applied (upper trace). (b) The stabilized steady-state intensity vs time with the control signal applied. The upper trace is the control signal; its fluctuations are submerged in the noise level of the digital oscilloscope.

level, reduced from the nearly 100% fluctuations in the chaotic state. These results demonstrate that it is possible to successfully stabilize the unstable steady state for a given pump power (about 50 mW) and control parameter settings.

We display in Fig. 3(a) the consequence of changing the pump power for fixed control parameters. The laser retains stable steady state only for the limited range of pump power indicated by the solid dots, giving rise to complex periodic and chaotic oscillations for small changes of the diode laser power. Figure 3(b) shows that the control signal fluctuations grow on either side of the control points as the pump power is varied, becoming several times larger ($\sim 3\%$ to 10% of the dc value) than those at the optimized control point (less than $\sim 1\%$).

Next, we show the results of application of the tracking procedure. The pump power was steadily increased in small steps from a value close to threshold, where stable steady state was obtained without control. When unstable oscillations of the output intensity were detected, control was switched on, and the reference intensity level I_{ref} was optimized to obtain an essentially zero dc component of the control signal. The standard deviations of the fluctuations of the control signal were also minimized by adjustment of T, δt, and A. It was found that the laser could be stabilized over the entire range of pump power shown in Fig. 4, by tracking the steady state through adjustment of I_{ref} as the pump power was increased, and through minor adjustments in T and δt. The intensity fluctuations about the stabilized steady state are typically more than an order of magnitude smaller than the almost full scale unstable periodic and chaotic fluctuations.

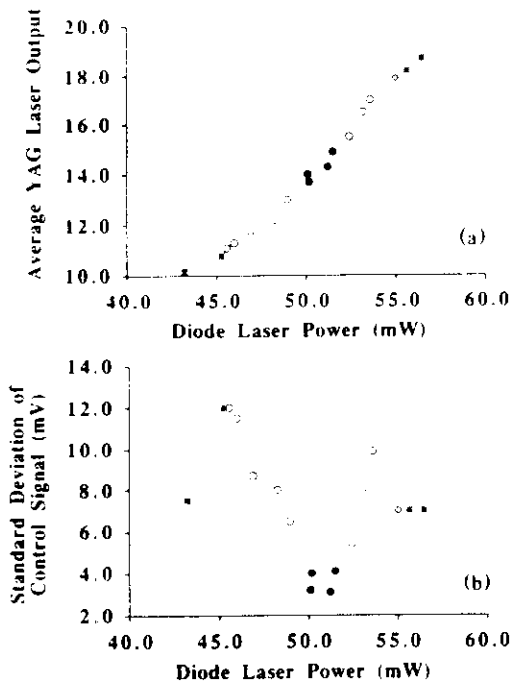

FIG. 3. (a) Stabilization of the laser achieved for a fixed setting of the control parameters is lost for small changes in the pump power. The solid dots indicate the range of stable operation. Period 1 (○), period 4 (□), period 10 (◇), and chaotic (*) operation were observed as the pump power was changed without any tracking procedure applied to the control parameters. (b) The standard deviation of the control signal fluctuations is shown for the range of pump powers investigated in (a). The fluctuations grow sharply on either side of the optimized control point.

A comparison of Figs. 1 and 4 immediately shows that the tracking technique allows us to obtain about 15 times more output power in a stable steady state for a given set of laser operating parameters. The stabilized steady-state values are very close to the average values of the fluctuating unstable laser output for the same pump power. The control signal fluctuations are a small perturbation and almost no extra pump energy input is required to stabilize the system. Steady-state operation achieved in this manner is extremely stable for long periods of time (many minutes).

In conclusion, we have introduced a new procedure to track an unstable steady state in a multimode laser system as the pump power is varied over a wide range. The results demonstrate over an order of magnitude extension of the stability regime, from a pump power about 20% above threshold to more than 300% above threshold. The control technique requires only small perturbations of the pump power and excellent stability is maintained in the laser output.

A detailed model of the system is not required. However, it is known [8] that the system has a higher-dimensional attractor, with no simple return map. Several globally coupled longitudinal modes oscillate simultaneously in different polarizations. Our results indicate that complex systems of nonlinear oscillators may be stabilized, and the regime of stability extended, through the combination of tracking and control procedures demonstrated here. The technique should be applicable to a wide variety of electronic, fluid, and mechanical systems as well as to chemical and biological processes.

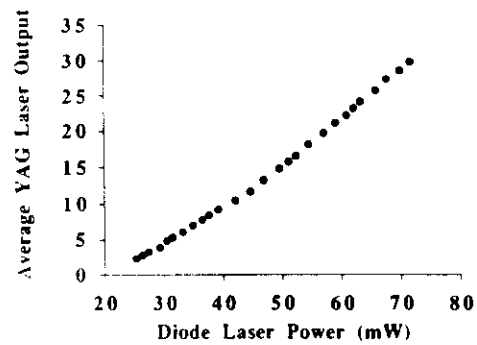

FIG. 4. Stable steady-state output of the laser (same scale as in Fig. 1) vs pump power. Control and tracking were both applied. The regime of stable operation was extended from about 20% above threshold to more than 300% above threshold.

R.R. thanks Pere Colet and Kurt Wiesenfeld for very helpful discussions. He also thanks Jack Hale for an early remark on tracking orbits and a discussion of control strategies for nonlinear systems. Z.G. was supported by an AT&T graduate fellowship. C.I. was supported by an NSF REU program, and R.R. by NSF Grant No. ECS-9114232. We thank Tom Maier for his constant help with electronics instrumentation. I.T. gratefully acknowledges the support of the Office of Naval Technology.

[1] W. L. Ditto, S. N. Rauseo, and M. L. Spano, Phys. Rev. Lett. **65**, 3211 (1990).

[2] J. Singer, Y-Z. Wang, and H. H. Bau, Phys. Rev. Lett. **66**, 1123 (1991).

[3] E. R. Hunt, Phys. Rev. Lett. **67**, 1953 (1991).

[4] Rajarshi Roy, T. Murphy, Jr., T. D. Maier, Z. Gills, and E. R. Hunt, Phys. Rev. Lett. **68**, 1259 (1992).

[5] E. Ott, C. Grebogi, and J. A. Yorke, Phys. Rev. Lett. **64**, 1196 (1990).

[6] B. Peng, V. Petrov, and K. Showalter, J. Phys. Chem. **95**, 4957 (1991); V. Petrov, B. Peng, and K. Showalter, J. Chem. Phys. **96**, 7506 (1992).

[7] Ira B. Schwartz and I. Triandaf, Phys. Rev. A (to be published); T. Carroll, I. Triandaf, I. B. Schwartz, and L. Pecora, Phys. Rev. A **46**, 6189 (1992). The tracking procedure is applied to an electronic Duffing oscillator in this paper.

[8] C. Bracikowski and Rajarshi Roy, Chaos **1**, 49 (1991); Rajarshi Roy, C. Bracikowski, and G. E. James, in Proceedings of the International Conference on Quantum Optics, edited by G. S. Agarwal and R. Inguva (Plenum, New York, to be published).

[9] Ira B. Schwartz, Ioana Triandaf, and Rajarshi Roy (to be published).

Coherence and phase dynamics of spatially coupled solid-state lasers

Larry Fabiny, Pere Colet,* and Rajarshi Roy
School of Physics, Georgia Institute of Technology, Atlanta, Georgia 30332-0430

Daan Lenstra
Department of Physics and Astronomy, Free University, Amsterdam, The Netherlands
(Received 27 July 1992)

We examine the mutual coherence and phase dynamics of two solid-state lasers, generated adjacent to each other in a single Nd:YAG rod. The coupling of the lasers is varied by changing the separation of the pump beams. A model is formulated to interpret the experimental results, and theoretical predictions are obtained that are in excellent agreement with the measurements.

PACS number(s): 42.60.−v, 42.55.Rz, 42.55.Px

I. INTRODUCTION

Laser arrays have been fabricated and their properties studied for many years. Most of these studies have been concerned with semiconductor laser arrays. Recent studies have shown [1] that although the total light output from the semiconductor arrays may be stable, the emission from individual elements of an array is often unstable and even chaotic, and a stable phase-locked operation is possible only over small parameter ranges. These results indicate that it is very important to study the conditions for the stable operation of coupled lasers [2,3] even in the simplest case of two lasers, in order to develop a thorough understanding of the factors that affect their stability.

It has also become clear that miniaturized solid-state lasers and their arrays are gaining importance through potential applications and through the development of new solid-state lasing media. There are indications that while semiconductor laser arrays demonstrate a stable phase-locked operation only over a small range of operating parameters, solid-state laser arrays may exhibit stable phase locking over a much wider range of coupling and operating parameters [4]. Therefore it is of great interest to examine both experimentally and theoretically the coherence and phase dynamics of two coupled solid-state lasers. In the system studied here, we vary the coupling between the lasers and study the mutual coherence of the lasers as revealed in the formation of interference fringes by the overlapped beams.

It is important to note the similarities and differences between solid-state and semiconductor lasers. Both are class B lasers [5], because the polarization dynamics may be adiabatically eliminated when cw operation is considered. Thus, the lasers are well described by coupled complex field and inversion equations. In both cases the decay rate of the cavity is larger than that of the inversion. For Nd:YAG (yttrium-aluminum-garnet) lasers these are $\rho_c \approx 10^6\ \mathrm{s}^{-1}$ and $\gamma_\perp \approx 4\times 10^3\ \mathrm{s}^{-1}$, respectively, while for a solitary semiconductor laser the corresponding values are $\rho_c \approx 10^{12}\ \mathrm{s}^{-1}$ and $\gamma_\perp \approx 10^9\ \mathrm{s}^{-1}$. This means that while solid-state laser dynamics may be studied with conventional detectors, streak cameras are often necessary for studies of semiconductor laser array dynamics [1]. We have used simple p-i-n photodiodes and a video camera system for the studies reported here. Another important distinction between solid-state and semiconductor lasing media is the large value of the "linewidth enhancement factor" α for semiconductors ($\alpha \approx 3$–5) compared with $\alpha \approx 0$ for solid-state systems. This difference makes solid-state lasers much more suitable for phase locking than semiconductor lasers.

We have fabricated solid-state laser arrays by several different procedures. A single pump beam may be split into several approximately equal components through the use of beam splitters, microlens arrays, specially designed binary optic gratings such as the Dammann grating, and fiber beam splitters. While we have generated arrays of multiple lasers by all of these methods, here we report the results of our study of the mutual coherence of two lasers created in a single Nd:YAG rod by two parallel pump beams obtained using beam splitters. We will describe the experimental system in Sec. II. Section III contains the experimental results obtained with the video camera system. Section IV describes a model for the two-laser system. We show that if the intensity of the two lasers is assumed to be more or less constant, and there is negligible coupling between intensity and phase fluctuations, we may obtain a single stochastic equation to describe the dynamics of the phase difference between the two lasers. The solution of the stochastic equation is the subject of Sec. V. The Langevin equation for the phase difference φ is converted to a Fokker-Planck equation and solved in the stationary state under the appropriate boundary conditions to yield a simple expression for the probability density of φ. The visibility of the two lasers may be calculated as a function of their separation and compared directly with experiment. Several numerical computations performed with the model of Sec. IV are given and we present a discussion of our results in Sec. VI.

II. EXPERIMENTAL SYSTEM

The experimental system for studying the coherence of two spatially coupled lasers is shown in Fig. 1. Two spa-

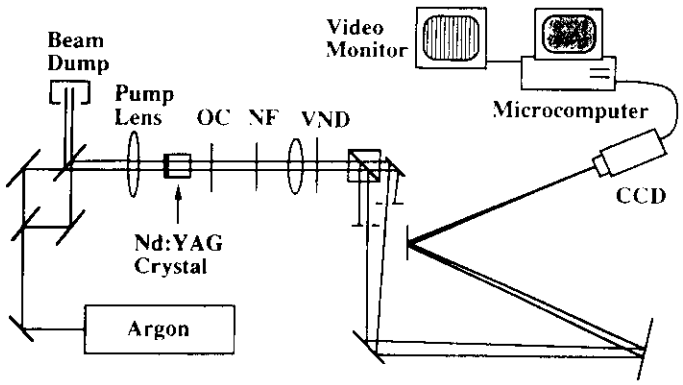

FIG. 1. Experimental system for generating two adjacent lasers in an Nd:YAG crystal and measuring their mutual coherence. The two beams overlap at the sensor of the CCD camera which has its imaging lens removed. OC is the output coupler; NF is the notch filter transmitting at 1064 nm; VND is the variable neutral density filter.

tially separated parallel lasing beams are created in a plane parallel cavity by end pumping a single Nd:YAG rod with two pump beams for an argon laser. Two pump beams are produced from a single Ar laser source by first splitting and then recombining the beams using two beam splitters. The YAG crystal is 5 mm in length and 5 mm in diameter, while the entire cavity is ≈ 1 cm in length. One end of the crystal serves as a flat cavity mirror and is coated to be highly reflecting at the lasing wavelength of 1064 nm and highly transmitting at 514.5 nm. The opposite crystal face is antireflection coated at both wavelengths.

Thermal lensing [4,6] induced in the crystal by the two pump beams is responsible for generating two separate stable cavities. This is a consequence of the temperature-dependent index of refraction ($dn/dT = 7.3\times10^{-6}$ K^{-1}) of the crystal, and is responsible for the creation in each cavity of an effective positive lens with a focal length of the order of ~ 1 m. A second mechanism, self-focusing, also contributes to the formation of a positive lens in the crystal, but to a significantly lesser degree. Self-focusing is the result of the dependence of the index of refraction on the intensity of the light propagating in the material. In these experiments, the effective lens generated by self-focusing was estimated to be of the order of $\sim 10^3$ m, so thermal lensing is the dominant effect in generating a stable resonator. However, self-focusing has the potential to be more important if the Nd:YAG lasers were to be operated as pulsed rather than cw lasers.

Unlike the fixed geometry inherent in coupled semiconductor lasers, here we have the freedom to continuously vary the overlap of the lasing fields by varying the pump beam separation. Typically, both pump beams are focused in the crystal to a radius, measured at $1/e^2$ of the peak intensity, of $r \approx 17$ μm while the lasing intensity beam radii are $r \approx 220$ μm. In this study, the separation d between the pump beam centers was always larger than 350 μm, which implies that the coupling between the lasers is entirely through spatial overlap of their fields, and not through direct coupling of the pump beams. For pump beam separations $d \leq 350$ μm, we find that the thermal lensing distorts the two distinct lasing beams and they tend to combine into a single higher-order lasing mode rather than maintain their separate identity as lasers.

We can determine whether some degree of coherence exists between the two lasers by observing the far-field output of the two lasers. As shown in Fig. 2(a), two parallel uncoupled TEM_{00} lasers will add incoherently to produce a far-field pattern similar to that of a single TEM_{00} laser. In this figure the experimentally measured incoherent sum is shown together with the profiles of the two separate lasers. The two lasers are generated as described above with a pump spot separation of $d = 1.5$ mm. Next, in Figs. 2(b) and 2(c), we show the far-field pattern of two strongly coupled lasers, for a pump separation of $d = 0.60$ mm. The two individual beams are now phase locked with a phase difference of π, and a two-lobed far-field pattern is obtained. This pattern is characteristic of *spatially separated* coherent TEM_{00} beams with a constant π phase difference and should not be confused with a TEM_{01} mode pattern. In fact, if one pump beam is blocked, a single TEM_{00} mode is still observed. If the two beams could be made to lase with zero phase difference, the output pattern would assume the more desirable form of a strong central peak with small side lobes. Although we are unable to force the two coupled lasers to lase intrinsically with zero phase difference, we can shift the phase of one beam relative to the other by using a binary optic phase plate with a π-phase step.

A binary phase plate was fabricated with this aim, but it turned out to create a $3\pi/4$ phase step instead of π, due to a difficulty in the etching process. However, it was still possible to produce a predominantly single-lobed far-field pattern with this plate. The result of insertion of this plate just beyond the output coupler is shown in Fig. 2(d). A comparison is made of the expected and measured profiles, with excellent agreement.

To provide a quantitative measurement of the coherence of the two lasers, we determined the visibility of the fringes formed by the interference of the two laser beams. A lens and a beam splitter produced two separate near-field images of the output (see Fig. 1), at which point apertures were used to select opposite beams in the two paths. The two beams were then overlapped at a small relative angle on the sensor of the charge-coupled-device (CCD) camera. The pattern was digitized by a framegrabber and analyzed on a microcomputer to calculate the visibility. Although the two beams propagate ≈ 4 m in air before reaching the camera, the generated fringe pattern is not affected noticeably by atmospheric phase fluctuations. The relative propagation angle was shallow enough such that both beams traveled nearly identical paths.

The fringes acquired by the camera-framegrabber system were averaged over a time of ≈ 10 ms. The video camera acquires 30 frames per second, allowing us to examine only slow variations in the visibility. An example of a high visibility fringe pattern is shown in Fig. 3. A line profile through the middle of this pattern allowed us

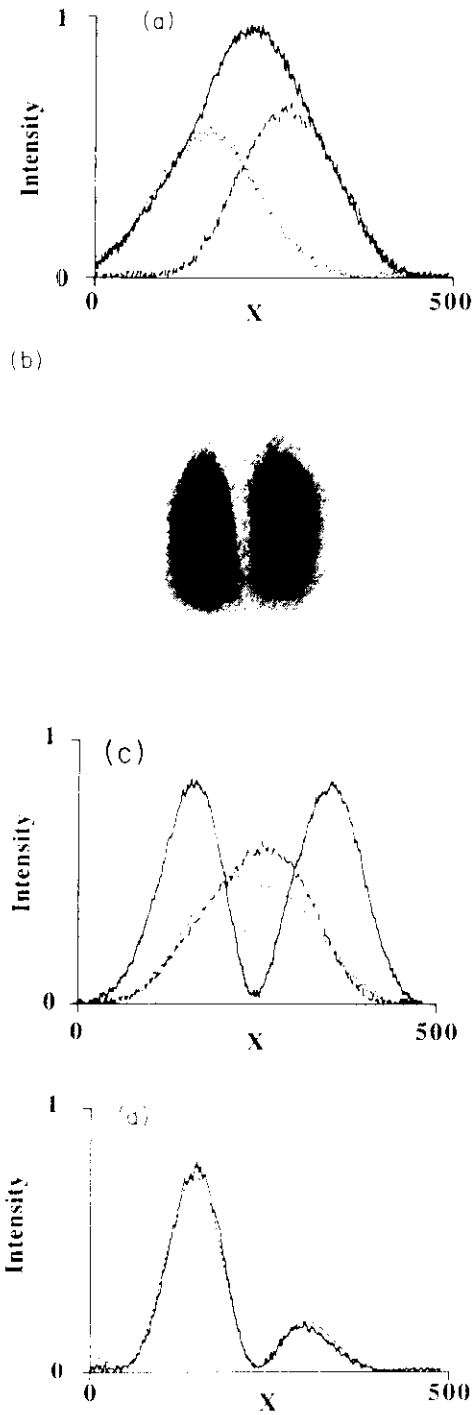

FIG. 2. Measured far-field output intensity. (a) Profile of the far-field intensity for two uncoupled lasers, showing the total intensity and the individual laser intensities. The separation of the two lasers is $d=1.5$ mm. Solid line, total intensity; dashed line, intensity of laser 1; dotted line, intensity of laser 2. The x axis gives the pixel number on the CCD sensor. (b) Two-lobed far-field intensity for two coupled lasers phase-locked π out of phase for $d=0.60$ mm. (c) Profile of the intensity for two coupled lasers, showing the total intensity and the individual laser intensities for $d=0.60$ mm. Solid line, total intensity; dashed line, intensity of laser 1; dotted line, intensity of laser 2. (d) Two-lobed output intensity profile corrected to a predominantly single-peaked profile by a binary phase plate. Dashed line, theoretically predicted profile after correction by phase plate; solid line, measured intensity profile.

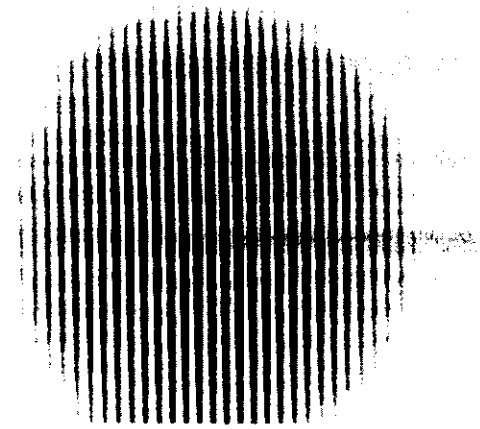

FIG. 3. A representative high visibility fringe pattern acquired by the camera-framegrabber system of Fig. 1, showing a high degree of coherence between the two lasers.

to calculate the visibility, as will be described in the next section. Measurements were made approximately at twice the threshold value for the pumping.

III. EXPERIMENTAL RESULTS

We recall [7] that the intensity of the interference pattern formed by the overlap of wave fronts from two light sources 1 and 2 is (after time averaging)

$$\langle I\rangle=\langle|u_1|^2\rangle+\langle|u_2|^2\rangle+2|\Gamma(\tau)|\cos(\omega\tau+\varphi_\Gamma)\ , \tag{3.1}$$

where u_1 and u_2 are the complex, slowly varying amplitudes of the two sources and

$$\Gamma(\tau)=\langle u_1(\mathbf{r}_1,t_1)u_2^*(\mathbf{r}_2,t_2)\rangle\ ,\quad \tau=t_2-t_1\ .$$

φ_Γ arises from an initial phase difference between the two waves. The visibility of the fringes is defined as

$$v=\frac{\langle I\rangle_{\max}-\langle I\rangle_{\min}}{\langle I\rangle_{\max}+\langle I\rangle_{\min}}=\frac{2|\Gamma(\tau)|}{\langle|u_1|^2\rangle+\langle|u_2|^2\rangle}\ . \tag{3.2}$$

If the two lasers are independent, we expect that the time-averaged interference pattern will have zero visibility if the averaging is done over a time long compared to the coherence time of each laser. In our case, the time average is taken over a $\approx$10-ms period, which is long compared to the coherence time of each separate laser ($\tau_{\rm coh}\lesssim 10\ \mu$s).

The calculation of the visibility utilizes the central five or six peaks of the interference pattern. Samples of interference patterns are shown for separations of the pump beams of 1.8, 1.1, and 0.40 mm in Figs. 4(a), 4(b) and 4(c), respectively. In Fig. 4(a), the two lasers are well separated, and the interference pattern yields $v\approx 0$. The visibility measured increases to $v=0.91$ in Fig. 4(c). The accompanying Figs. 4(d)–4(f) show the corresponding separations of the laser beams, represented by their intensity profiles and the circles of $1/e^2$ radii. It is clear that a very small amount of field overlap creates a transition from an incoherent to a coherent phase relationship.

Visibility measurements were performed for pump beam separations d, in the range $0.35<d<2.0$ mm. The

maximum visibility calculated as described above is shown plotted as a function of the pump beam separation d in Fig. 5. A sharp transition in the visibility is seen for a separation slightly greater than 1 mm, from $v \approx 1$ to 0. We will discuss possible reasons for the scatter of points in the high visibility end of this plot in Sec. V. To interpret these experimental measurements we present a model for these two coupled lasers in the next section, and examine the predictions from it in the subsequent sections.

IV. LASER MODEL

We have chosen the simplest model that will provide an interpretation of our experimental results; there are many possible refinements and these will be discussed in Sec. VI. The model for the two coupled lasers consists of equations for the complex fields E and the gains G of the lasers,

$$\frac{dE_1}{dt} = \frac{1}{\tau_c}[(G_1 - \alpha_1)E_1 + \kappa E_2] + i\omega_1 E_1 + \sqrt{\epsilon_1}\xi_1(t) , \tag{4.1}$$

$$\frac{dG_1}{dt} = \frac{1}{\tau_f}[p_1 - G_1 - G_1|E_1|^2] , \tag{4.2}$$

$$\frac{dE_2}{dt} = \frac{1}{\tau_c}[(G_2 - \alpha_2)E_2 + \kappa E_1] + i\omega_2 E_2 + \sqrt{\epsilon_2}\xi_2(t) , \tag{4.3}$$

$$\frac{dG_2}{dt} = \frac{1}{\tau_f}[p_2 - G_2 - G_2|E_2|^2] . \tag{4.4}$$

In these equations, τ_c is the cavity round trip time (0.2 ns), τ_f is the fluorescence time (240 μs) of the upper lasing level of the Nd^{3+} ion (1064-nm transition), p_k and

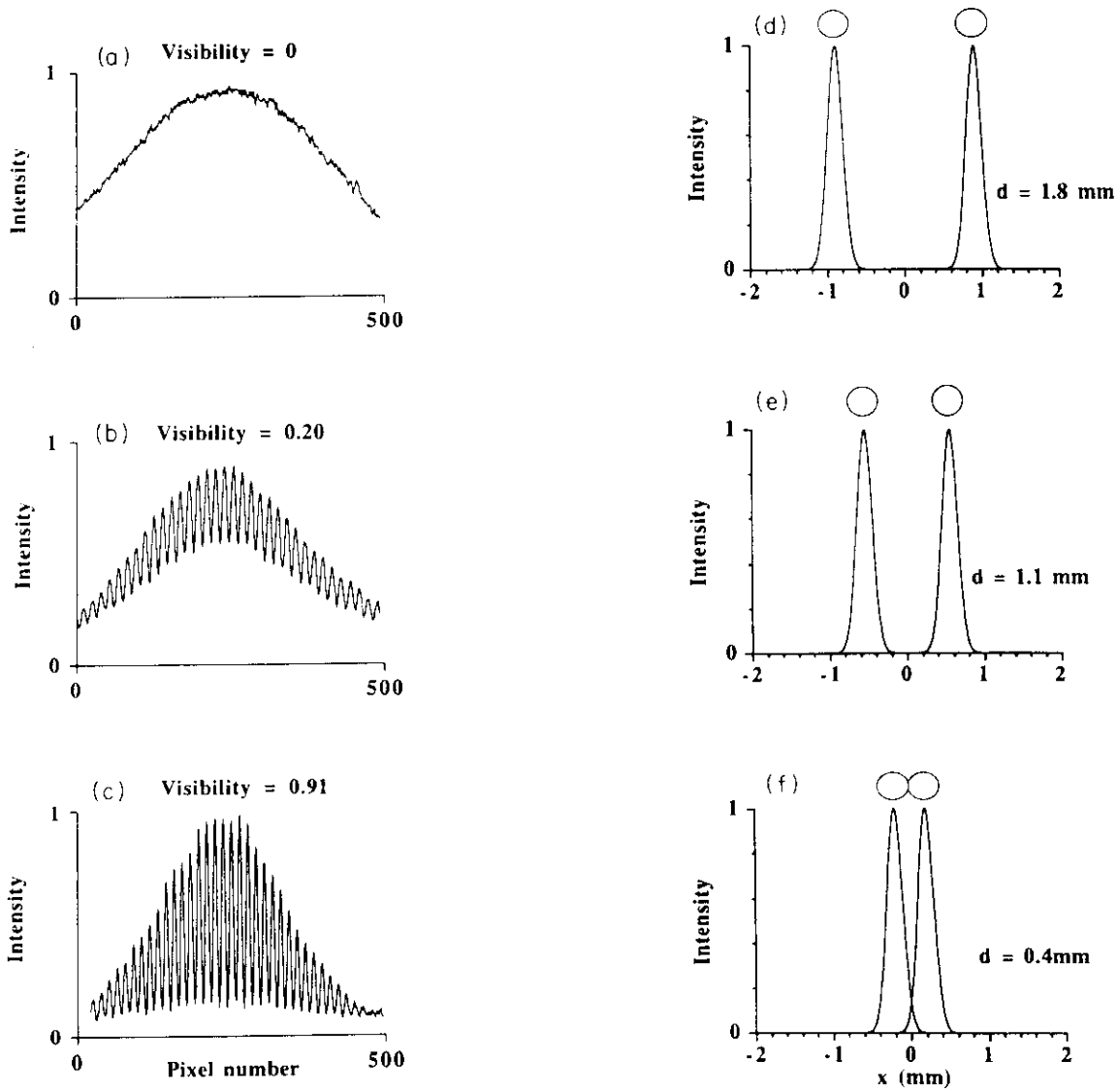

FIG. 4. (a)–(c) Experimentally measured low, medium, and high visibility interference fringes obtained for different pump beam separations of $d = 1.8$, 1.1, and 0.40 mm, respectively. (d)–(f) Intensity profiles of the laser beams and circles of $1/e^2$ radii ($r = 220$ μm) for $d = 1.8$, 1.1, and 0.40 mm, respectively, showing the small amount of spatial overlap between lasers that is sufficient to induce mutual coherence between the two lasers.

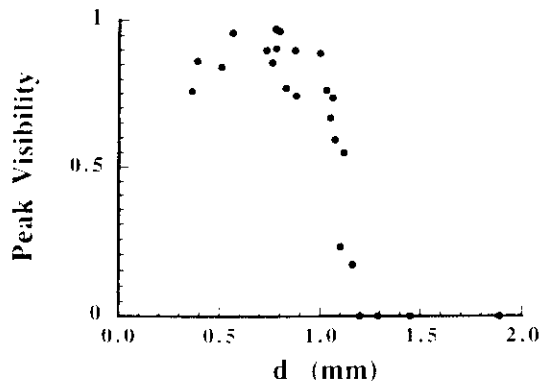

FIG. 5. Experimental values of the maximum fringe visibility as a function of the separation d between the two lasers.

α_k (≈ 0.01) are the pumping and cavity loss coefficients, while ω_k are the detunings of the lasers from a common cavity mode. The index $k=1,2$ stands for the two lasers. The last terms on the right-hand sides of the gain equations (4.2) and (4.4) account for self-saturation of the gains. Spontaneous emission, present in both lasers, is modeled by the noise source terms $\sqrt{\epsilon_k}\xi_k(t)$, where

$$\langle \xi_j(t)\xi_k^*(t')\rangle = 2\delta_{jk}\delta(t-t') . \tag{4.5}$$

The noise sources are independent, Gaussian, and δ-function correlated in time.

The κE_k terms in the field equations represent the coupling between the two lasers through spatial overlap of the electric fields. We have not included any coupling of the lasers through sharing of the inversions, since the pump beams do not overlap to any appreciable extent. Assuming that each laser field has a Gaussian intensity profile and a constant phase front, the transverse field can be written as

$$E_k'(x,y,t) = \frac{E_k(t)}{2\pi\sigma^2}\exp\left[-\frac{x^2+y^2}{2\sigma^2}\right] , \tag{4.6}$$

where σ is related to the $1/e^2$ radius of the intensity profile by $r=\sqrt{2}\sigma$. The overlap integral of the two beams separated by a distance d is given by

$$\int_{-\infty}^{\infty}\int_{-\infty}^{\infty} dx\,dy E_1'(x+d,y,t)E_2'^*(x,y,t) = \frac{E_1(t)E_2^*(t)}{4\pi\sigma^2}\exp\left[-\frac{d^2}{4\sigma^2}\right] . \tag{4.7}$$

The coupling coefficient κ is obtained from the overlap integral through appropriate normalization such that $|\kappa|=1$ when $d=0$. Then,

$$\kappa = \pm\exp\left[-\frac{d^2}{4\sigma^2}\right] . \tag{4.8}$$

The question arises whether κ should be complex. A strictly imaginary coupling coefficient corresponds to conservative coupling, while a strictly real coefficient corresponds to nonconservative (dissipative) coupling. Considering the nature of coupling between the lasers, we take the simple point of view that κ is predominantly real, and choose its sign in the equations to correspond to the experimentally observed results for the relative phases of the two coupled lasers, as will be explained later in this section.

Equations (4.1) and (4.3) can be written in terms of the intensity I_k and phase φ_k of each beam. In the Stratonovich calculus, Eqs. (4.1)–(4.4) are equivalent to the following [8]:

$$\frac{dI_1}{dt} = \frac{2}{\tau_c}[(G_1-\alpha_1)I_1 + \kappa\sqrt{I_1I_2}\cos(\varphi_2-\varphi_1)] + \epsilon_1 + 2\sqrt{\epsilon_1 I_1}\eta_1^I(t) , \tag{4.9}$$

$$\frac{d\varphi_1}{dt} = \omega_1 + \frac{1}{\tau_c}\left[\frac{I_2}{I_1}\right]^{1/2}\kappa\sin(\varphi_2-\varphi_1) + \left[\frac{\epsilon_1}{I_1}\right]^{1/2}\eta_1^{\varphi}(t) , \tag{4.10}$$

$$\frac{dG_1}{dt} = \frac{1}{\tau_c}[p_1 - G_1 - G_1I_1] , \tag{4.11}$$

$$\frac{dI_2}{dt} = \frac{2}{\tau_c}[(G_2-\alpha_2)I_2 + \kappa\sqrt{I_1I_2}\cos(\varphi_1-\varphi_2)] + \epsilon_2 + 2\sqrt{\epsilon_2 I_2}\eta_2^I(t) , \tag{4.12}$$

$$\frac{d\varphi_2}{dt} = \omega_2 + \frac{1}{\tau_c}\left[\frac{I_1}{I_2}\right]^{1/2}\kappa\sin(\varphi_1-\varphi_2) + \left[\frac{\epsilon_2}{I_2}\right]^{1/2}\eta_2^{\varphi}(t) , \tag{4.13}$$

$$\frac{dG_2}{dt} = \frac{1}{\tau_f}[p_2 - G_2 - G_2I_2] . \tag{4.14}$$

The $\eta_j^{\alpha}(t)$ are real Gaussian white-noise sources of zero mean and obey

$$\langle \eta_j^{\alpha}(t)\eta_k^{\beta}(t')\rangle = \delta_{jk}\delta_{\alpha\beta}\delta(t-t') . \tag{4.15}$$

We assume that a stable steady state exists for the intensity of each laser. The intensity of each beam fluctuates about the mean value due to spontaneous emission noise. Neglecting these fluctuations and assuming equal average intensities for the two beams, we get from equations (4.10) and (4.13) the following single equation for the phase difference $\varphi \equiv (\varphi_2-\varphi_1)$ of the two lasers:

$$\frac{d\varphi}{dt} = (\omega_2-\omega_1) - \frac{2}{\tau_c}\kappa\sin(\varphi) + \left[\frac{\epsilon_2}{\langle I_2\rangle}\right]^{1/2}\eta_2^{\varphi}(t) - \left[\frac{\epsilon_1}{\langle I_1\rangle}\right]^{1/2}\eta_1^{\varphi}(t) . \tag{4.16}$$

The deterministic part of this equation corresponds to the Adler equation [9] which has been widely used in the study of coupled oscillators. The synchronization of an electronic oscillator with an externally injected signal gives rise to the same stochastic equation for the phase when the amplitude evolves so rapidly that it can be adiabatically eliminated as was studied by Stratonovich [10]. A similar stochastic equation also describes the voltage due to thermal noise in the dc Josephson effect, as shown

by Ambegaokar and Halperin [11]. Through combination of the noise source terms, Eq. (4.16) may be rewritten as the Langevin equation

$$\frac{d\varphi}{dt} = -\frac{dV(\varphi)}{d\varphi} + \sqrt{D_\varphi}\eta(t) , \tag{4.17}$$

where

$$D_\varphi = \frac{\epsilon_1}{\langle I_1 \rangle} + \frac{\epsilon_2}{\langle I_2 \rangle} . \tag{4.18}$$

$\eta(t)$ is a Gaussian white-noise source of zero mean and correlation

$$\langle \eta(t)\eta(t') \rangle = \delta(t-t') \tag{4.19}$$

and

$$V(\varphi) = -(\omega_2-\omega_1)\varphi - \frac{2}{\tau_c}\kappa\cos\varphi \tag{4.20}$$

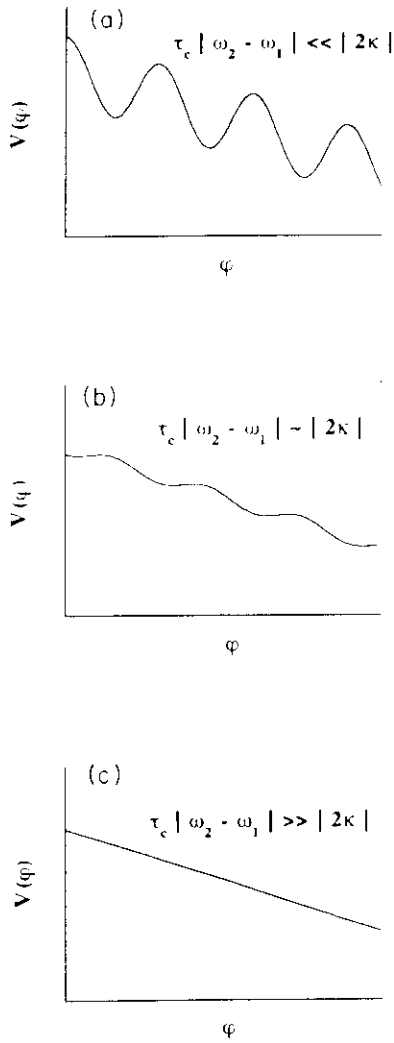

FIG. 6. Schematic plot of the "potential" $V(\varphi)$ of Eq. (4.20) for different relative magnitudes of detuning frequency $(\omega_2-\omega_1)$ and coupling strength κ. (a) Potential which produces phase locking, $\tau_c|\omega_2-\omega_1| \ll |2\kappa|$. (b) Potential at transition region between phase-locking and free-running phases, $\tau_c|\omega_2-\omega_1| \approx |2\kappa|$. (c) Potential when the detuning dominates the coupling strength and no phase locking occurs, $\tau_c|\omega_2-\omega_1| \gg |2\kappa|$.

is the associated "potential" for the overdamped motion of the phase.

Figures 6(a)–6(c) show representative plots of the potential $V(\varphi)$ for three different sets of values of κ and $\tau_c|\omega_2-\omega_1|$. When $\tau_c|\omega_2-\omega_1| \ll |2\kappa|$, V is a sinusoidal potential, and the system resides in one of the local minima, located at $\varphi = 2n\pi$ $(n=0,1,2,\ldots,)$ for $\kappa>0$ and at $\varphi=(2n+1)\pi$ for $\kappa<0$. Experimentally, we have only observed $\varphi=\pi$ for the two phase-locked lasers, thus we will only consider $\kappa<0$. With the choice of $\kappa<0$ in the model equations (4.1)–(4.4), the nonconservative nature of the coupling causes two out-of-phase fields to reinforce each other while two in-phase fields are mutually destructive. For small noise strengths, jumps from one minimum to another will occur extremely infrequently. When $\tau_c|\omega_2-\omega_1| \approx |2\kappa|$, the potential shape of Fig. 6(b) is realized, and noise is most important in this regime. The system motion is a combination of sliding down the edges of the "staircase" with diffusion on the plateaus. The lasers lock imperfectly and we may expect that large fluctuations in the visibility will be observed for operation in this range of coupling. The measured visibility fluctuations are apparent in successive averages over the ~10-ms time window for which v is calculated.

For the extreme situation $\tau_c|\omega_2-\omega_1| \gg |2\kappa|$ [Fig. 6(c)], the linear term dominates the potential and the phase difference φ evolves toward $\pm\infty$, depending on the sign of $(\omega_2-\omega_1)$. The lasers will be completely unlocked in phase, and we may expect zero visibility in this case.

In our experiments there may be fluctuations in the value of the detuning of the lasers $(\omega_2-\omega_1)$ due to environmental changes. The coupling coefficient κ can be changed by varying the pump beam separation, and small fluctuations in beam diameter will produce large fluctuations in κ. To a certain extent these fluctuations can be effectively accounted for in the diffusion coefficient D_φ. In the next section we interpret the experimental results of Sec. III by comparison with the predictions of the theoretical model.

V. THEORETICAL PREDICTIONS AND COMPARISON WITH EXPERIMENTAL OBSERVATIONS

The Langevin equation (4.17) may be simulated numerically, and the phase dynamics of the two lasers examined from stochastic realizations of the time trajectories of the phase difference $\varphi \equiv (\varphi_2-\varphi_1)$. We will present some results obtained from numerical simulations at the end of this section. However, for many purposes, it is very informative to consider the related Fokker-Planck equation for $P(\varphi,t)$, the probability density of the phase difference. This equation is immediately obtained from an examination of Eq. (4.17) as [8]

$$\frac{\partial P(\varphi,t)}{\partial t} = -\frac{\partial}{\partial\varphi}J(\varphi,t) , \tag{5.1}$$

which has the form of a continuity equation where

$$J(\varphi,t) = \left[-\tfrac{1}{2}D_\varphi\frac{\partial}{\partial\varphi} - \frac{dV(\varphi)}{d\varphi}\right]P(\varphi,t) \tag{5.2}$$

is the probability current density. Because any physical observable is periodic in φ with period 2π, the densities P and J must also be periodic. Therefore Eqs. (5.1) and (5.2) must be solved subject to periodic boundary conditions for P, i.e., $P(\varphi+2n\pi,t)=P(\varphi,t)$, for $n=0,\pm1,\pm2,\ldots$.

The physical significance of J can be easily revealed by considering the time-averaged Langevin equation (4.17),

$$\langle\dot{\varphi}\rangle=-\left\langle\frac{dV}{d\varphi}\right\rangle . \tag{5.3}$$

Assuming that the system is ergodic, the right-hand side of Eq. (5.3) can be expressed, using Eq. (5.2), as

$$\begin{aligned}-\left\langle\frac{dV}{d\varphi}\right\rangle&=-\int_0^{2\pi}d\varphi'\frac{dV}{d\varphi'}P(\varphi,t)\\&=\int_0^{2\pi}d\varphi'\left[J+\tfrac{1}{2}D_\varphi\frac{\partial P}{\partial\varphi'}\right]\\&=\int_0^{2\pi}d\varphi' J(\varphi') ,\end{aligned} \tag{5.4}$$

where we have assumed periodic boundary conditions for the probability density $P(0,t)=P(2\pi,t)$. Combining Eqs. (5.3) and (5.4) we conclude that the integrated current $\int_0^{2\pi}d\varphi' J(\varphi')$ is just the effective detuning frequency between the laser fields, i.e.,

$$\Omega_{\rm eff}=\langle\dot{\varphi}\rangle=\int_0^{2\pi}d\varphi' J(\varphi') . \tag{5.5}$$

Note that in the stationary state J will be independent of φ, so that the right-hand side of Eq. (5.5) is simply $2\pi J$.

Because the experimental data do not involve any short-time transients, we look for the stationary solution of Eqs. (5.1)–(5.2). This solution is characterized by the fact that P is independent of t, and J is constant, independent of φ and t. Note that, unlike many other problems where $J=0$, in this case the tilt of the potential requires $J\neq0$. We get [10]

$$P(\varphi)=C\exp\left[-\frac{2}{D_\varphi}V(\varphi)\right]\int_\varphi^{\varphi+2\pi}d\varphi'\exp\left[\frac{2}{D_\varphi}V(\varphi')\right] , \tag{5.6}$$

and the probability current is

$$J=C\frac{D_\varphi}{2}\left[1-\exp\left[\frac{4\pi}{D_\varphi}(\omega_2-\omega_1)\right]\right] , \tag{5.7}$$

where C is a constant normalizing $P(\varphi)$ to unity.

The visibility of the interference fringes formed by the superposition of the laser beams can be calculated from Eq. (5.6), since

$$v=\frac{2|\langle E_1^*E_2\rangle|}{\langle|E_1|^2\rangle+\langle|E_2|^2\rangle}=|\langle\exp(i\varphi)\rangle| \tag{5.8}$$

for fields of equal magnitude. Then,

$$v=\sqrt{\langle\cos\varphi\rangle^2+\langle\sin\varphi\rangle^2} . \tag{5.9}$$

The averages of the $\sin\varphi$ and $\cos\varphi$ functions are obtained using $P(\varphi)$. From (4.20), (5.3), and (5.5), we have

$$\langle\sin\varphi\rangle=-\frac{\tau_c}{2\kappa}[\Omega_{\rm eff}-(\omega_2-\omega_1)] , \tag{5.10}$$

but we could not find a similar expression for $\langle\cos\varphi\rangle$.

From Eqs. (4.20) and (5.6) it is clear that there are only two effective independent dimensionless parameters, namely

$$A=\frac{D_\varphi}{(\omega_2-\omega_1)}\ \text{and}\ B=\frac{2\kappa}{\tau_c(\omega_2-\omega_1)} , \tag{5.11}$$

where according to Eq. (4.8) κ depends on the pump separation d and the beamwidth σ. The parameter A plays the role of an effective diffusion rate whereas parameter B is the effective coupling rate. In the limit $|B|\ll1$ (weak coupling) the exponent $(2/D_\varphi)V(\varphi)$ in Eq. (5.6) can be approximated as $(2/D_\varphi)V(\varphi)\approx-2\varphi/A$, so that the probability distribution P becomes constant, independent of φ. Normalizing, we have $P(\varphi)=1/2\pi$. As φ is uniformly distributed in the interval $[0,2\pi]$, the averages $\langle\sin\varphi\rangle$ and $\langle\cos\varphi\rangle$ vanish, so that the visibility vanishes as well. For weak coupling and in the limit $D_\varphi\to0$, the Langevin equation (4.17) reduces to the well-known Adler equation [9,12]. It has the analytic stationary state solution

$$\tan\left[\frac{\varphi}{2}\right]=\frac{\Omega_{\rm eff}}{(\omega_2-\omega_1)}\tan\left[\frac{\Omega_{\rm eff}(t-t_0)}{2}\right]-\frac{2\kappa}{\tau_c(\omega_2-\omega_1)} , \tag{5.12}$$

where $\Omega_{\rm eff}=[(\omega_2-\omega_1)^2-(2\kappa/\tau_c)^2]^{1/2}$. In this case, both lasers are monochromatic, but due to the nonzero frequency difference, the visibility will vanish.

In the limit $|B|\gg1$ (strong coupling) the lasers will phase lock to each other, i.e., $\langle\dot{\varphi}\rangle\approx0$. The locking angle φ_0 corresponds to a minimum of the potential given by Eq. (4.20), so that $\varphi_0=\pi-\arcsin[(\omega_2-\omega_1)\tau_c/(2\kappa)]$. We can approximate the potential by a quadratic form and the probability density by a Gaussian, since φ will stay close to this lock angle, i.e.,

$$\begin{aligned}V(\varphi)&\approx V(\varphi_0)-\frac{\kappa}{\tau_c}(\varphi-\varphi_0)^2\cos(\varphi_0)\\&=V(\varphi_0)+\tfrac{1}{2}\gamma_{\rm eff}(\varphi-\varphi_0)^2 ,\end{aligned} \tag{5.13}$$

$$P(\varphi)=\left[\frac{\gamma_{\rm eff}}{\pi D_\varphi}\right]^{1/2}\exp\left[-\frac{\gamma_{\rm eff}}{D_\varphi}(\varphi-\varphi_0)^2\right] , \tag{5.14}$$

where $\gamma_{\rm eff}=[(2\kappa/\tau_c)^2-(\omega_2-\omega_1)^2]^{1/2}$. The visibility in this approximation is given by

$$v=\exp(-D_\varphi/4\gamma_{\rm eff}) . \tag{5.15}$$

Figure 7 shows a comparison of the experimental measurements of the visibility versus beam separation with those predicted from the theory, for several sets of parameters. We have a reasonable estimate for σ because we can measure the beam radii when the beams are well separated. However, there is some distortion of the beams when they are overlapped, and σ can only be taken to be an estimate, not an accurately determined pa-

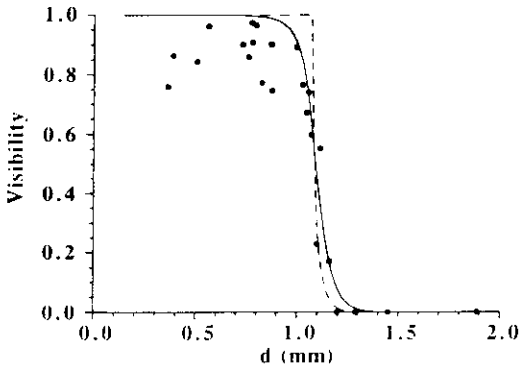

FIG. 7. Experimental and theoretical results for the visibility as a function of the beam separation. Dots correspond to the experimental measurements shown in Fig. 5. The theoretical visibility is calculated from Eqs. (5.6) and (5.9) for $(\omega_2-\omega_1)=5000$ rad/s, $\sigma=0.141$ mm, and $D_\varphi=8\ s^{-1}$ (dashed line); $(\omega_2-\omega_1)=5000$ rad/s, $\sigma=0.175$ mm, and $D_\varphi=1\times10^6\ s^{-1}$ (solid line).

rameter. The parameter A which measures the ratio between noise strength and the detuning is a parameter that is not determined easily. From estimates of the spontaneous emission noise, one would arrive at a value of $A\approx10^{-3}$, but external sources of noise are far greater in magnitude, and may give $A\approx10^{2}$. The theoretical curves shown in Fig. 7 reveal that the fits are not very sensitive to the noise strength, over several orders of magnitude. The observed transition from coherent to incoherent behavior is very well reproduced by theoretical predictions. For the phase-locked regime we note that the visibility measurements are quite scattered, and consistently lower than the predictions. There are several possible reasons for this feature. We have neglected the multimode nature of the laser fields, as well as the possibility of intensity fluctuations in the laser beams. Pump fluctuations have been entirely neglected as well. Given these many sources of fluctuations that are not accounted for, it is not surprising that the theory provides an upper bound to the visibility measurements in Fig. 7. With these points in mind, the agreement between theory and experiment is very good.

The Langevin equation (4.17) may be directly simulated to examine the behavior of the phase difference φ in time for different characteristic shapes of the potential $V(\varphi)$. Ten trajectories each are plotted in Figs. 8(a)–8(c), corresponding to the potentials of Figs. 6(a)–6(c). In Fig. 8(a) the phase difference locks quickly at π, and remains locked thereafter, while in Fig. 8(b), φ jumps at random times from one step of the potential to the next. In Fig. 8(c), the evolution of φ is almost linear in time, indicating the absence of phase locking between the lasers.

The three situations discussed above are characterized by the measurements of visibility versus time shown in Fig. 9. The visibility itself is a time-averaged measurement, but the camera system shown in Fig. 1 predeter-

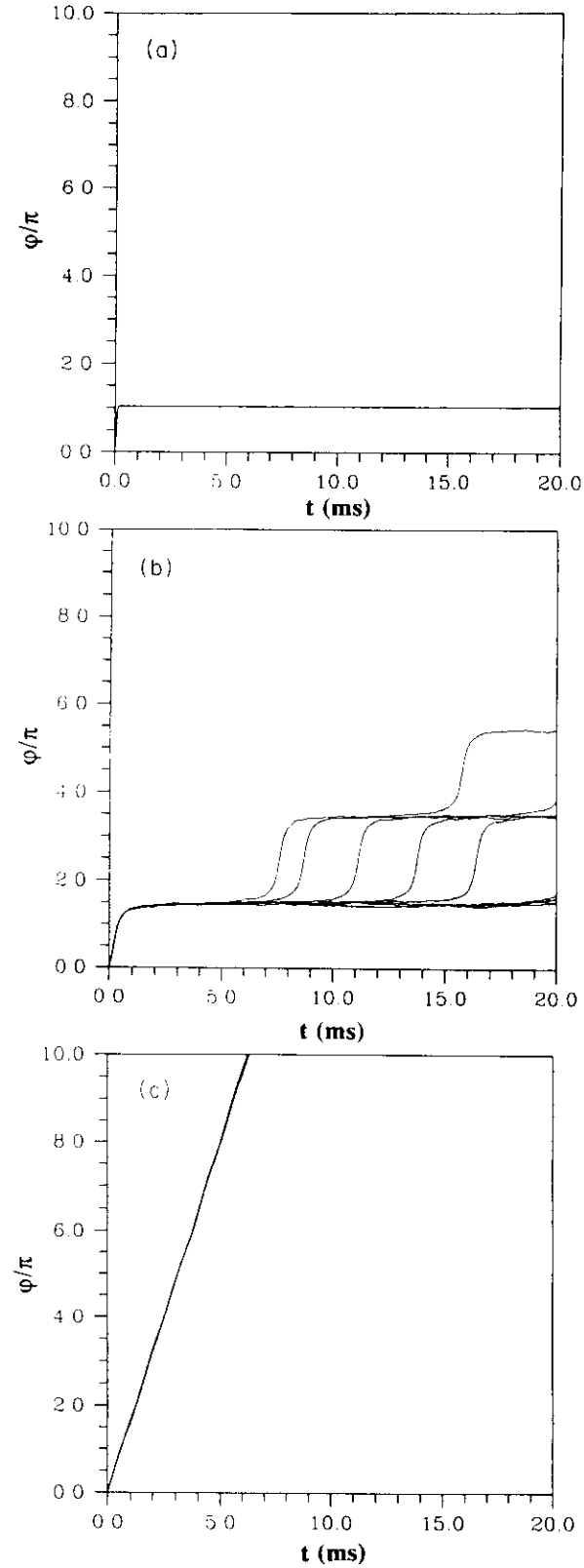

FIG. 8. Plots of ten phase trajectories obtained from the numerical integration of Eq. (4.17) for $(\omega_2-\omega_1)=5000$ rad/s, $D_\varphi=4\ s^{-1}$, and different values of the coupling coefficient: (a) The two lasers quickly lock at π out of phase, for $2\kappa/\tau_c=-5\times10^4\ s^{-1}$. (b) Intermediate transient locking regime, where the noise induces 2π phase jumps at random time intervals between "constant" phase states, for $2\kappa/\tau_c=-5\times10^3\ s^{-1}$. (c) Unlocked regime, where the phase difference evolves nearly linearly in time, for $2\kappa/\tau_c=-5\times10^2\ s^{-1}$.

mines the time averaging-window to be of the order of 10 ms. Figure 9(a) shows that, for strongly coupled lasers that produce high visibility fringes, the visibility remains relatively constant in time. When the distance between the two lasers is increased so that it is within the narrow transition region shown in Fig. 5, large fluctuations are seen in the visibility, as shown in Fig. 9(b). Increasing the laser separation beyond the transition region reduces the visibility to zero for all time, as shown in Fig. 9(c). The visibility measurements of Figs. 9(a)–9(c) correspond to the respective phase dynamics of Figs. 8(a)–8(c).

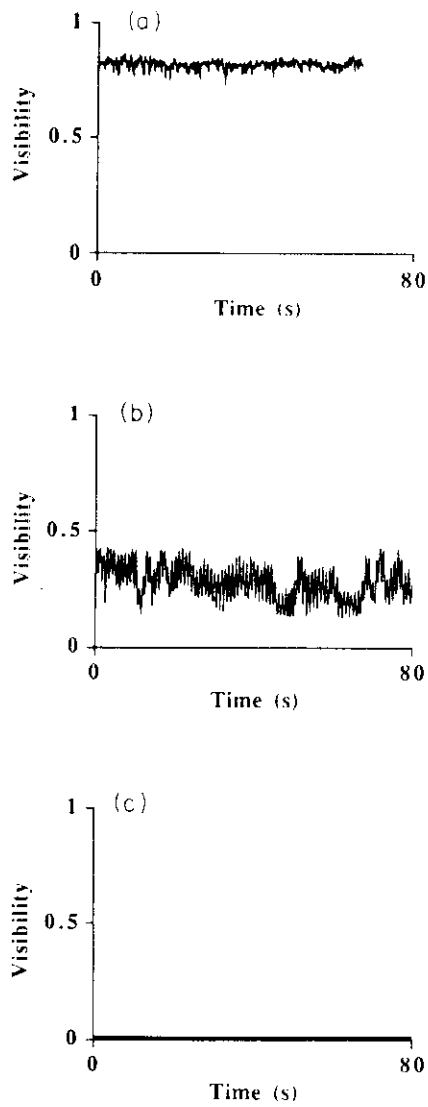

FIG. 9. Experimentally measured visibility as a function of time for different laser separations d. (a) Two strongly coupled lasers produce stable interference fringes for $d=0.39$ mm. (b) In the intermediate transient locking regime, large fluctuations are seen in the visibility for $d=1.03$ mm. (c) Uncoupled lasers produce zero visibility fringes for $d=1.5$ mm.

VI. DISCUSSION

The experimental results and theoretical predictions presented in the previous sections showed that a critical separation exists for phase locking of two spatially coupled Nd:YAG lasers. The two lasers exhibited stable phase-locking π out of phase for separations less than a critical value. In contrast, evanescently coupled semiconductor lasers display phase locking only in a narrow window of coupling strength, a window which is not always physically achievable [1,2]. It was also demonstrated that a simple phase plate can be used to compensate for the 180° phase difference between the lasers and generate a predominantly single-lobed far-field intensity.

Although the agreement between experimentally measured data and theoretical predictions was quite good, there are several enhancements to the laser model which could be made. The laser model predicted perfect phase locking with $v \approx 1$ for sufficiently small laser separations, but Fig. 5 shows a scatter of corresponding experimentally measured visibilities, with $v < 1$. The model does not include several sources of noise which can reduce the visibility below $v=1$. The model neglected fluctuations in the population inversion induced by spontaneous emission, intensity fluctuations of the pump laser, and fluctuations in the overlap of the laser fields. These additional sources of noise can also contribute to decreased visibility. Furthermore, each laser typically operates with two to five longitudinal modes rather than the single mode assumed in Eqs. (4.1)–(4.4), thus introducing the possibility of fluctuations due to mode competition. The noise strength D_φ was varied from $D_\varphi \sim 10$ to $D_\varphi \sim 10^6$. The effect of increasing D_φ by five orders of magnitude is to cause a smoothing of the visibility curve in Fig. 7 and a slight decrease of the critical separation. The larger value of D_φ may to some extent account for fluctuations in the detuning of the lasers as well as some of the other sources of noise mentioned above that are responsible for the scatter of visibility values when measured on a ~10-ms time scale. It is clear, however, that the theoretical predictions should be regarded as an upper bound to the measured values of the visibility.

It was assumed in the reduction of the model to a single Langevin equation for the phase difference of the two lasers that the intensities have negligible fluctuations, and that there exists a stable steady state. This assumption needs to be reexamined, particularly since the complete form of the coupling coefficient κ and contributions from different coupling mechanisms are not fully understood for the present system. κ was chosen to be real and negative in the model, since this was consistent with the experimental observations, but there is no *a priori* reason for κ to have this form. We can calculate only the magnitude of κ from Eq. (4.8). A more comprehensive calculation of the coupling coefficient is desirable for various coupling mechanisms.

Finally, we mention the existence of solid-state laser arrays with geometries more complex than that of the two parallel lasers studied here, geometries which induce

phase locking at relative phases other than π. A square configuration of four Nd:YAG lasers has been observed to lase with adjacent elements phase-locked π out of phase, but a three-laser triangle was found to be phase locked with a $\pm 2\pi/3$ phase difference between lasers [4]. The only stable phase-locked mode for an odd number N of solid-state lasers arranged in a ring has been predicted [13] to have a constant phase difference between adjacent lasers, where the phase difference is given by $\varphi = \pm\pi(N-1)/N$. The dynamics of both intensity and phase of such complex configurations of lasers remain to be explored.

ACKNOWLEDGMENTS

We thank Jim Beletic, Donald O'Shea, and Menelaos Poutous for fabricating the binary phase plate. We thank Surendra Singh for pointing out some relevant references. L.F. and R.R. were supported by Grant No. DE-FG05-87ER13708 from the Division of Chemical Sciences, Office of Basic Energy Sciences, Office of Energy Research, U.S. Department of Energy. P.C. acknowledges the Dirección General de Investigación Científica y Técnica (DGICYT) (Spain) for support under the MEC-Fulbright program.

*Permanent address: Departament de Física, Universitat de les Illes Balears, E-07071 Palma de Mallorca, Spain.

[1] S. S. Wang and H. G. Winful, Appl. Phys. Lett. **52**, 1774 (1988); H. G. Winful and S. S. Wang, *ibid.* **53**, 1894 (1988). N. Yu, R. K. DeFreez, D. J. Bossert, R. A. Elliot, H. G. Winful, and D. F. Welch, Electron. Lett. **24**, 1203 (1988).

[2] P. Mandel, R-D. Li, and T. Erneux, Phys. Rev. A **39**, 2502 (1989); R-D. Li, P. Mandel, and T. Erneux, *ibid.* **41**, 5117 (1990).

[3] S. A. Shakir and W. W. Chow, Phys. Rev. A **32**, 983 (1985); S. E. Falvey and W. W. Chow, J. Opt. Soc. Am. B **6**, 1894 (1989).

[4] M. Oka, H. Masuda, Y. Kaneda, and S. Kubota, IEEE J. Quantum Electron. **28**, 1142 (1992).

[5] F. T. Arecchi, G. L. Lippi, G. P. Puccioni, and J. R. Tredicce, Opt. Commun. **51**, 308 (1984).

[6] W. Koechner, *Solid-State Laser Engineering* (Springer-Verlag, Berlin, 1988), 2nd ed.

[7] R. Loudon, *The Quantum Theory of Light* (Oxford University, New York, 1983).

[8] H. Risken, *The Fokker-Planck Equation* (Springer-Verlag, Berlin, 1984); C. W. Gardiner, *Handbook of Stochastic Methods* (Springer-Verlag, Berlin, 1983); R. L. Stratonovich, *Topics in the Theory of Random Noise* (Gordon and Breach, New York, 1967), Vol. 1.

[9] R. Adler, Proc. IRE **34**, 351 (1946), reprinted in Proc. IEEE, **61**, 1380 (1973).

[10] R. L. Stratonovich, *Topics in the Theory of Random Noise* (Gordon and Breach, New York, 1967), Vol. 2, Chap. 9.

[11] V. Ambegaokar and B. I. Halperin, Phys. Rev. Lett. **22**, 1364 (1969).

[12] A. Siegman, *Lasers* (University Science Books, Mill Valley, CA, 1986), p. 1143.

[13] M. Silber, L. Fabiny, and K. Wiesenfeld (unpublished).

Experimental Synchronization of Chaotic Lasers

Rajarshi Roy and K. Scott Thornburg, Jr.
School of Physics, Georgia Institute of Technology, Atlanta, Georgia 30332
(Received 30 August 1993)

We report the observation of synchronization of the chaotic intensity fluctuations of two Nd:YAG lasers when one or both the lasers are driven chaotic by periodic modulation of their pump beams.

PACS numbers: 05.45.+b, 42.50.Lc

The synchronization of chaotic nonlinear oscillators has attracted much attention in recent years, motivated by the possibility of practical applications of this fundamental phenomenon. Several papers [1,2] have shown that such synchronization may be achieved in electronic oscillator circuits, with applications in the transmission of information signals masked in a background of chaos, followed by real-time recovery of signals at the receiver. A theory of synchronization of coupled, chaotic, nonlinear oscillators has been developed independently by Rabinovich and co-workers [3] in the context of turbulence in fluids. It has also been known for several years that lasers can exhibit chaotic intensity fluctuations under different circumstances. Winful and Rahman have theoretically investigated the possibility of synchronization of chaotic lasers, and some evidence of such behavior has been found in semiconductor laser arrays [4]. However, a direct test of their predictions on an experimental system where the coupling between the lasers is systematically varied has yet to be performed.

The scheme for chaotic synchronization developed by Pecora and Carroll [1,2] requires that a chaotic system exists, from which one can separate a stable subsystem with only negative Lyapunov exponents. When a chaotic system and a stable response subsystem are linked with a common drive signal, the two may display synchronized chaos. An example of this construction is given by the Lorenz system $dx/dt=\sigma(y-x)$, $dy/dt=rx-y-xz$, $dz/dt=xy-bz$ and the response system $dx'/dt=\sigma(y'-x')$, $dy'/dt=rx-y'-xz'$, $dz'/dt=xy'-bz'$ [2]. While this ingenious scheme has been practically implemented with electronic oscillators, it appears impossible to separate the elements of a chaotic laser and obtain a stable subsystem in precisely this manner.

In this paper we report the observation of synchronization of two coupled, chaotic, Nd:YAG (neodymium doped yttrium aluminum garnet) lasers. The equations that describe the lasers are of the form

$$\frac{d}{dt}\begin{pmatrix}E_1\\N_1\end{pmatrix}=\vec{f}(E_1,N_1,\kappa E_2)$$

and

$$\frac{d}{dt}\begin{pmatrix}E_2\\N_2\end{pmatrix}=\vec{g}(E_2,N_2,\kappa E_1),$$

where the E's and N's are the complex electric fields and the population inversions for the two lasers and κ is a parameter that provides a measure of the mutual coupling between the lasers [4,5]. One or both the lasers may be driven chaotic through a periodic modulation of their pump excitation, and synchronized, chaotic intensity fluctuations may be observed in both cases when the lasers are sufficiently coupled. Thus it is possible, by a somewhat less restrictive procedure than that of Refs. [1] and [2], to obtain synchronized chaotic intensity fluctuations for two lasers. In particular, we show that a master-slave relationship is not necessary to obtain synchronization of chaotic oscillators. Mutual coupling can be used to obtain chaotic synchronization even for the case where the two uncoupled oscillators are both chaotic.

The laser system [Fig. 1(a)] consists of two Nd:YAG lasers of wavelength 1.06 μm generated in the same crystal by two almost equal intensity 514.5 nm pump beams obtained from an argon laser [5]. The spatial separation d of the parallel pump beams may be varied and is much larger (>0.5 mm) than their radius (about 20 μm) within the crystal. There is thus virtually no coupling through overlap of the population inversions of the two lasers; instead, the coupling between the lasers is provided by overlap of the intracavity laser fields of approximate radius 200 μm. The laser cavity consists of a high reflectivity coating (at 1.06 μm) on one end of the 5 mm long laser rod and a flat output mirror with 2% transmittance. The cavity length is 1.5 cm, and the output power of the lasers was measured to be about 5 mW each with a pump excitation of about twice above threshold.

A simple measure of the coupling is obtained from the overlap integral of the two fields, normalized such that the coupling coefficient $|\kappa|=\exp(-d^2/4\sigma^2)$ is unity for $d=0$ and where σ is related to the $1/e^2$ radius r of the intensity profile by $r=\sigma\sqrt{2}$ [5]. At the smallest separation of the beams in this study ($d\sim0.6$ mm) the overlap of the fields is $|\kappa|\sim1.1\times10^{-2}$, while at the largest separation ($d\sim1.5$ mm) $|\kappa|\sim6.1\times10^{-13}$. The coupling between the lasers is varied experimentally by translating the beam combiner in Fig. 1(a), which changes the separation of the pump beams.

The far field of the output from the lasers is observed on a video camera. When the lasers are phase locked (this occurs with a π-phase difference), the far field is a double-lobed pattern with a node in the center. When the lasers are mutually incoherent, the far-field pattern is

0031-9007/94/72(13)/2009(4)$06.00

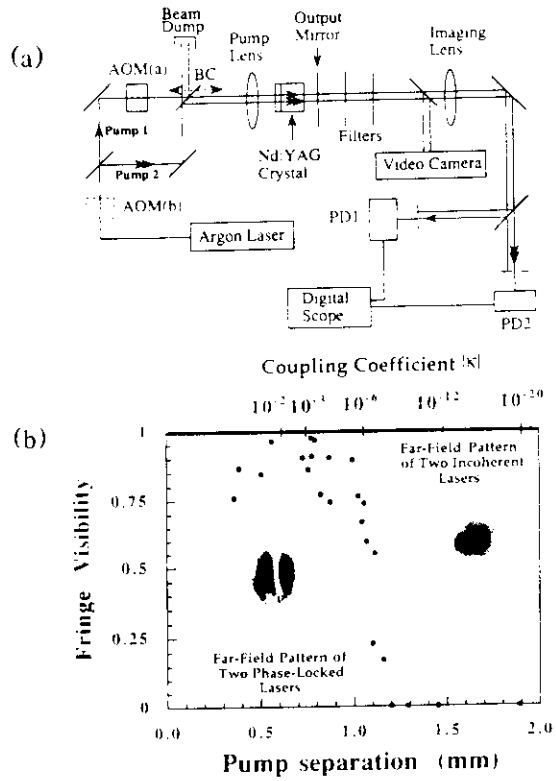

FIG. 1. (a) Experimental system for generating two spatially coupled chaotic lasers and monitoring their outputs. An acousto-optic modulator (AOM) can be placed in position (a) to modulate only laser 1, or in position (b) to modulate both lasers simultaneously. Beam splitters divide the argon laser output into two beams, each of which pumps a spatially separate region in the Nd:YAG crystal. The separation of the beams can be varied by moving the beam combiner, BC. The video camera is used to monitor the beam profiles. A lens is used to image the lasers so that the individual beams can be resolved and monitored by the photodiodes PD1 and PD2. The time traces of the two lasers can be displayed and stored by the digital oscilloscope. (b) Visibility of interference fringes for the superposed laser fields vs pump separation (from Ref. [5]). Also shown are two representative far-field intensity patterns for pump beam separations of $d=0.6$ mm and $d=1.5$ mm.

Gaussian. The lasers are found to be phase locked for separations of less than about 1 mm ($|\kappa| \sim 3.7\times10^{-6}$), and display a very sharp transition from incoherence to coherence with decreasing separation of the pump beams. A plot of the visibility of the interference fringes formed by the superposition of the beams from the two lasers versus the separation of the pump beams is shown in Fig. 1(b), along with representative far field intensity patterns as described above. An imaging lens allows us to examine the near fields of the lasers as well, and two fast photodetectors connected to a digital oscilloscope display the temporal fluctuations of the individual laser intensities. A detailed description of this system of two coupled lasers is contained in Ref. [5], where the phase locking of the lasers through spatial overlap of their electric fields was investigated.

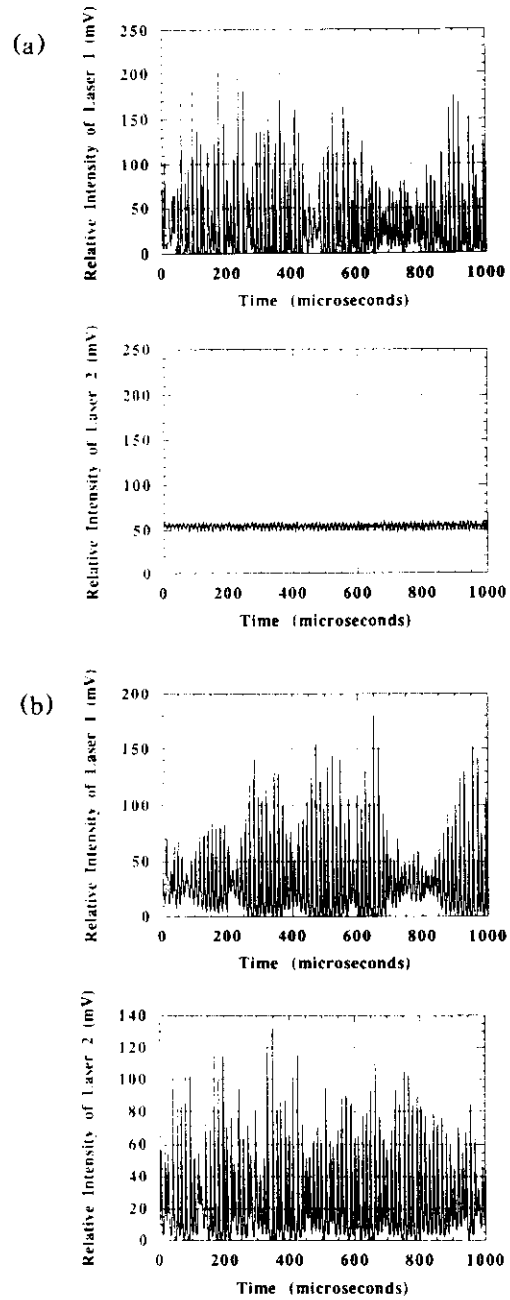

FIG. 2. (a) Relative intensity of the uncoupled lasers, for $d\sim1.5$ mm. Only laser 1 is modulated, and there is no appreciable interaction between the two lasers. (b) Relative intensities of lasers 1 and 2, with the AOM in position (b). Notice the asynchronous fluctuations of the two intensities, typical of the uncoupled case, even though both lasers experience the same pump modulation.

In the Nd:YAG lasers studied here, the decay time of the upper lasing level is $\tau_f\sim240$ μsec, while the round-trip time of light in the cavity is $\tau_c\sim0.12$ nsec. This leads to relaxation oscillations at a frequency $\nu_{\rm rel}=(1/2\pi)[\delta(\gamma/\gamma_{\rm th}-1)/\tau_f\tau_c]^{1/2}$, where $\gamma_{\rm th}$ and γ are the threshold and actual pump rates, δ is the fractional cavity loss ($\sim2\%$) per pass [6]. At a pump excitation of twice the threshold value, $\nu_{\rm rel}\sim130$ kHz. This is in very good

agreement with measured relaxation oscillation frequencies for our laser system. An acousto-optic modulator (AOM) may be used to sinusoidally amplitude modulate a single pump beam in position (a), or to modulate both pump beams simultaneously in position (b), indicated by the dotted lines in Fig. 1(a). If the pump beam of one of the lasers is modulated at close to the relaxation oscillation frequency, the laser intensity may be driven into chaotic fluctuations, as seen in Fig. 2(a). A wide variety of periodic wave forms, including period-doubled oscillations, may be observed for different frequencies and amplitudes of modulation. Similar behavior in other modulated laser systems has been extensively studied in the past [7].

With the AOM in position (a), and for a large separation $d \sim 1.5$ mm of the pump beams within the crystal, the two lasers are effectively *uncoupled*. We see in Fig. 2(a) that laser 1 shows chaotic intensity fluctuations when the frequency and amplitude of modulation of the pump beam are appropriately adjusted. In these experiments, the maximum depth of modulation was adjusted to be about 50%. For a modulation frequency close to the relaxation oscillation frequency of the laser, the intensity fluctuations increase markedly in amplitude and become chaotic. Laser 2 is unaffected by the fluctuations of laser 1 and shows a steady intensity.

If the pump beams of the two uncoupled lasers are both modulated with the AOM in the position shown by the dotted lines, both lasers display chaotic intensity fluctuations that are not synchronized, as shown in Fig. 2(b). This is to be expected, since the lasers are not coupled to any appreciable extent at this large separation, as may be verified from the Gaussian far-field pattern of the laser intensities monitored by the video camera system.

For *intermediate coupling* at a somewhat smaller separation ($d \sim 1$ mm), close to the phase-locking threshold, the two laser intensities are both found to be chaotic and irregular when only the pump beam for laser 1 is modu-

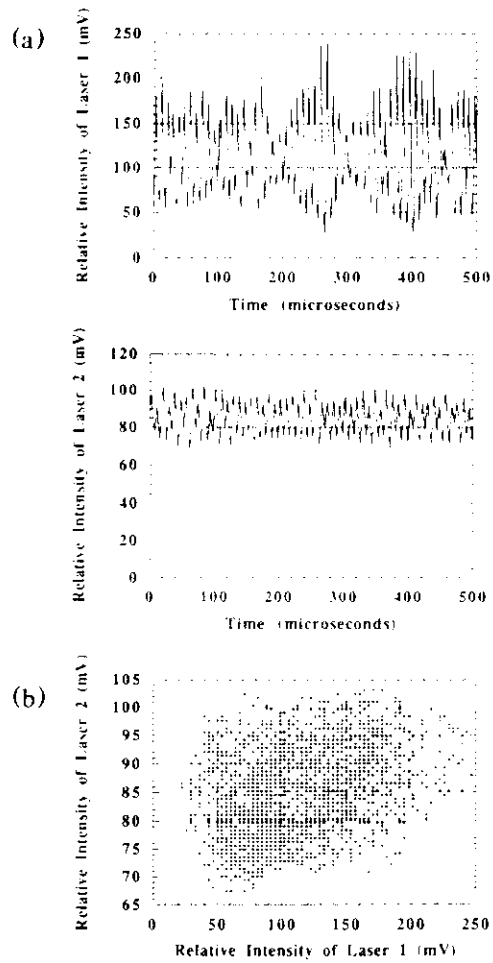

FIG. 3. (a) Relative intensities of two intermediately coupled lasers ($d \sim 1.0$ mm) when only the pump beam for laser 1 is modulated. Although still asynchronous, the modulation of one laser now affects the other appreciably. (b) X-Y plot of the two laser intensities shown in (a). The dispersion of the points indicates that they are not synchronized.

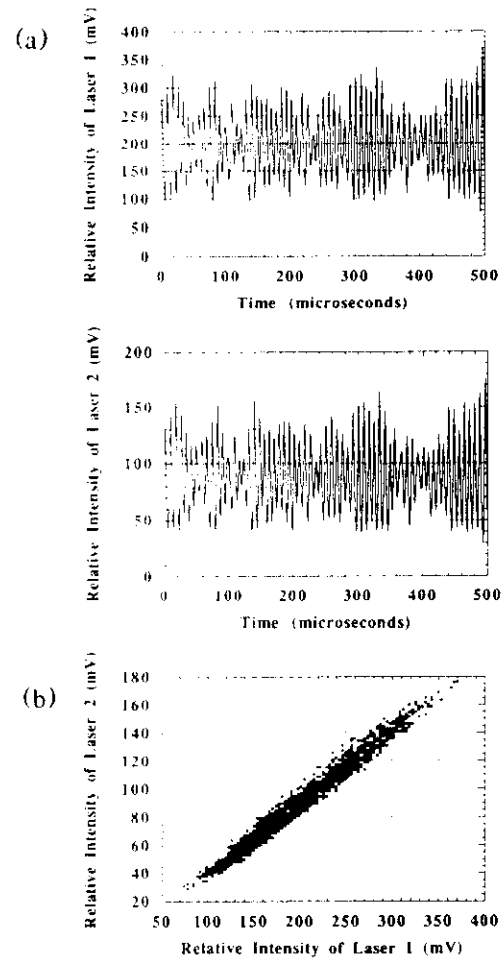

FIG. 4. (a) Relative intensities of two strongly coupled lasers ($d \sim 0.75$ mm) with the pump beam for laser 1 modulated by the AOM. Note the strong synchronization of the two laser intensities. (b) X-Y plot of the two laser intensities shown in (a). Note the strong linearity of this figure, indicating the synchronized nature of the time traces. Compare this figure to Fig. 3(b).

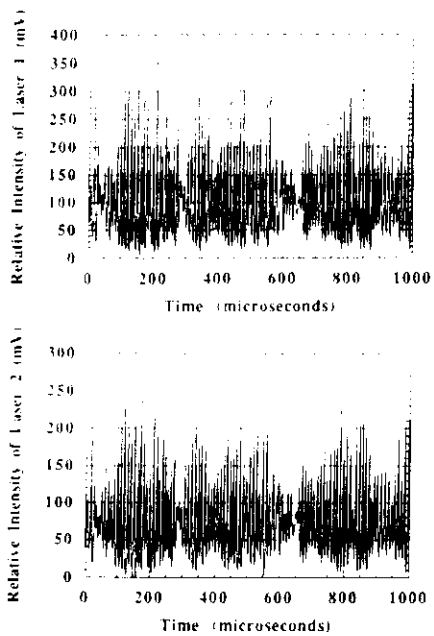

FIG. 5. Relative intensities of two strongly coupled lasers ($d \sim 0.60$ mm), with the AOM in position (b). Notice that, in contrast to the uncoupled case shown in Fig. 2(b), the lasers now fluctuate synchronously.

lated, as shown in Fig. 3(a). Clearly, the chaotic behavior of laser 1 now has a significant influence on its neighbor and destabilizes the intensity of laser 2. However, the plot of the fluctuations of laser 1 vs those of laser 2 displayed in Fig. 3(b) show a random set of points, indicating that the fluctuations are unsynchronized.

For *strong coupling* at a smaller separation ($d \sim 0.75$ mm) of the pump beams, the far-field pattern is distinctly double lobed; this reveals that the lasers are phase locked. Even in this "strong coupling" regime, the overlap of the two laser intensity profiles is extremely small, $|\kappa| \sim 8.8 \times 10^{-4}$. Modulation of the pump beam for laser 1 now leads to well synchronized chaotic fluctuations of the two laser intensities, as shown in the time traces of Fig. 4(a). A plot of the intensity of laser 1 vs the intensity of laser 2 [Fig. 4(b)] is now remarkably different from the random scatter of points shown in Fig. 3(b), and the synchronized nature of the chaotic lasers is evident. Synchronization of the chaotic lasers persists stably over periods of tens of minutes, as long as the temperature and other environmental conditions are maintained constant.

Figure 5 shows the result of modulating both the pump beams simultaneously for strongly coupled lasers with the pump beams separated by 0.6 mm. In contrast to Fig. 2(b), where both the uncoupled lasers are independently chaotic (and thus would have positive Lyapunov exponents), we now see that the two mutually coupled chaotic lasers are well synchronized. The scheme for synchronization is more general than those developed earlier [1,2] where a stable subsystem with negative Lyapunov exponents is necessary.

The laser outputs, though adjusted to be roughly equal in intensity, produce different voltages due to the difference in sensitivity of the photodetectors and differences in apertures, beam splitters, etc. The lasers themselves are of course not identical, due to imperfections in the crystal and mirror, or nonparallelism of the pump beams. One laser may thus have a somewhat higher pump threshold than the other, and therefore a relaxation oscillation frequency that differs by as much as 10% from that of the other laser. Synchronization is achieved despite these differences, and is remarkably robust in nature. We also note that the coupled lasers remain phase locked with a π-phase difference even when their intensities exhibit synchronized chaotic fluctuations.

In conclusion, we have reported the direct observation of the synchronization of intensity fluctuations of two chaotic lasers. It should be possible to extend these observations to large arrays of coupled nonlinear oscillators, including linear and two-dimensional arrays of lasers, Josephson junctions, and other physical and chemical systems.

We acknowledge support from the Division of Chemical Sciences, Office of Basic Energy Sciences, Office of Energy Research, U.S. Department of Energy. It is a pleasure to thank Val Afraimovich, Neal Abraham, Pere Colet, Larry Fabiny, Darlene Hart, Lou Pecora, and Herbert Winful for many helpful discussions.

[1] L. M. Pecora and T. L. Carroll, Phys. Rev. Lett. **64**, 821 (1990); L. M. Pecora and T. L. Carroll, Phys. Rev. A **44**, 2374 (1991).

[2] K. M. Cuomo and A. V. Oppenheim, Phys. Rev. Lett. **71**, 65 (1993).

[3] A. V. Gaponov-Grekhov, M. I. Rabinovich, and I. M. Starobinets, Pis'ma v Zh. Eksp. Teor. Fiz. **39**, 561 (1984); (b) V. S. Afraimovich, N. N. Verichev, and M. I. Rabinovich, Izvest. Vyss. Uch. Zavedenii, Radiofizika **29**, 1050 (1986).

[4] H. G. Winful and L. Rahman, Phys. Rev. Lett. **65**, 1575 (1990); R. K. DeFreez *et al.*, in *Nonlinear Dynamics in Optical Systems*, edited by N. B. Abraham, E. M. Garmire, and P. Mandel (Optical Society of America, Washington, D. C., 1991), p. 106.

[5] L. Fabiny, P. Colet, R. Roy, and D. Lenstra, Phys. Rev. A **47**, 4287 (1993).

[6] A. E. Siegman, *Lasers* (University Science Books, Mill Valley, CA, 1986), p. 963.

[7] F. T. Arecchi, R. Meucci, G. Puccioni, and J. Tredicce, Phys. Rev. Lett. **49**, 1217 (1982); W. Klische, H. R. Telle, and C. O. Weiss, Opt. Lett. **9**, 561 (1984); A. V. Bondarenko *et al.*, in *Laser Noise*, edited by Rajarshi Roy (Proc. SPIE Int. Soc. Opt. Eng. 1376, 1991), p. 117; H. G. Winful, Y. C. Chen, and J. M. Liu, Appl. Phys. Lett. **48**, 616 (1986); L. E. Everett, C. Iwata, N. B. Janicki, and N. B. Abraham, in Proceedings of Laser Optics '93, edited by A. Mak (SPIE, Bellingham, to be published).